SURFACE INTEGRAL FINITE ELEMENT HYBRID METHOD FOR LOCALIZED PROBLEMS IN CONTINUUM MECHANICS

BY

BALKRISHNA SHRINIWAS ANNIGERI

D.M.E., Govt. Polytechnic, Nagpur, India
1970

B.E., Govt. College of Engineering, Aurangabad, India
1973

M.M.E., Illinois Institute of Technology, Chicago, Illinois
1976

Submitted to the Department of
Mechanical Engineering in partial fulfillment
of the requirements for the degree of
DOCTOR OF SCIENCE
at the
MASSACHUSETTS INSTITUTE OF TECHNOLOGY
April 1984

Signature of Author Balkrishna S. Annigeri
Department of Mechanical Engineering

Certified by Michael P. Cleary
Michael P. Cleary
Thesis Supervisor

Accepted by Warren Rohsenow
Warren Rohsenow
Chairman Departmental Graduate Committee

SURFACE INTEGRAL FINITE ELEMENT HYBRID METHOD FOR LOCALIZED PROBLEMS IN CONTINUUM MECHANICS

by

BALKRISHNA SHRINIWAS ANNIGERI

Submitted to the Department of Mechanical Engineering on April 24, 1984 in partial fulfillment of the requirements for the Degree of Doctor of Science.

ABSTRACT

An effective surface integral and finite element hybrid (SIFEH) method has been developed to model localized problems in continuum mechanics; in this research the method has been developed for fracture mechanics. This hybridization by (incrementally) linear superposition combines the best features of both component methods. Displacement based finite elements are used to model the finite domain (including material nonlinearity) while continuous distribution of dislocations (resulting in surface integral equations) are used to model the fracture (i.e. displacement discontinuity). Quasi-static fracture propagation of surface and internal cracks has been modelled effectively. This method has been implemented for linear and materially nonlinear analysis in a computer program and results of representative problems are presented: these compare very well with known analytical and experimental solutions and they demonstrate the computational advantages of SIFEH over other numerical methods (including the individual components).

Thesis Supervisor: Dr. Michael Patrick Cleary

Title: Associate Professor of Mechanical Engineering

ACKNOWLEDGEMENTS

I wish to express my sincere gratitude to Professor Michael P. Cleary for the suggestion of this thesis topic, for his advice and encouragement, and especially the freedom I was accorded in pursuing this research. I have great respect for his knowledge in continuum mechanics and I have enjoyed developing this hybrid method and working with him.

Thanks are due to Professor Klaus-Jurgen Bathe who encouraged me to pursue this thesis topic. He has been my co-advisor and I have benefited greatly from his excellent courses in finite element analysis and from the numerous discussions pertaining to this research, especially with respect to adaptation of this hybrid method for NONSAP and nonlinear analysis.

I thank Professor David M. Parks for his help, especially with plasticity aspects of fracture and inelastic deformation in general. His insight into asymptotic analysis for multilinear constitutive models was especially useful. I thank Professor Herbert H. Einstein for his help and advice. Thanks are also due to Professor Frank A. McClintock who referred me to a recent thesis on fatigue crack propagation and who also impressed me with the importance of being able to model displacement discontinuities in media with nonlinear constitutive behavior.

Pertaining to my research I was happy to be associated with my colleagues Mohan Narendran, Daniel Wium, Bill Keat and Tom Greene; I thank them all. I am confident that Bill Keat will sucessfully continue furthering this research for 3-D applications. I thank Mr. Art Anger of the IPC Computer Center at M.I.T. for his help. I wish to thank all my

colleagues and friends who have made this stay at M.I.T. enjoyable.

This research was supported by the National Science Foundation (under Grant #CEE-8119364), and the M.I.T. UFRAC project sponsored by a number of production and service companies in the oil and gas industry; their support is acknowledged with thanks.

My sincere thanks to Mr. Sandy Squires of the Commercial Union Insurance Company for the use of the word processing system. I thank Andrea Viscione for the excellent typing, and Leslie Regan for typing the equations superbly and also for being a friend. Thanks to Benge Ambrogi for doing a superb job with the drawings. I want to thank Sandy Williams Tepper for her help.

On a personal note I want to thank my parents for their love and advice and for always encouraging me to pursue my goals.

Lastly but most importantly I want to thank my wife Ujwal who has sacrificed a lot so that I could achieve my doctorate at M.I.T. She has helped me with the typing of this thesis and with her love and patience has helped its completion. I thank our sons Anand and Vinay who have been patient enough to let me finish my work. I dedicate this thesis to Ujwal, Anand and Vinay.

I end this thesis on a sad note for the sudden loss of my mother and younger brother in an unfortunate car accident in India.

B.S.A.

TABLE OF CONTENTS

TABLE OF CONTENTS (Continued)

TABLE OF CONTENTS (Continued)

LIST OF TABLES

LIST OF FIGURES

NOTATION

All the notation used in this thesis is defined in the text when first used.

CHAPTER 1

INTRODUCTION

1.1 MOTIVATION FOR PRESENT RESEARCH AND A BRIEF REVIEW OF EXISTING METHODS

The motivation for this research was provided by a need to develop an effective procedure to solve localized problems in continuum mechanics. The characteristic of a localized problem is the existence of a disturbance or a perturbation in an otherwise unperturbed field or domain. An example of such a problem is a fracture in a solid where the perturbation is caused by the fracture (displacement discontinuity) in an otherwise continuous and finite solid defined by its boundaries. Some sample problems which have localized character are:

- o Fracture propagation in arbitrarily shaped bodies, e.g. evolution of fracture in structures (typical aerospace, nuclear, or automotive industry application), growth of hydraulic fractures in rocks (typical resource recovery industry application) [35] - (refer to figure 1.1);

- o Propagation of localized rupture (viz. non-opening shear bands)
  e.g. in flow of granular material through hoppers [21] (refer to figure 1.2), formation of localized bands in sheet metal forming, and in glassy metals and polymers [31,32], etc.;

- o Dynamic fracture problems;
  e.g. unstable brittle fracture of glass, ceramics and rock [74].

- o Potential flow problems in fluid mechanics
  e.g. flow over an air foil in a wind tunnel [34] (refer to figure 1.3);

- o Diffusion of heat and mass near surfaces or fractures
  e.g. heat and mass transfer around a fracture in a porous medium [36].

The scope of the localized problems is very broad, but attention is concentrated on fracture mechanics in this thesis.

There are various numerical procedures available for solving problems in continuum mechanics. Of the existing methods, the finite element method [24,25] and the boundary integral method [8,12] have gained wide acceptance. There are many general purpose finite element computer programs commercially available. The finite element method has been used extensively to solve elastic and elastic-plastic problems in fracture mechanics [1-7] and is very effective for solving problems with material and geometric nonlinearities, dynamics and inhomogeneity (e.g. boundaries, inclusions, interfaces). However, finite element analysis (which uses local interpolation in variables over the element subspace) is not most effective for problems with singularities (e.g. a mathematically sharp crack) or any localized events such as point sources and sinks (e.g. in field problems of heat and mass transfer). A fine mesh is needed near a crack tip to capture the rapidly varying stress and displacement field. The topology of the finite elements is dictated by the shape and orientation of the fractures. Propagation of fractures necessitates redefining the finite element topology which may present difficulties, especially in nonlinear analysis since a reliable continuum mechanics based method has not yet been developed to

facilitate remeshing (note: this is also a problem posed in large strain and large displacement analysis [24,37]).

Finite elements are not most effective for infinite domain problems: e.g. unbounded surface wave problems, deep underground cavities, etc. However "Infinite Elements" which for instance use exponentially decaying shape functions [14] have been reported in literature [14-16] which enable application of the finite element analysis to infinite domains.

The boundary integral equation (BIE) method [8-13] has also been developed and extensively used for analysis of problems in continuum mechanics. This method reduces the order of the problem, basically by using the divergence theorem of Gauss; however the system matrix is full and unsymmetric so the reduction in order may be achieved only superficially. This is particularly effective for problems with singularities and dominantly linear response; and also for modelling infinite domains. The method has recently also been applied to materially nonlinear analysis [38]. This method has been used for analyzing fracture problems [9,10,13]; difficulties which existed in modelling sharp cracks [9] have been overcome by use of multidomain modelling or substructuring [13].

The surface integral method has been developed for solving a variety of solid mechanics and field problems [17,19,20,33,35,36]. It basically involves setting up the governing integral equation for the problem by using known fundamental solutions to events such as dislocations, dipoles, fluid or heat point sources and sinks etc. and by using boundary collocation. Fracture problems in infinite domains have been modelled effectively using the surface integral method [19,20]. The fracture is modelled as a

continuous distribution of dislocations [17], which are displacement discontinuities defined in the sense of Volterra [23], and this results in a singular integral formulation [17]. Gauss-Chebyshev quadrature is best used to perform numerical integration. Mathematical foundations and convergence criteria for numerical integration of the singular integral equations using global interpolation has been provided by Erdogan and Gupta [18]. This surface integral method has been extended to analyze multiple, branched, arbitrarily shaped cracks [19, 20] and also for quasi-static crack propagation [35]. It is to be pointed out that displacement discontinuities (fracture) for a sharp crack can be modelled effectively using the surface integral method, which distinguishes it from the BIE method. However as mentioned earlier, substructuring techniques [13] or Green's functions [9] (for traction free crack) have been eventually implemented to model a sharp (flat) crack with BIE methods.

A dislocation superposition computer program to solve plane elasticity fracture problems has also been developed [44,45] for finite and infinite domains. Finite domains are modelled by distributing dislocations not only along the crack but also along the boundaries of the finite body. This program uses local interpolation for discretizing the singular integral equation which is in contrast to the global Gauss-Chebyshev interpolation scheme used in the surface integral formulation. Mixed mode fracture propagation in titanium specimens due to fatigue was modelled using this dislocation superposition program as described in [46]. However the development of the SIFEH method was motivated to extract the best features of the component methods especially for materially nonlinear analysis.

1.2 SCOPE OF PRESENT RESEARCH

The objective of combining the finite element and surface integral methods was to simultaneously implement the best features of the two methods. The procedure of combining these two methods in a hybrid formulation will be explained after commenting on its features. This SIFEH method allows modelling of the crack "independently" of the finite element mesh. The crack can penetrate "through" the finite elements and this is very desirable, especially in the context of crack propagation and also for initiation of new cracks. In conventional finite element analysis the mesh depends on the shape of the crack and a refined mesh is required at the crack tips (even when special elements [1,2,3] are used). A need to have such a hybrid method was also arrived at earlier [21], and a computer program was written to solve a specific shear box problem (central crack in a plate with pure shear loading). However, the computer implementation was very limited; also, the formulation incorporated dislocation dipoles, with crack opening/slip as a variable, and a local interpolation which did not allow direct relation to the stress intensity factor, for instance. The research presented in this thesis is based on computer implementation of a general two dimensional program capable of modelling multiple cracks and branched cracks. The amplitude of the "dislocation density" (which is the derivative of the crack opening/slip) is used as a variable, which is directly related to the stress intensity factor at the crack tip [22,39].

The formulation of the SIFEH method for linear analysis is presented in Chapter 2. The fracture problem is shown to be the sum of the finite element and surface integral models using linear superposition. Governing equations are derived for the linear case.

Sample analyses of linear elastic fracture problems are presented in Chapter 3. Results for representative problems of internal and surface cracks and cracks in nonhomogeneous domains are presented.

The formulation for quasi-static crack propagation is developed in Chapter 4. Results for a plate with an internal crack and a beam with a surface crack are presented. Evolution of shear bands in flow of granular material through hoppers is presented.

Incorporation of the SIFEH method in a nonlinear finite element computer program is presented in Chapter 5. The governing equations for nonlinear analysis are developed. The decoupled method of solution of the incrementally linear equations is derived. Sample analysis of fracture problems for incompressible hypoelastic bi-linear materials are presented.

Finally, conclusions and recommendations for further research are summarized in Chapter 6. Further topics of research where this hybrid method can be effectively applied are discussed.

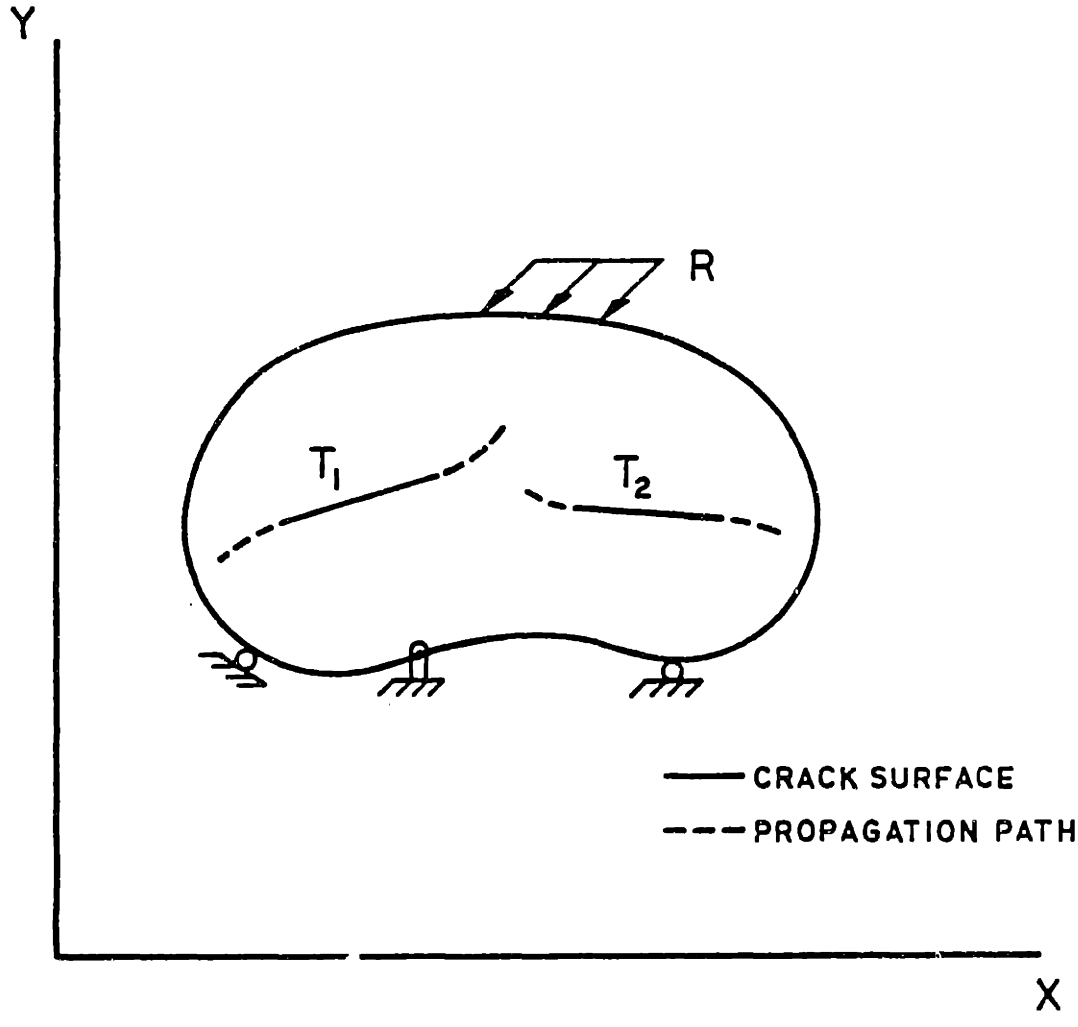

Figure 1.1 Crack propagation in arbitrarily shaped bodies

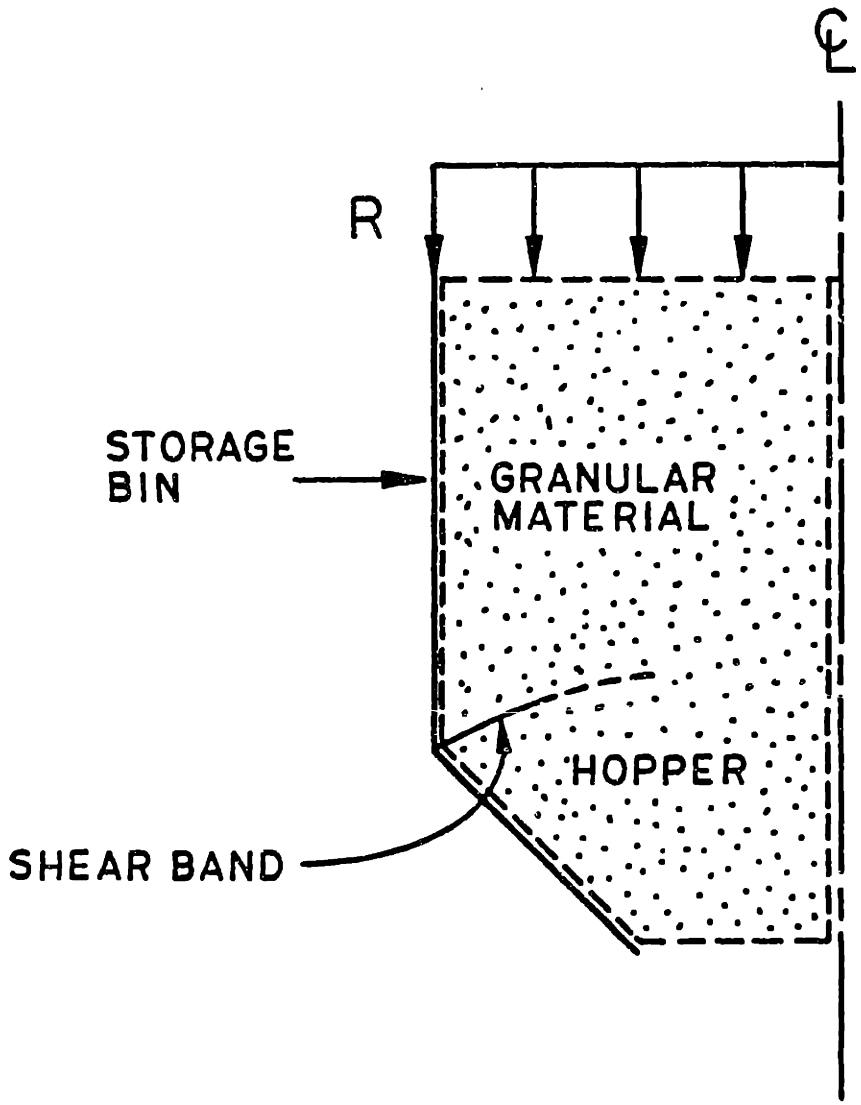

Figure 1.2 Propagation of shear bands in granular materials

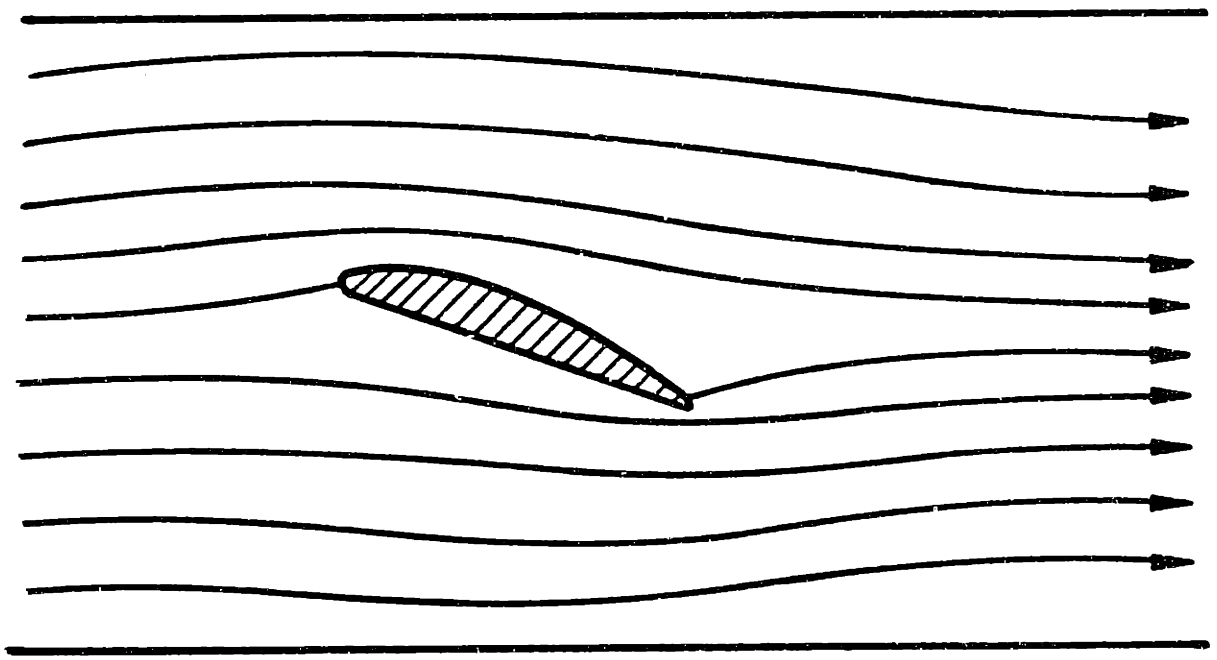

Figure 1.3 Potential flow over an airfoil

CHAPTER 2

THEORETICAL FORMULATION OF THE SIFEH METHOD FOR LINEAR ANALYSIS

2.1 LINEAR ELASTIC FRACTURE ANALYSIS

In this chapter the governing equations for linear elastic fracture analysis in the plane are developed. Consider a mixed boundary value problem (shown in figure 2.1) of a center cracked plate with a tensile load R and traction T applied along the crack surface. The aim of the analysis is to compute the stress and displacement field and the stress intensity factors. The above problem can be analyzed using linear superposition as shown in figure 2.2.

Linear superposition allows representation of the actual problem as a sum of a finite plate without the crack (discretized by a finite element model) and a finite plate with a crack cut out from an infinite region (discretized by a surface integral model). The vector R^c is the correction applied (only at the boundary) to the load vector R in the finite element model to account for the presence of a crack. The vector T^c is the correction applied (only along the crack surface) to the traction vector T in the surface integral model to account for the finite boundary of the actual problem. What has been achieved is a force matching along the outer boundary of the actual plate and traction matching along the crack surface; displacement matching will be analogously achieved.

Using variational or virtual work formulations which

have been discussed in depth elsewhere [24-25] and for completeness in Appendix A, the governing finite element equations for the center cracked plate without the crack (refer to figure 2.3) are given by:

$$K\ U^{FE} = R - R^{C} \qquad (2.1)$$

K = Stiffness matrix of the plate without the crack.

U^{FE} = Finite element nodal displacement vector (only continuous field).

R = Applied load vector.

R^{C} = Correction to the applied load vector due to the presence of the crack.

As is evident from figure 2.4 the load correction vector R^{C} is a function of the displacements of the crack faces and can be expressed as a function of the dislocation density (which is derivative of crack face displacements) amplitude vector F by defining matrix G (refer to Appendix D):

$$R^{C} = G\ F \qquad (2.2)$$

G = Boundary force correction matrix

Combining equations (2.1) and (2.2):

$$K\ U^{FE} + G\ F = R \qquad (2.3)$$

The product GF represents a correction to the applied force R due to the presence of a crack in the finite body.

The surface integral model is the result of modelling cracks in an infinite medium using continuous distributions of dislocations [17,19,20,39,40]. Basically a dislocation is a displacement discontinuity [26,42] and a continuous distribution of such dislocations can be used effectively to model a crack or a slip band. A brief discussion of the formulation is presented here and additional details can be found in reference [20].

Consider an infinite linear elastic domain with cracks, loaded as shown in figure C.1 in Appendix C. This problem of the infinite domain is also solved using linear superposition of the infinite domain without the cracks and the same infinite domain with the cracks with applied tractions reversed along the cracks. The first problem does not have singularities; the second one does, and this is modelled effectively using a singular integral formulation. The resulting singular equation takes the form [17]:

$$\int_{S_c} \Gamma(\underset{\sim}{X}_o, \underset{\sim}{X}) \cdot \mu(\underset{\sim}{X}) \, dS_c = T(\underset{\sim}{X}_o) \qquad (2.4)$$

$\underset{\sim}{X}_o$ = Evaluation point along the crack.

$\underset{\sim}{X}$ = Interpolation point along the crack.

$\Gamma(\underset{\sim}{X}_o, \underset{\sim}{X})$ = Stress tensor at $\underset{\sim}{X}_o$ due to an edge dislocation at $\underset{\sim}{X}$ (known from elastic theory of dislocations).

$\mu(\underset{\sim}{X})$ = Dislocation density at $\underset{\sim}{X}$.

S_c = Crack surface

$T(\underset{\sim}{X}_o)$ = Traction vector at $\underset{\sim}{X}_o$.

The above singular (since the kernel $\Gamma(\underset{\sim}{X}_o, \underset{\sim}{X})$ is singular) integral equation is evaluated in the Cauchy principle value sense using a Gauss-Chebyshev integration scheme [17,19,20]. The details of the discretization process is described in [19,20] and for completeness is described in Appendix C. The discretized equations for the plate cut out from the infinite domain with appropriate force R^c acting on the boundary (refer to figure 2.4) are given by:

$$C\ F = T - T^c \qquad (2.5)$$

C = Coefficient matrix for the singular integral equation (refer to Appendix C).

F = Vector of amplitudes of the dislocation density.

T = Applied traction vector.

T^c = Correction to the applied traction vector due to the finite domain.

The traction correction vector T^c can be expressed as a function of the finite element nodal displacement vector U^{FE} by defining matrix S (refer to Appendix B):

$$T^c = S\ U^{FE} \qquad (2.6)$$

S = Stress feedback matrix

Using equations (2.5) and (2.6):

$$S\ U^{FE} + C\ F = T \qquad (2.7)$$

The product S U^{FE} represents the stress feedback correction to the line of the crack due to the continuous displacement field at the finite element nodes.

Equations (2.3) and (2.7) result in a coupled matrix equation:

$$\begin{bmatrix} K & G \\ S & C \end{bmatrix} \begin{Bmatrix} U^{FE} \\ F \end{Bmatrix} = \begin{Bmatrix} R \\ T \end{Bmatrix} \qquad (2.8)$$

In equation (2.8) it is to be noted that the vector U^{FE} represents the continuous displacement field at the finite element nodes. The total displacement U at the finite element nodes is the sum of the continuous field U^{FE} and the discontinuous field U^{SI} resulting from the surface integral discretization of the infinite domain with fracture (refer to figure 2.2).

$$U = U^{FE} + U^{SI} \qquad (2.9)$$

To be able to solve a displacement or a mixed boundary value problem it is necessary to change the U^{FE} vector in equation (2.8) to U. The U^{SI} vector (evaluated at the finite element nodes) can be expressed as a function of the dislocation density amplitude vector F by defining matrix L (refer to Appendix E).

$$U^{SI} = L\ F \qquad (2.10)$$

L = Displacement matrix.

Physically this means that the displacement at any point in the surface integral model is proportional to the F vector. The L matrix has been worked out (Appendix E) using

the displacement influence function for an edge dislocation [26], and integrating the effect of a continuous distribution of dislocations along the surface of the crack. The displacement influence functions model the displacement discontinuity, and special care has to be exercised to correctly derive the L matrix as shown in the Appendix and in [43]. Using equations (2.8), and (2.9):

$$\begin{aligned} K\ (U - U^{SI}) + G\ F &= R \\ S\ (U - U^{SI}) + C\ F &= T \end{aligned} \tag{2.11}$$

Using equations (2.10) and (2.11)

$$\begin{aligned} K\ U + (G - K\ L)F &= R \\ S\ U + (C - S\ L)F &= T \end{aligned} \tag{2.12}$$

Defining:

$$\begin{aligned} G^* &= G - K\ L \\ C^* &= C - S\ L \end{aligned} \tag{2.13}$$

The resulting matrix equation becomes:

$$\begin{bmatrix} K & G^* \\ S & C^* \end{bmatrix} \begin{Bmatrix} U \\ F \end{Bmatrix} = \begin{Bmatrix} R \\ T \end{Bmatrix} \tag{2.14}$$

Equation (2.14) is the governing matrix equation for the SIFEH method for linear analysis. Arbitrary force and displacement boundary conditions can be imposed using standard procedures for imposing these constraints [24]. The details of obtaining the K, G, S, C and L matrices are

explained in Appendices A through E. Evaluation of crack opening and slip displacements is explained in Appendix E.

Fracture problems in nonhomogeneous media can be solved by substructuring techniques. The G* and C* matrices are evaluated for the substructure with cracks and the stiffness of the whole domain is assembled in matrix K. Essentially this procedure involves providing correct boundary data of the substructure with the cracks to compute G and evaluating L only for this substructure. As a degeneration of the substructuring concept it is readily deduced for a homogeneous domain that the G matrix can be obtained by taking any closed contour (along the finite element edges) around the fracture as far as the L matrix is evaluated for this substructure.

2.2 CONVERGENCE CRITERIA

The convergence of the finite element method has been studied in great detail by many researchers, some of whom have used functional analyses to quantify in rigorous mathematical terms the errors associated with the discretization process and the manner in which these errors propagate [24,25,48,49]. For this hybrid method the requirement of the finite element discretization is that it should be adequate to capture the $R-R^c$ field. However, since this method is coupled it is important to note that the R^c vector depends on how adequately the crack is modelled using a given distribution of dislocations. The crack can be modelled effectively using a relatively few degrees of freedom on dislocation density. Convergence of the surface integral scheme has been presented in a recent associated research effort as exemplified in [50] (See also [75]). The singular crack tip stress and displacement

fields have been compared with both asymptotic and complete solutions (when they were available), and superb accuracies have been obtained for the problems that have been analyzed. Curved and kinked cracks do need more number of dislocations to model the crack [20,35] as compared with straight cracks.

By examining the convergence characteristics of these individual methods it is then possible to qualitatively assess the convergence characteristics of the hybrid method. Stress jumps at common nodal points (for different finite elements) can be used as a guide in determining convergence.

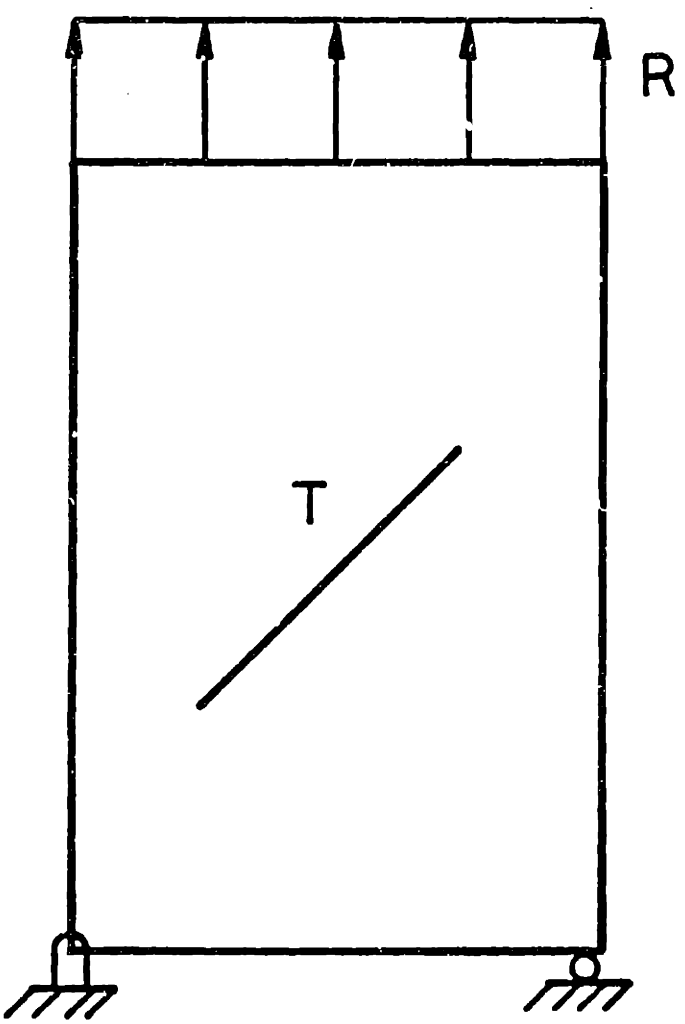

Figure 2.1 Center cracked plate with tensile load

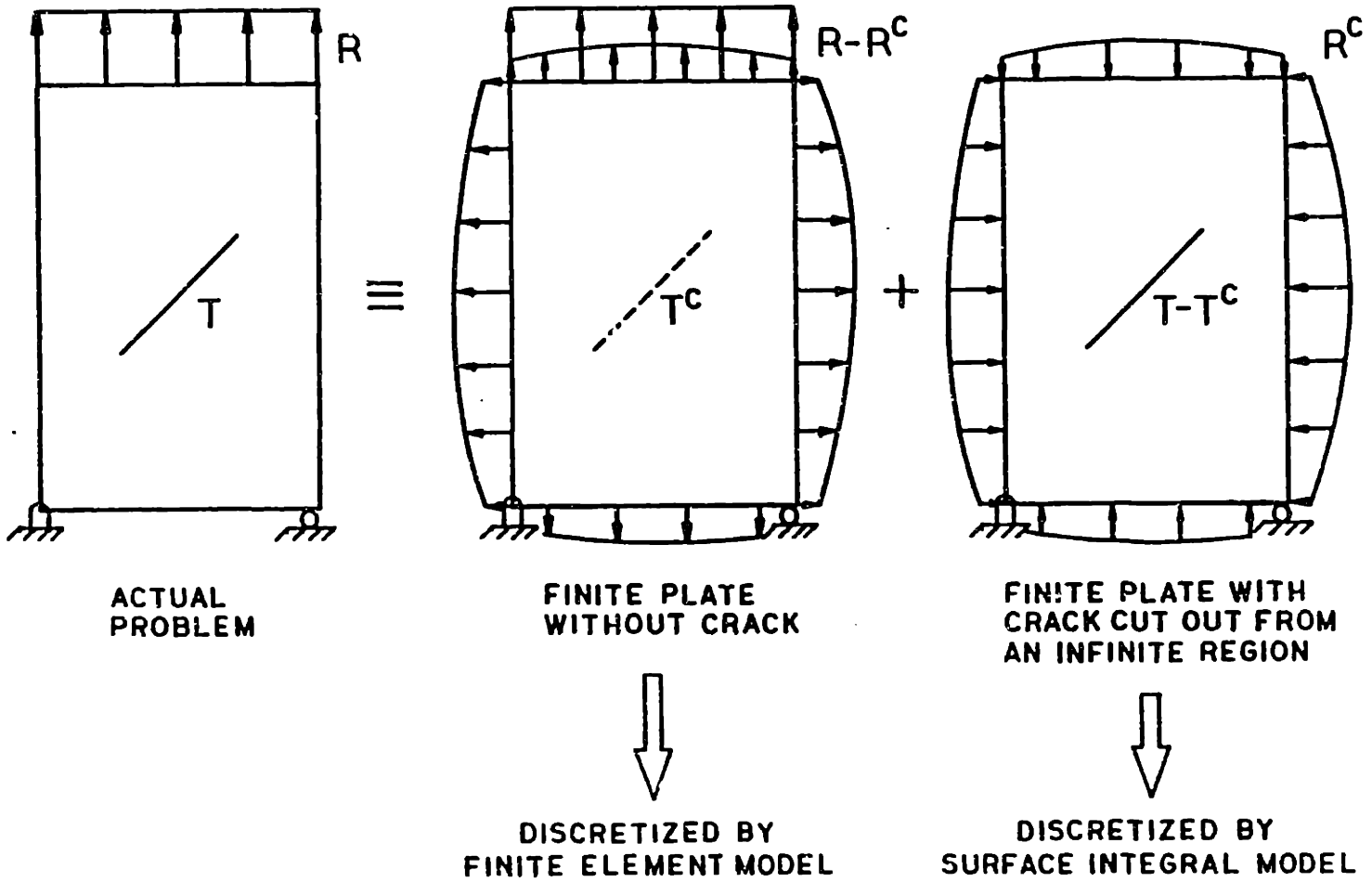

Figure 2.2 Linear superposition of the finite element and surface integral models

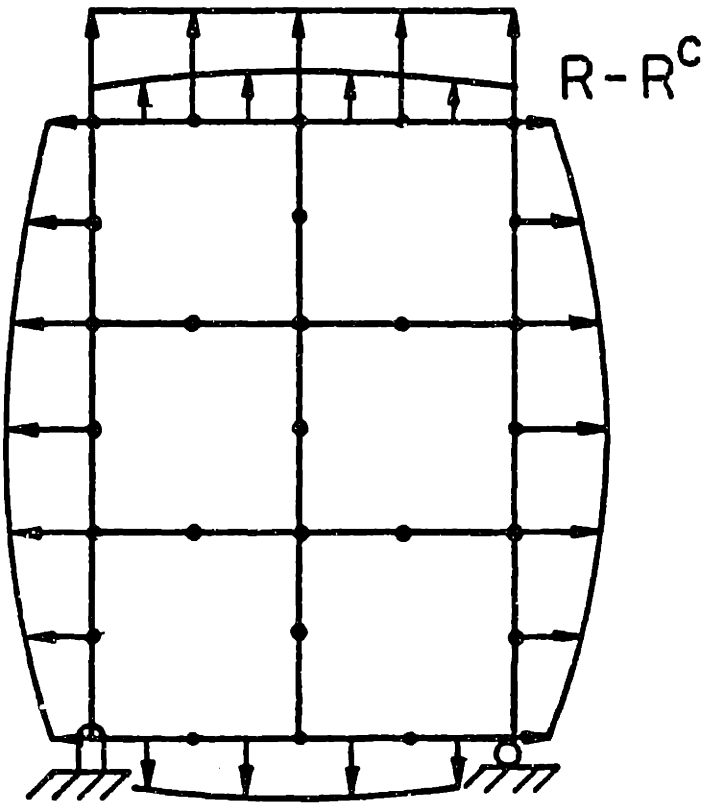

Figure 2.3 Finite element model using eight noded isoparametric elements

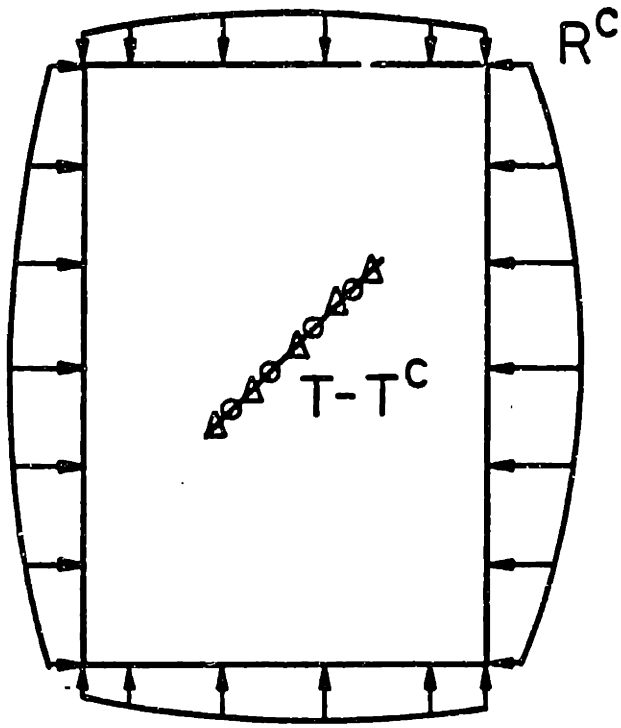

Figure 2.4 Surface integral model using continuous distribution of dislocations to model the crack

CHAPTER 3

RESULTS FOR LINEAR ELASTIC STATIC ANALYSES OF FRACTURE PROBLEMS

Results are presented for fractures in plates under plane strain conditions.

3.1 CENTRAL SYMMETRIC CRACK WITH TENSILE LOAD

The finite element discretization of this problem along with the number of interpolation points (S_{nk} points used to evaluate the C matrix) is shown in figure 3.1.

The stress intensity factors (SIF's) are as plotted in figure 3.1. The length of the crack is varied maintaining the same finite element mesh and number of S_{nk} points defining the crack. With this SIFEH model it can be seen that good agreement with analytical solution of Isida [27] is obtained up to a ratio of $a/b = 0.5$. For $a/b > 0.5$ the SIF's are lower than the analytical values. A second SIFEH model was analyzed as shown in Figure 3.2. The resulting SIF's agreed very well up to a ratio of $a/b = 0.9$. The reason for using more finite elements rather than more S_{nk} points is that for this problem, theoretically, only two S_{nk} points per crack wing (using an origin and two wings to define the crack) are sufficient to model the crack; since for a square root singular dislocation density and the given loading, the variation of the amplitude vector F is linear. However, to place the interpolation (S_{nk}) points near the crack tips using the Gauss-Chebyshev integration scheme, five S_{nk} points per wing or a total of ten points have been

used. With this reasoning more finite elements were used in the second model (Figure 3.2) and as is evident, convergence in the SIF's were obtained over a wide range.

3.2 CENTRAL SYMMETRIC CRACK WITH MOMENT LOAD

The finite element and surface integral discretization is shown in figure 3.3. SIF for this problem is shown in Table 3.1. Good agreement with analytical solution [27] has been obtained.

Table 3.1 Stress intensity factor for center cracked test specimen (Refer to figure 3.3)

$\frac{K_I^{SIFEH}}{\sigma\sqrt{\pi a}}$	$\frac{K_I^{[27]}}{\sigma\sqrt{\pi a}}$	$\frac{K_I^{SIFEH}}{K_I^{[27]}}$
0.477	0.513	0.93

3.3 CENTRAL UNSYMMETRIC CRACK WITH TENSILE LOAD

The finite element and surface integral discretization is shown in figure 3.4. SIF's for this problem are shown in Table 3.2. Results agree well with analytical solution [27].

Table 3.2 Stress intensity factors for center cracked test specimen - unsymmetric crack - (Refer to figure 3.4)

	$\frac{K_I^{SIFEH}}{\sigma\sqrt{\pi a}}$	$\frac{K_I^{[27]}}{\sigma\sqrt{\pi a}}$	$\frac{K_I^{SIFEH}}{K_I^{[27]}}$
Tip 1	1.392	1.405	0.99
Tip 2	1.184	1.200	0.98

3.4 ANGLED CRACK IN A LARGE PLATE

The finite element and surface integral discretization is shown in figure 3.5. The results for this mixed mode angled crack problem for various angles of crack inclination are shown in Table 3.3. Since the boundaries of the plate are removed from the crack, the correction R^c (refer chapter 2) will be small. As expected the results are very close to the solution for an angled crack in an infinite medium [13,27].

Table 3.3 Stress intensity factors for an angled crack in a large plate (Refer to figure 3.5).

Crack angle β	$\frac{K_I^{SIFEH}}{\sigma\sqrt{\pi a}}$	$\frac{K_{II}^{SIFEH}}{\sigma\sqrt{\pi a}}$	$\frac{K_I^{[27]*}}{\sigma\sqrt{\pi a}}$	$\frac{K_{II}^{[27]*}}{\sigma\sqrt{\pi a}}$
0^o	0.	0.	0.	0.
30^o	0.253	0.434	0.250	0.433
45^o	0.520	0.507	0.500	0.500
60^o	0.758	0.434	0.750	0.433
90^o	1.007	0.000	1.000	0.000

* Analytical solution for an angled crack in an isotropic infinite medium is given by:

$$K_I^{\infty} = \sigma\sqrt{\pi a}\ \sin\beta$$

$$K_{II}^{\infty} = \sigma\sqrt{\pi a}\ \sin\beta\ \cos\beta$$

3.5 ANGLED CRACK IN A PLATE

The finite element and surface integral discretization is shown in figure 3.6. Results for this problem are shown in table 3.4. Good agreement with analytical solutions [13,27] has been obtained for 45^o and 90^o cracks for which analytical results were available.

Table 3.4. Stress intensity factors for an angled crack in a plate (Refer to figure 3.6)

Crack Angle β	K_I^{SIFEH} / $\sigma\sqrt{\pi a}$	K_{II}^{SIFEH} / $\sigma\sqrt{\pi a}$	$K_I^{[27]}$ / $\sigma\sqrt{\pi a}$	$K_{II}^{[27]}$ / $\sigma\sqrt{\pi a}$	K_I^{SIFEH} / $K_I^{[27]}$	K_{II}^{SIFEH} / $K_{II}^{[27]}$
30°	0.387	0.516	-	-	-	-
45°	0.708	0.553	0.730	0.600	0.97	0.92
60°	1.013	0.458	-	-	-	-
90°	1.446	0.	1.488	0.	0.97	-

3.6 MULTIPLE CRACKS

The computer program has been written to model multiple cracks. Figure 3.7 shows a sample analysis. The SIF obtained numerically as shown in Table 3.5 was compared to that for an infinite strip with an array of parallel cracks [27] as an analytical solution to the problem was not available for comparison.

Table 3.5. Stress intensity factor for multiply cracked plate (refer to figure 3.7).

K_I SIFEH	K_I^{∞} STRIP [27]
1.014	0.960

3.7 SINGLE EDGE NOTCHED (SEN) SPECIMEN

The finite element and surface integral discretization is shown in figure 3.8. The single edge notched problem lacks symmetry in both geometry and loading, and it was determined using various SIFEH models that a greater number of finite elements were needed to attain convergence of results as compared with the double edge notched (DEN) specimen (figure 3.9). The greater number of finite elements were necessary to model the $R - R^c$ field; the surface integral discretization used was determined to be adequate. Good agreement with analytical [51] and BIE [9] results has been obtained as shown in table 3.6. For the ratios of a/b greater than 0.3 an improved finite element discretization is needed. This contrasts with the DEN specimen results presented next where due to geometric and load symmetry good results are obtained over a wide range of a/b.

Table 3.6 Stress intensity factors for a single edge notched specimen (refer to figure 3.8)

a/W	Pressure P (psi.)	$\frac{K_I^{SIFEH}}{\sigma\sqrt{\pi a}}$	$\frac{K_I^{[9]}}{\sigma\sqrt{\pi a}}$	$\frac{K_I^{[51]}}{\sigma\sqrt{\pi a}}$	$\frac{K_I^{SIFEH}}{K_I^{[51]}}$
0.125	313.19	1.26	1.27		-
0.150	278.66	1.30	1.34		-
0.200	223.91	1.40	1.48	1.49	0.94
0.300	152.89	1.67	1.82	1.85	0.90

3.8 DOUBLE EDGE NOTCHED (DEN) SPECIMEN

The finite element and surface integral discretization is shown in figure 3.9. Good agreement with analytical results [27] over a wide range of a/b has been obtained as shown in figure 3.9.

3.9 INTERNAL CRACK IN A NONHOMOGENEOUS PLATE

As a further example of application of the SIFEH method an internal crack in a nonhomogeneous plate was analyzed. As described in Chapter 2 a substructuring technique has been used to model the problem. The finite element and surface integral discretization is shown in figure 3.10. Good agreement with analytical [41] and BIE [9] solutions has been obtained as shown in table 3.7.

Table 3.7 Stress intensity factors for a bi-material panel with an internal crack (refer to figure 3.10).

$K_I/\sigma_m\sqrt{\pi L}$

$L/(W_1 + W_2)$	E_1/E_2	Bowie[41] et. al.	Cruse & Wilson[9]	SIFEH*
	3	1.03	1.03	.994
0.15	1	1.01	1.01	.995
	1/3	0.99	0.99	.998
	3	1.06	1.06	1.009
0.20	1	1.02	1.02	1.008
	1/3	0.98	0.98	1.009
	3	1.10	1.11	1.048
0.25	1	1.03	1.03	1.044
	1/3	0.97	0.97	1.040

* The boundary conditions are slightly different for this model. Bowie et. al. and Cruse et. al. have used displacement boundary conditions. This has been approximately modelled for convenience in the SIFEH model by applying the stresses proportional to the moduli as shown in figure 3.10; however constant displacements can be imposed.

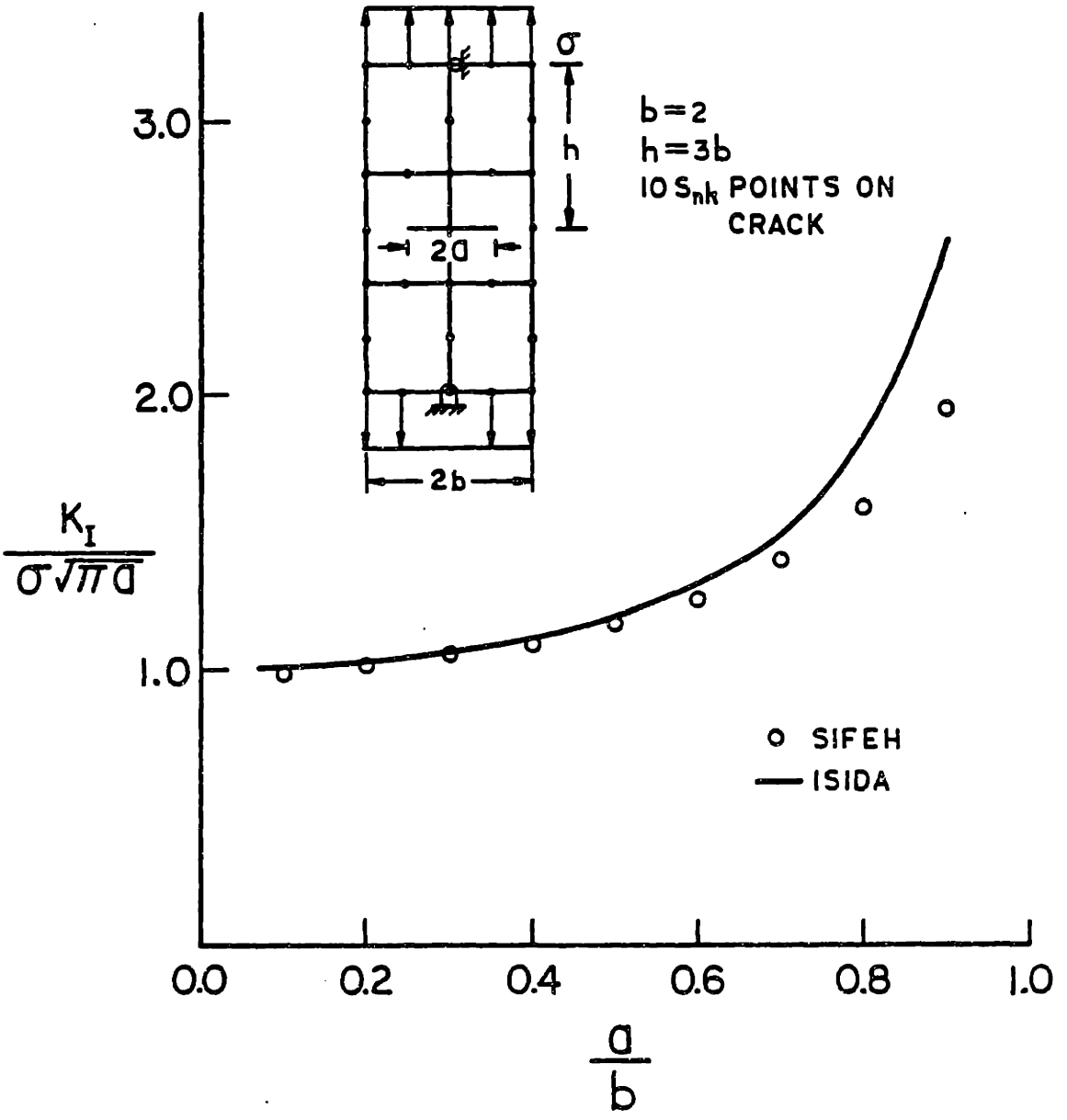

Figure 3.1 Center cracked test specimen

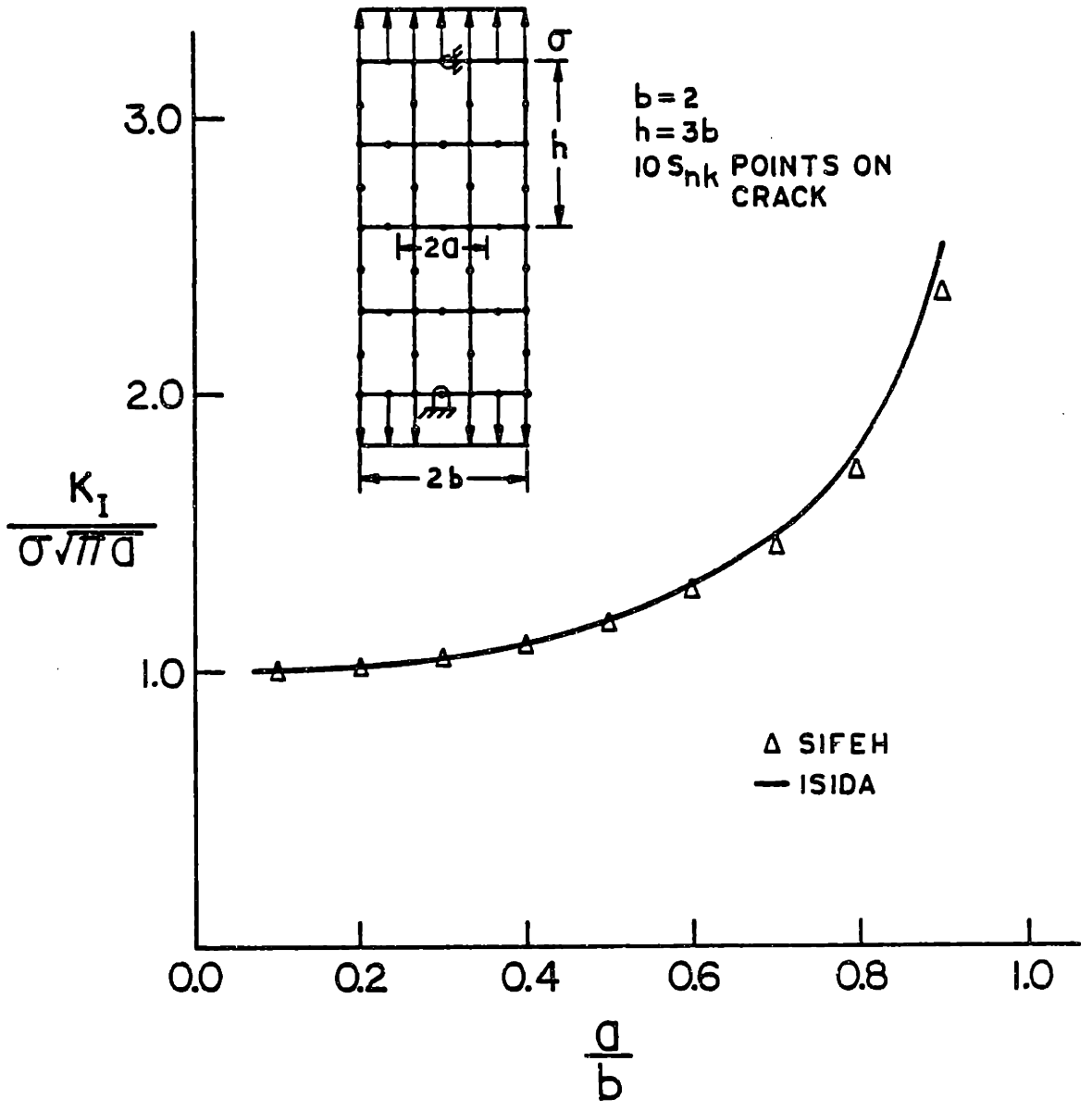

Figure 3.2 Center cracked test specimen

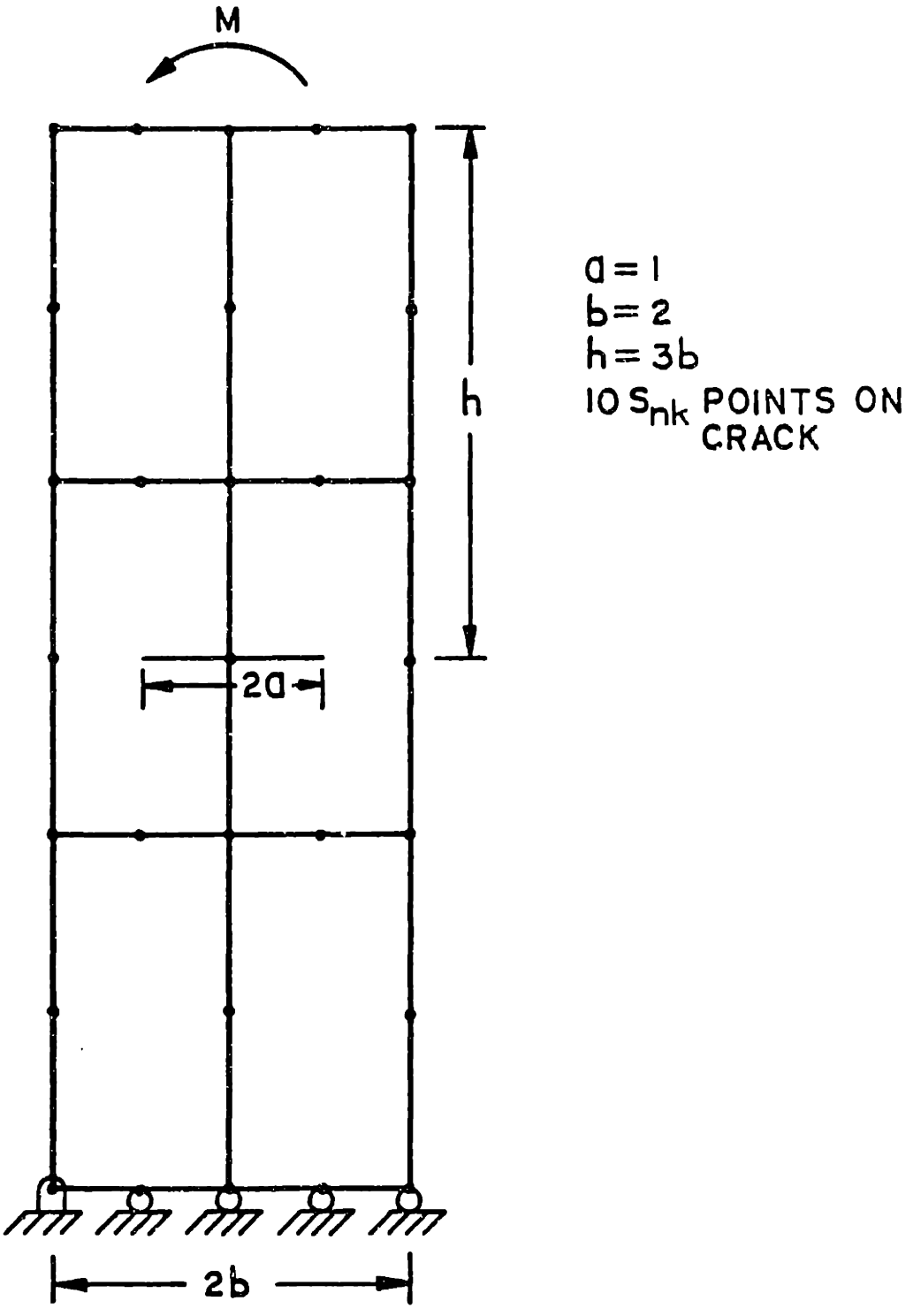

Figure 3.3 Center cracked test specimen with moment loading

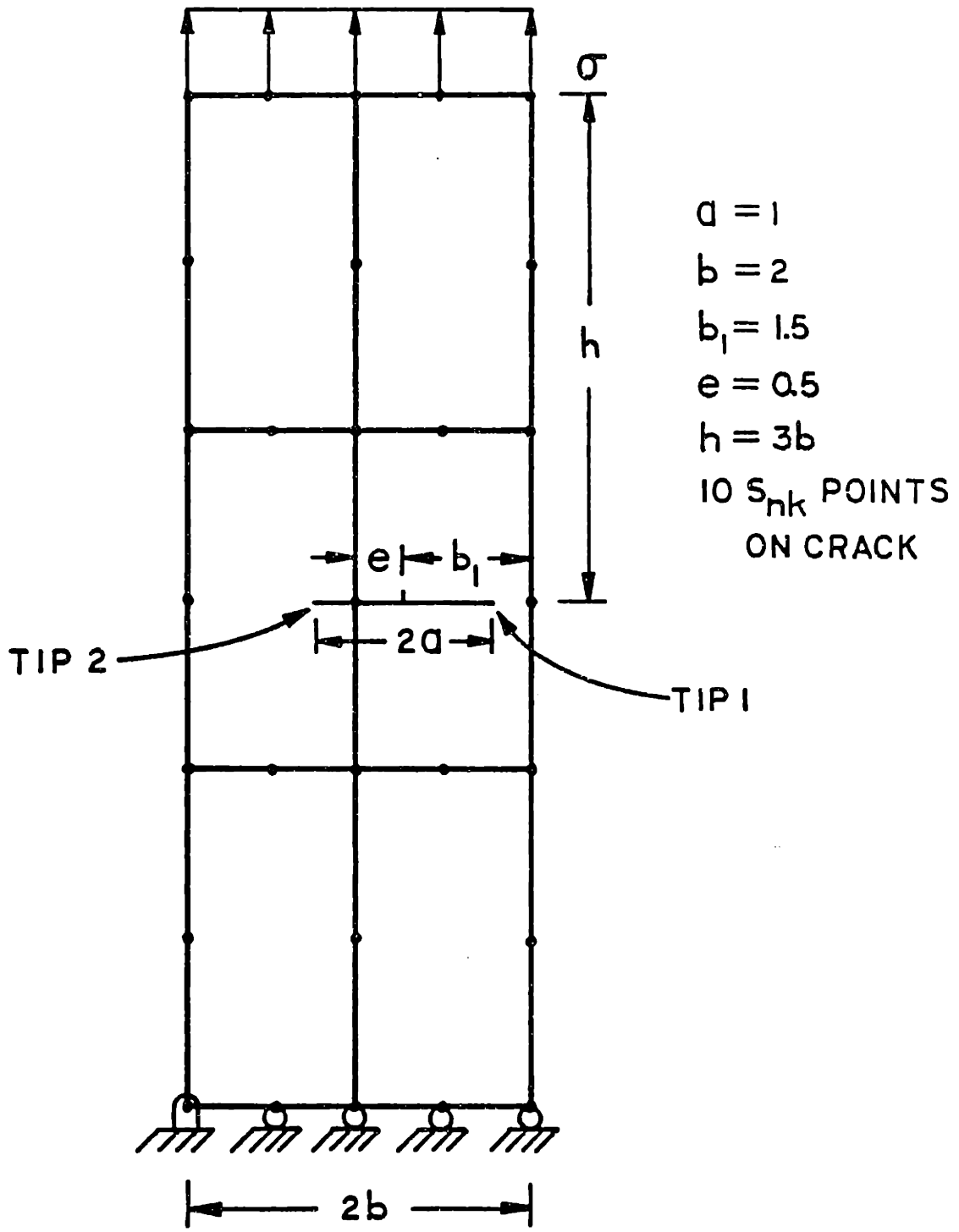

Figure 3.4 Unsymmetric crack

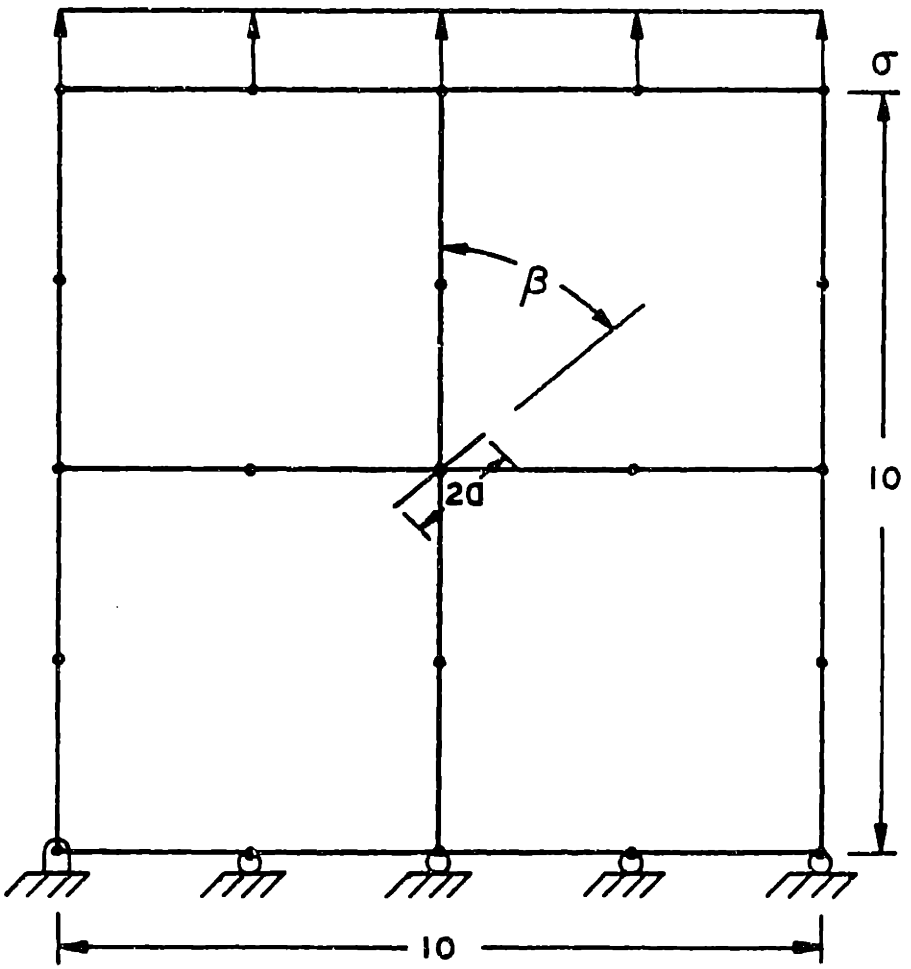

$2a = \sqrt{2}$

10 S_{nk} POINTS ON CRACK

$K_I^* = \sigma\sqrt{\pi a}\ \sin^2\beta$

$K_{II}^* = \sigma\sqrt{\pi a}\ \sin\beta\ \cos\beta$

Figure 3.5 Angled crack in a large plate

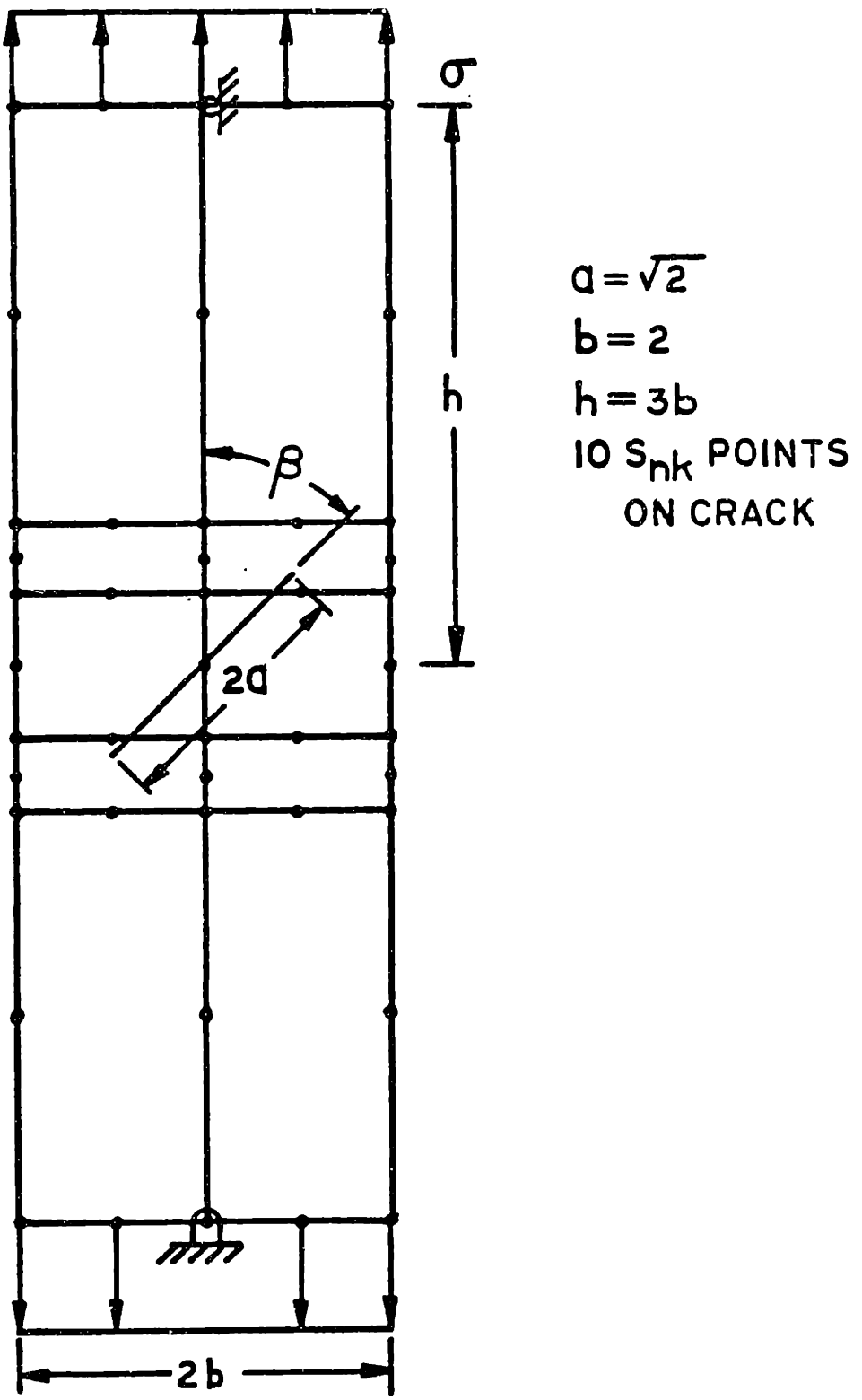

Figure 3.6 Angled crack in a plate

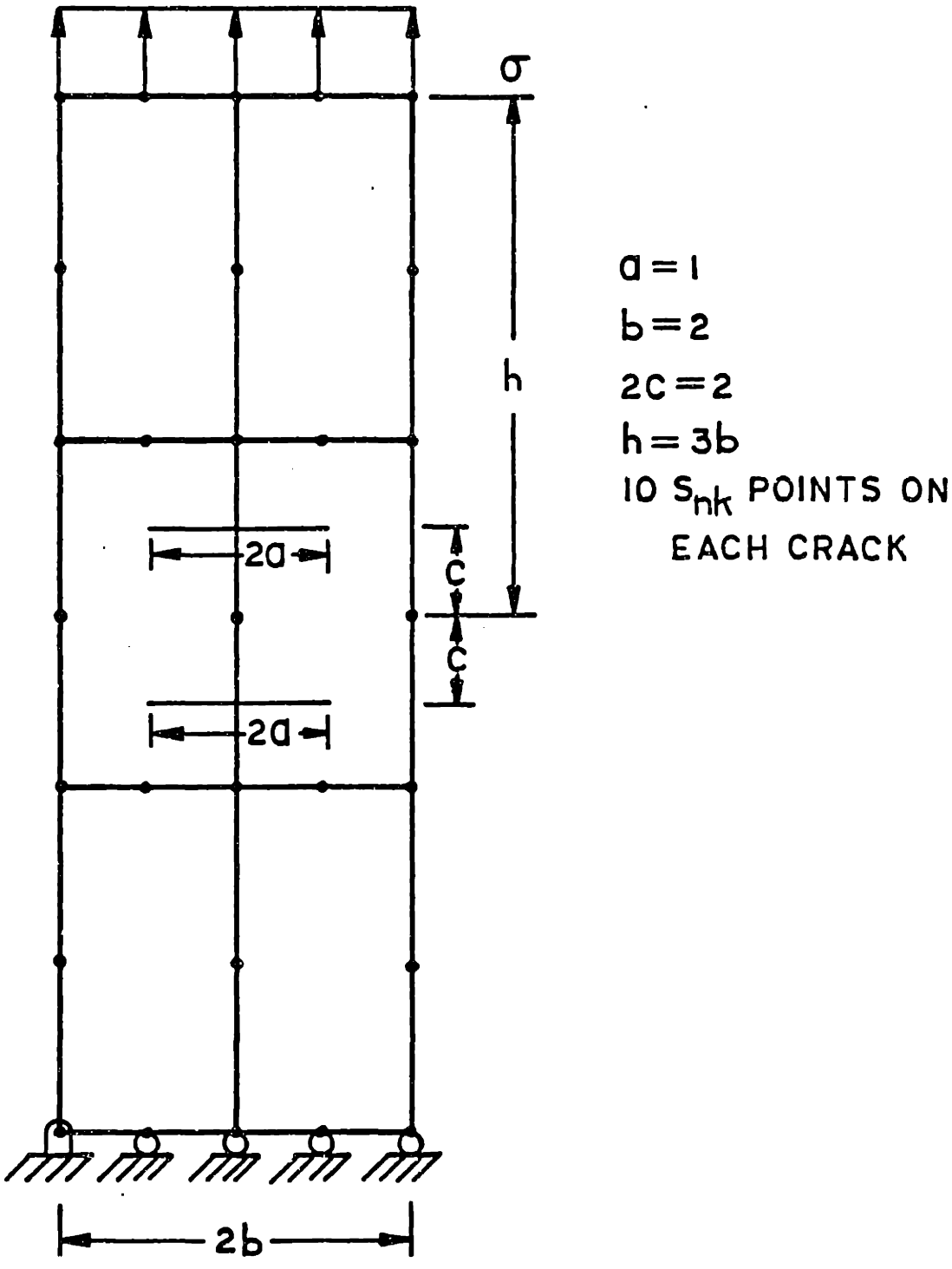

Figure 3.7 Multiple cracks

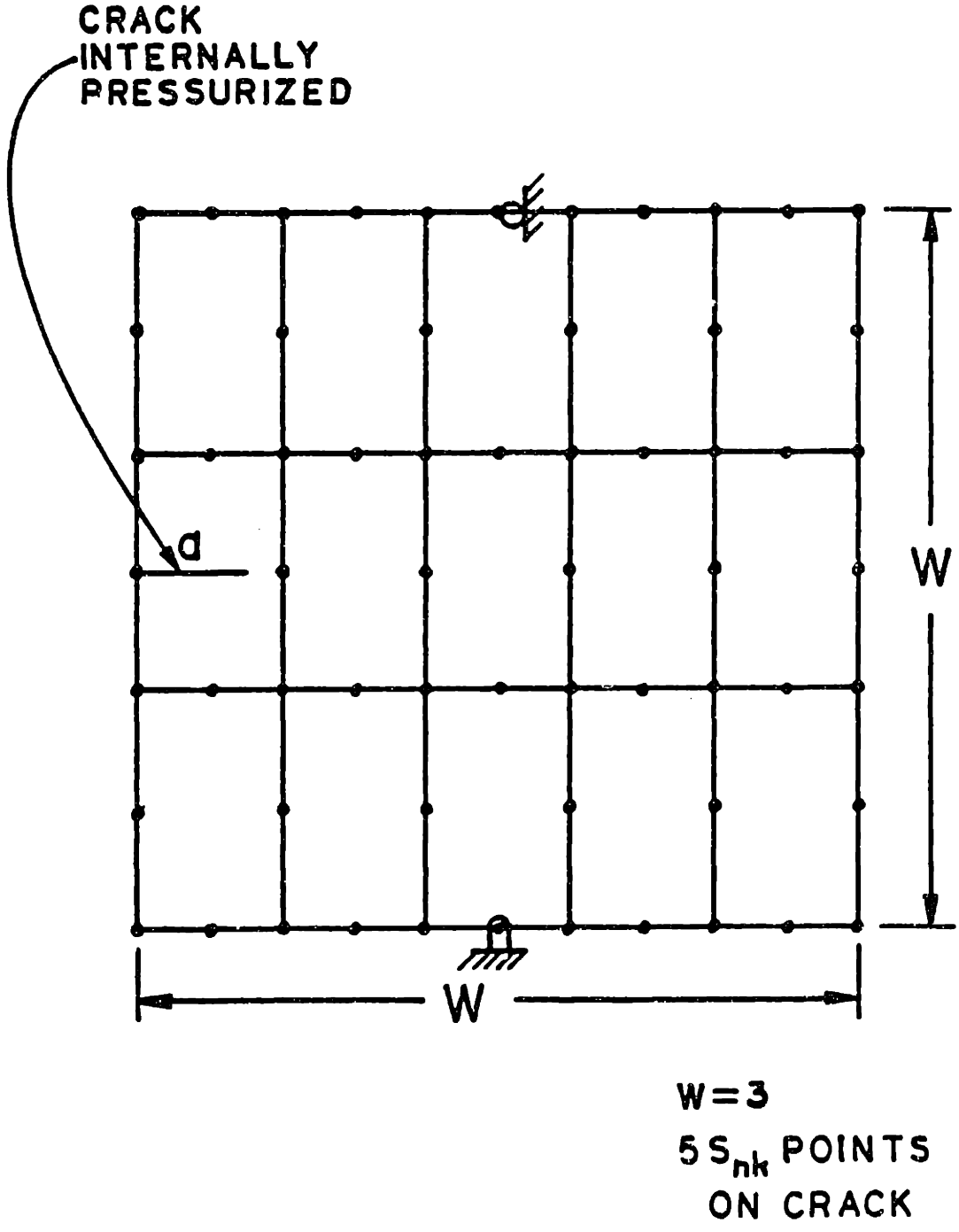

Figure 3.8 Single Edge Notched Specimen

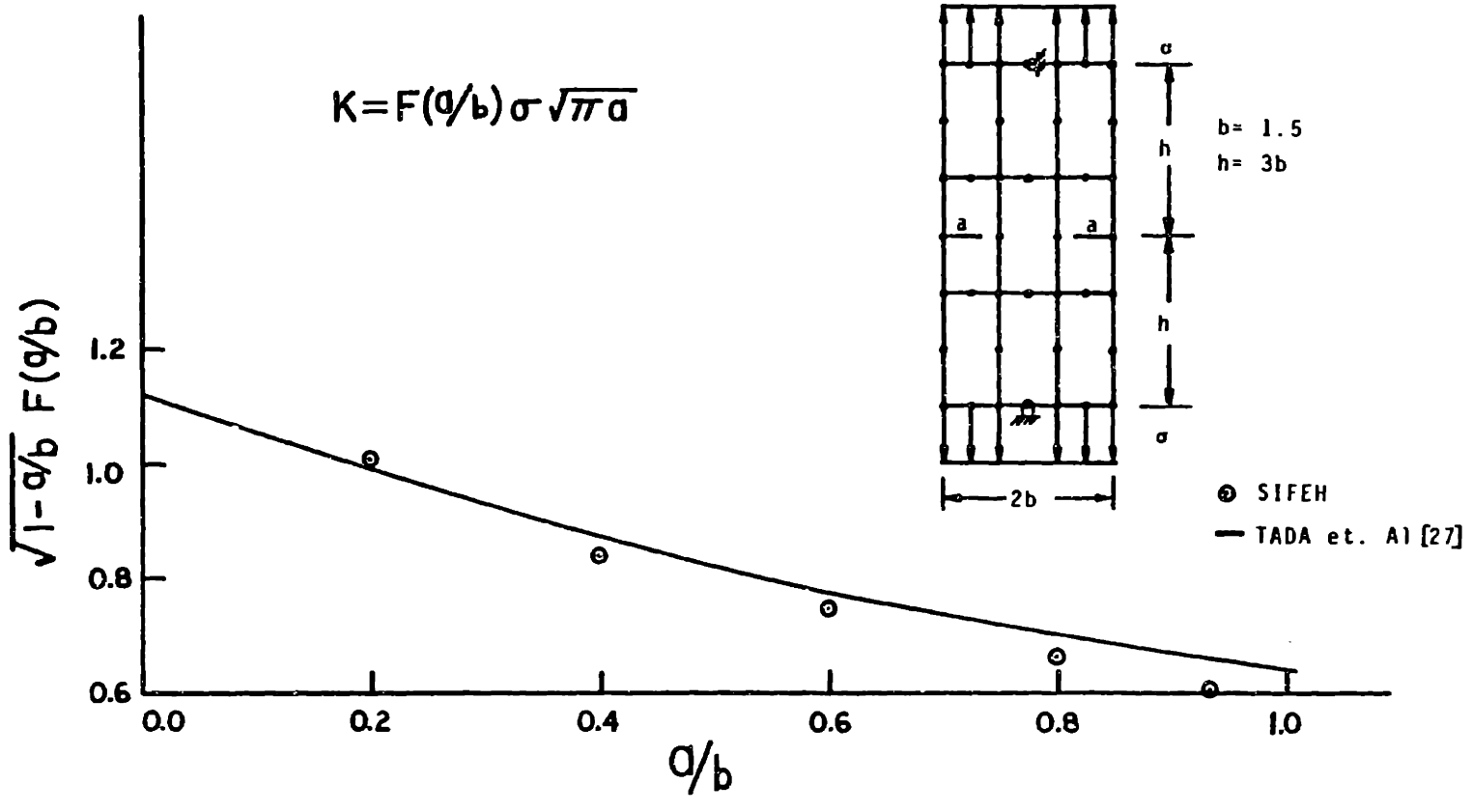

Figure 3.9 Double edge notched specimen

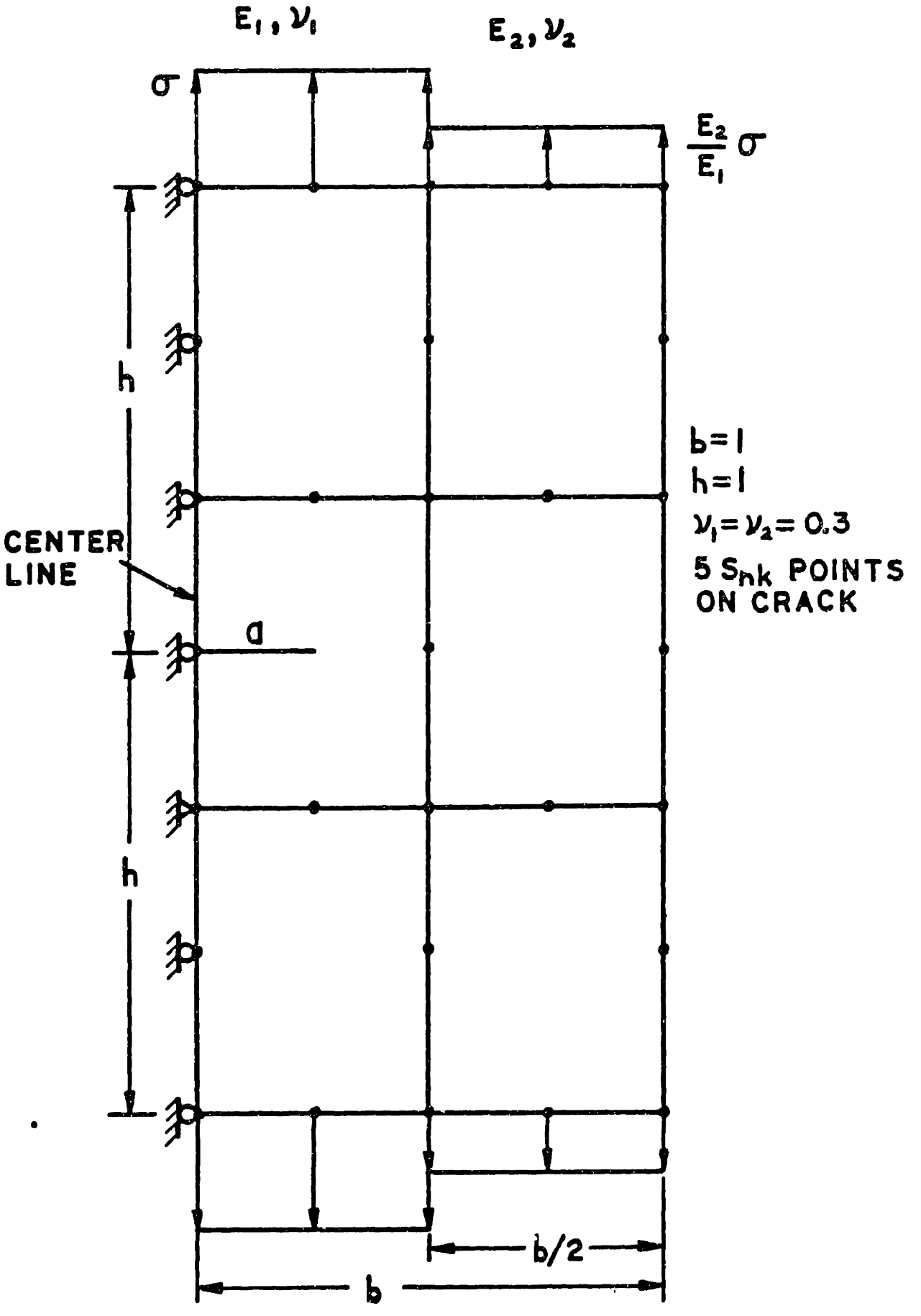

Figure 3.10 Center crack in a bi-material panel

CHAPTER 4

QUASI-STATIC FRACTURE PROPAGATION

4.1 GENERAL DISCUSSION

As has been already described in Chapter 1, this SIFEH method was developed out of necessity for effectively modelling fracture and it is appropriate to underscore that the method has its most significant application for fracture propagation. In the SIFEH model the finite element discretization has to be adequate only to capture the $R-R^c$ field which is much well behaved than if the finite elements were expected to model the singular fields at the crack tip. The crack can penetrate "through" the finite elements which is one of the major advantages in this formulation. The development presented here is within the bounds of linear elastic fracture mechanics (LEFM) with quasi-static propagation (i.e. no dynamic effects). Quasi-static propagation dictates, for instance, having a test machine which is very stiff so that dynamic effects are minimized. It is important to note that fracture mechanics has one additional aspect aside from continuum assumptions, and that is the length of the crack. If the plastic zone at the crack tip is small compared to the length of the crack and other dimensions of the finite body (47) then small scale yield (s.s.y) conditions exist and LEFM can be used satisfactorily to model the fracture. The extent of the plastic zone are given by [27,47]:

$$\begin{aligned} r_p &= (1/3\pi)\ (K/\sigma_o)^2\ , \text{for plane strain.} \\ r_p &= (1/\pi)\ \ (K/\sigma_o)^2\ , \text{for plane stress.} \end{aligned} \tag{4.1}$$

$$r_p = (\pi/8)\ (K/\sigma_o)^2 \text{ , for Dugdale model.}$$

where r_p = Extent of the plastic zone as shown in figure 4.1 [27,47].

σ_o = Tensile yield stress for the material.

In typical structures (e.g. aerospace structures etc.) the study of the propagation of cracks is usually in the context of low cycle fatigue (LCF) life prediction or damage tolerant design where the aim is avoidance of growth of cracks beyond a critical size. For resource extraction applications the intent is to grow fractures in underground reservoirs by hydraulic fracturing. Quasi-static fracture propagation in infinite domains has been effectively modelled using the surface integral method [35] and at present the SIFEH method developed in this research is being applied for modelling hydraulic fracturing of laboratory specimens to study effects of finite boundaries on the propagation path [35].

4.2 CRITERIA FOR PROPAGATION

Various criteria for mixed mode crack propagation can be found in the fracture mechanics literature; in particular a good discussion is provided in [13]. Viewing the fracture process within the context of continuum mechanics and LEFM, propagation occurs when some parameter (e.g. stress intensity factor, strain energy, energy release rate etc.) reaches or exceeds a critical value of the same parameter for that material. A brief discussion of the various propagation criteria is given below; additional details can be found in [13].

4.2.1 THE MAXIMUM CIRCUMFERENTIAL STRESS THEORY

This theory proposes that crack propagation will occur when the stress intensity factor reaches a critical value [54]. The maximum stress and the associated direction is given by (using polar co-ordinates):

$$\frac{\sigma_{\theta\theta}\sqrt{2\pi r}}{K_{Ic}} = 1 = \cos\frac{\theta_o}{2}\left[\frac{K_I}{K_{Ic}}\cos^2\frac{\theta_o}{2} - \frac{3}{2}\frac{K_{II}}{K_{Ic}}\sin\theta_o\right] \tag{4.2}$$

$$\sigma_{r\theta} = 0 = \cos\frac{\theta_o}{2}\left[K_I\sin\theta_o + K_{II}(3\cos\theta_o - 1)\right] \tag{4.3}$$

The angle can be found from (4.3):

$$K_I\sin\theta_o + K_{II}(3\cos\theta_o - 1) = 0 \tag{4.4}$$

Using trigonometric identities:

$$\sqrt{1 - \cos^2\theta_o} = -\frac{K_{II}}{K_I}(3\cos\theta_o - 1) \tag{4.5}$$

Using $\cos\theta_o = t$ and $\frac{K_{II}}{K_I} = \alpha$ and squaring, equation (4.5) becomes:

$$1 - t^2 = \alpha^2(9t^2 - 6t + 1) \tag{4.6}$$

or, $$(9\alpha^2+1)t^2 - 6\alpha^2 t + (\alpha^2 - 1) = 0 \tag{4.7}$$

Solving the quadratic equation,

$$t = \frac{6\alpha^2 \pm \sqrt{36\,\alpha^4 - 4(9\alpha^2 + 1)(\alpha^2 - 1)}}{2(9\alpha^2 + 1)} \tag{4.8}$$

$$\theta_o = \cos^{-1}\left[\frac{6\alpha^2 \pm \sqrt{4 + 32\alpha^2}}{2(9\alpha^2 + 1)}\right] \qquad (4.9)$$

This criterion proposes that the crack propagation occurs along a radial direction and in a plane along the direction θ_o as given by equation (4.9) when K reaches a critical value as given by equation (4.2).

This criterion for propagation has been implemented in the computer program as this is physically more appealing. There are other criteria given below which could also be implemented in the computer program very easily.

4.2.2. THE MINIMUM STRAIN ENERGY DENSITY THEORY

This theory proposes that fracture will occur in a radial direction where the strain energy density is the minimum [55]. The angle θ_o at which propagation occurs is given by:

$$\frac{\partial S}{\partial \theta} = 0, \quad \frac{\partial^2 S}{\partial \theta^2} > 0 \qquad (4.10)$$

S = Strain energy density.

Crack propagation occurs when $S(\theta_o)$ reaches a critical value S_c. Other details can be found in [55] and [13].

4.2.3 THE MAXIMUM ENERGY RELEASE RATE THEORY

This theory proposes that the crack extension will occur in the direction along which the strain energy release rate G per unit of crack extension is maximum. Crack propagation occurs when the energy release rate reaches a

critical value G_c.

$$G = \frac{1}{\bar{E}} (K_I^2 + K_{II}^2) \qquad (4.11)$$

$\bar{E} = E/(1 - \nu^2)$ for plane strain

$\bar{E} = E$ for plane stress

The value of θ_o along which crack propagation occurs can be found from:

$$\frac{\partial G}{\partial \theta} = 0 \quad \frac{\partial^2 G}{\partial \theta^2} < 0 \qquad (4.12)$$

Other theories that use the J integral are discussed in [13]. It should be noted that the minimum strain energy or the maximum energy release rate theory should be applied for those angles for which the Mode I stress intensity factor K_I is positive, as negative K_I would mean interpenetration of the crack surfaces.

4.3 IMPLEMENTATION OF THE MAXIMUM CIRCUMFERENTIAL STRESS THEORY

The basic method of modelling evolution of fractures or (non-opening) shear bands is based on propagating the crack or shear band a certain distance and then determining the load required to keep the propagation quasi-static. Consider a finite domain with a system of cracks: "probes" or branch cracks are inserted at each tip (Refer to figure 4.2) in turn and certain sensitivities are determined. Then for a given load increment (decrement) the increase in the

length of the crack is determined. The propagation is performed automatically in the computer program. User inputs include a fixed length or a percentage length (percentage of the wing length) for the probe and the direction of propagation is computed using the following two methods:

4.3.1 PROPAGATION BASED ON THE STATE OF STRESS AT THE PRESENT CRACK TIP

This option is based on propagating at an angle as given by equation (4.9) in section 4.2.1. The angle given by equation (4.9) is valid in the infinitesimal sense. The probe length for the propagating crack should be small enough so that equation (4.9) is applicable; however the probe length should be large enough so as to keep computer costs down. Experience indicates that a probe length of around 10% to 15% of the main wing length is adequate for the problems that have been analyzed. The following procedure is adopted for this method:

1. Insert a probe of length L_p (modelled by additional dislocations) at the end of a wing at the angle θ_o given by equation 4.9. The probe is modelled as part of the main wing but can also be modelled as a branch wing. (Modelling the probe as part of the main wing has been determined to be more accurate numerically and is in the current version of the computer program).

2. Compute the increase or decrease in load required to drive this wing with the probe to K_{Ic} (fracture toughness for the material). Compute $\left[\frac{L_p}{\Delta R}\right]_i$ where:

L_p = Length of the probe.

ΔR = Increment or decrement in load required to keep the propagation quasi-static.

i = Crack wing number.

3. Remove the probe from this wing.

4. Repeat steps 1,2 and 3 for all the wings.

5. Compute the increment in the wing length L_{p_i} (for all the N wings) for a given increment (decrement) in load, as follows:

$$L_{p_i} = \left(\frac{L_p}{\Delta R}\right)_i \Delta R \quad , i = 1, \ldots N \qquad (4.13)$$

Usually, $$\Delta R = \max|\Delta R_i| \quad , i = 1, \ldots N \qquad (4.14)$$

6. Insert probes of lengths L_{p_i} at all the wing tips.

This option for crack propagation is economical as iterations are not required to determine the angles of propagation. However, this method is not realistic for propagation of shear bands: Since for pure mode II (i.e. $K_I=0$) the angle predicted by equation (4.9) is -70.5° and the shear band will branch at this angle at every time step. The second method given below can be used for cracks and shear bands and has also been incorporated in the computer program.

4.3.2 PROPAGATION BASED ON $K_{II} = 0$ AT THE TIP OF THE PROBE

This method has been used successfully in modelling propagation of cracks in an infinite domain, using the surface integral method [35]. The following procedure is adopted for this method.

1. Insert a probe of length L_p at the end of a wing along the local tangent at the tip.

2. Compute the stress intensity factors K_I and K_{II} at the tip of the probe. If $K_{II} = 0$ (i.e. less than a small tolerance) no further calculations are necessary, proceed to step 5.

3. Rotate the probe at the wing tip and determine a range of angles within which K_{II} changes sign.

4. Use "Regula Falsi" procedure with interval halving [58] to find the angle θ_i (for the wing i) at which $K_{II}=0$.

5. Compute the ratio $\left(\frac{L_p}{\Delta R}\right)_i$ for this wing.

6. Remove the probe for this wing.

7. Repeat steps 1 through 6 for all the wings.

8. Compute the increment in wing length L_{p_i} (for all the N wings) for a given increment (decrement) in load, as per equations 4.13 and 4.14.

9. Insert probes of lengths L_{p_i} at all the wing tips.

This option is more expensive as iterations are necessary to determine the direction for which $K_{II} = 0$.

4.4 RESULTS FOR LINEAR ELASTIC FRACTURE PROPAGATION

Results for propagation of internal and surface cracks for plane strain conditions are given below.

4.4.1 PROPAGATION OF INTERNAL CRACKS

Two mixed mode fracture problems (refer to figures 4.3 and 4.4) have been analyzed. The finite element and surface integral discretization, the dimensions of the plates and orientation of the cracks are as shown in the figures. The results of the propagation paths predicted by SIFEH analysis based on the theory presented in section 4.3.1 agreed very well with known experimental results published in [46,56,57]. The experimental tests were performed for fatigue loading of titanium Ti-6Al-4V specimens containing these oblique center-cracks at 45° and 30° respectively. Material parameters were [46,56,57,13]:

$$\begin{aligned} E &= 16000 \text{ ksi} \\ \nu &= .33 \\ K_{Ic} &= 75 \text{ ksi} - \text{in}^{1/2} \end{aligned} \qquad (4.15)$$

Growth of fatigue cracks can be explained in terms of initiation (Stage I), steady growth (Stage II) and rapid failure (Stage III) (Consult reference [13] for further details). It is the steady growth that can be modelled, for example, by the Paris equation:

$$\frac{da}{dN} = C(\Delta K_{eff})^{n} \qquad (4.16)$$

Where,

a = Length of crack.

N = Number of cycles.

C,n = Material constants.

(ΔK_{eff}) = The range of effective stress intensity factor. (ΔK_{eff}) is a function of the range of the mode I (K_I) and mode II (K_{II}) stress intensity factors [13]. Note that there is a $\Delta K_{THRESHOLD}$ below which fatigue propagation does not occur. Also note that $\Delta k = F_c \Delta\sigma\sqrt{\pi a}$ where F_c is the correction factor due to finite boundaries and a is half the crack length for an internal crack or crack length for a surface crack; $\Delta\sigma$ is the stress range.

To further investigate fatigue propagation it was desired that the ΔK_I and ΔK_{II} as obtained in the elastic stress analysis using the SIFEH formulation should be correlated to the same quantities as was done in [46] and [13]. (In Reference [13] the same problem was analyzed using the BIE method). These results are presented in Tables 4.1 and 4.2 (for the 45° crack) and the ΔK_I and ΔK_{II} ranges of Pustejovsky's analysis are obtained from [46]. Pustejovsky gave these results in the form of a plot; while these were tabulated in [13] using an incorrect stress range of 27 ksi. instead of the 22.5 ksi. used in the actual experiments [46]. Good agreement of SIFEH and Pustejovsky's results has been obtained. Results presented in [13] for

the ΔK's were consistently higher than the results of [46]. The number of cycles to failure can be easily computed by integrating equation (4.16) once the material constants C and n of equation (4.16) can be determined from base-line fatigue data. Pustejovsky has correlated the ΔK ranges from his analysis to the crack growth da/dN for both base line and mixed mode specimens. Good agreement is shown in figure 4.5. SIFEH analysis shows good agreement with Pustejovsky's ΔK's. Hence the agreement of ΔK's to the fatigue life of the material has been established for the titanium specimens. The stress range $\Delta\sigma$ used for the 45° specimen was 22.5 ksi. (2.5-25 ksi.) and for the 30° specimen was 27 ksi. (3-30 ksi). The lower value of the cyclic stress is usually positive (tensile) so as to prevent buckling while testing. The plastic zone at the crack tip for the maximum stress of 30 ksi. was 0.01 in. [46] which was less than 10% of the specimen thickness (0.125 in. thick); thus ensuring plane strain conditions at the crack tip.

Computer CPU time required for the SIFEH and BIE (13) methods for the 45° specimen is listed in table 4.2 and table 4.3.; SIFEH analysis required considerably less time than the BIE method. The SIFEH analysis was performed on an IBM 370-3033 computer system at M.I.T., an IBM 370-168 computer was used for the BIE analysis. The IBM 370-3033 is approximately twice as fast as the IBM 370-168 (based on the number of millions of instructions per second). Pustejovsky [46] did not report the CPU time required for this problem using the dislocation superposition analysis.

The computer time for the SIFEH analysis is given for the decoupled method of solution (Refer to Chapter 5) which has been incorporated in the computer program NONSAP (62). Correlation of the ΔK's has been obtained for the 45° crack; similar correlation can be obtained for the 30° crack.

Table 4.1 Pustejovsky's results from [46] for mixed mode propagation (45^{o} crack).

Crack Increment Number	Crack Length increment Δs (in)	Lower Crack Tip ΔK_I (ksi$\sqrt{in}$)	Lower Crack Tip ΔK_{II} (ksi$\sqrt{in}$)	Upper Crack Tip ΔK_I (ksi$\sqrt{in}$)	Upper Crack Tip ΔK_{II} (ksi$\sqrt{in}$)
1	0.0118	19.01	2.55	18.99	0.61
2	0.0161	20.06	0.49	19.65	0.06
3	0.0318	21.11	0.17	20.70	1.16
4	0.0263	21.97	0.58	21.63	1.39
5	0.0318	23.08	0.41	22.85	0.20
6	0.0145	23.57	1.02	22.09	4.59
7	0.0196	23.95	1.74	22.50	4.79
8	0.0496	25.57	0.12	25.35	0.49
9	0.0216	26.19	0.06	25.84	1.83
10	0.0255	26.83	1.77	26.65	1.45

* Note: $\Delta K = \Delta\sigma\, k\sqrt{\pi}\,\sqrt{\ell}$, where ℓ = initial length of the crack (0.53 in.), k's are given in [46].

Table 4.2 SIFEH results for the mixed mode propagation (45^{o} crack).

Crack Increment Number	Crack Length Increment (in.)	ΔK_I* (ksi$\sqrt{in}$)	ΔK_{II}* (ksi$\sqrt{in}$)	CPU Time (Seconds)
1	0.0265	21.24	1.66	2.55
2	0.0291	20.58	2.60	3.57
3	0.0320	23.16	2.40	4.82
4	0.0352	22.55	2.65	6.33
5	0.0387	24.76	0.18	8.12
6	0.0426	26.37	0.15	10.10
7	0.0469	27.99	0.25	12.34
TOTAL				47.83

* Note: Symmetric boundary conditions and the method of crack propagation resulted in the same values for both crack tips.

Table 4.3 BIE [13] results (CPU time) for the mixed mode propagation (45^{o} crack).

Crack Increment Number	Crack Increment Length (in.)	CPU Time (Seconds)
INITIAL	-	15.98
1	0.09	59.66
2	0.09	73.06
3	0.09	87.66
4	0.09	104.36
TOTAL		340.72

4.4.2 PROPAGATION OF SURFACE CRACKS

The SIFEH method has also been sucessfully applied to a concrete beam with a surface crack (Refer to figure 4.6). The analysis was performed by Daniel Wium of the Civil Engineering Dept. at M.I.T. and he has extended this method to model the nonlinear traction transfer across the crack faces in concrete [59]. The finite element and surface integral discretization is as shown in figure 4.6. Propagated path predicted by the SIFEH analysis (Refer to figure 4.7) is in excellent agreement with experimental results [60]. The load at which quasi-static propagation occurs were lower than the experimental loads (Refer to figure 4.8) when traction transfer was not modelled. Introducing traction transfer via a simple constitutive model improved the result and further research in understanding the traction transfer due to aggregate interlock in concrete etc. has been recommended [59].

4.4.3 PROPAGATION OF SHEAR BANDS

A shear band can be considered as a non-opening crack where there is slip (shear discontinuity) along its trajectory. Shear bands are observed in a variety of phenomena e.g.: in flow of granular material through hoppers [21,61], faults in the geophysical context [17], and in metals, polymers etc. [31,32,42]. Conditions for this localization of deformation have been discussed, for example in [30].

In this section a problem of shear band evolution in the two dimensional flow of granular material through hoppers will be analyzed. Mass flow bunkers (Refer to figure 1.2) are used to handle materials. The storage

bunker consists of a bin section and hopper section; the hopper section may be gently inclined (shallow) or steep. In either case there are conditions under which the flow of material can be continuous or intermittent, with a switch regime for the intermittent flow. It is important for the design of the bunker that the wall stresses be determined, especially during this switching regime. Experimental research reported in [61] for dense sand has shown that there is localization of deformation and formation of shear bands (rupture zones) where the displacement field is discontinuous. The observation of these rupture zones were made using radiographic techniques [61]. This problem has been modelled using the finite element method [21] where the prospective locus of the shear band was modelled by finite elements using constraints for displacements in the local normal direction and allowing for tangential slippage at the nodes; which is similar to modelling a contact problem. The disadvantage, however, is that the prospective locus has to be known a-priori and this is a limitation. The granular material was modelled [21] using various constitutive models available in the computer program ADINA [73]. The problem was also analyzed by the surface integral method (using plane elasticity) [21]. Frictional constraints along the shear band were also imposed using both these methods. A similar problem is analyzed here using the SIFEH method. The opening mode is condensed out for this shear band using standard procedures. The intent is to be able to model the evolution of the shear band. The actual problem of modelling the hopper problem can be very complex if all the features viz., constitutive model of the granular material, friction along the bin and hopper walls etc. were all to be accounted for. However, it was ascertained that the central feature of this problem was initiation and propagation of a shear band and it is this dominant behavior that is being modelled using the SIFEH method. For simplicity, a linear

elastic constitutive law has been used, and attention is concentrated on the propagation aspects assuming that initiation has already occured.

A SIFEH model of the hopper problem is shown in figure (4.9). The propagated path using the method described in section 4.3.2 and zero friction along the shear band is shown in figure (4.10); this predicted path is similar to the experimentally observed path [61]. It was found that the material on the top side of the shear band was moving to the left and vice versa, this agreed with the results of the experimental test. Experimental observations of the shear band is shown schematically in figure (4.11). Computer CPU time is given in table 4.4. Simple Coulomb friction conditions along the shear band have been modelled by imposing the shear traction to be equal in magnitude to μ times the normal traction. The propagated path as predicted by the SIFEH model for a shear band with friction ($\mu = 0.1$) showed reverse slip along the trajectory; this effect is not physically observed (thus suggesting additional features are needed in the model). Modelling nonlinear effects (material nonlinearity) outside the shear band and using constitutive laws for granular materials would probably alleviate this condition.

Table 4.4 Computer CPU time for shear band problem (coefficient of friction $\mu = 0$).

Shear Band Increment	CPU time (Seconds)
Initial	1.04
1	9.21
2	11.63
3	8.13
4	17.05
TOTAL	47.06

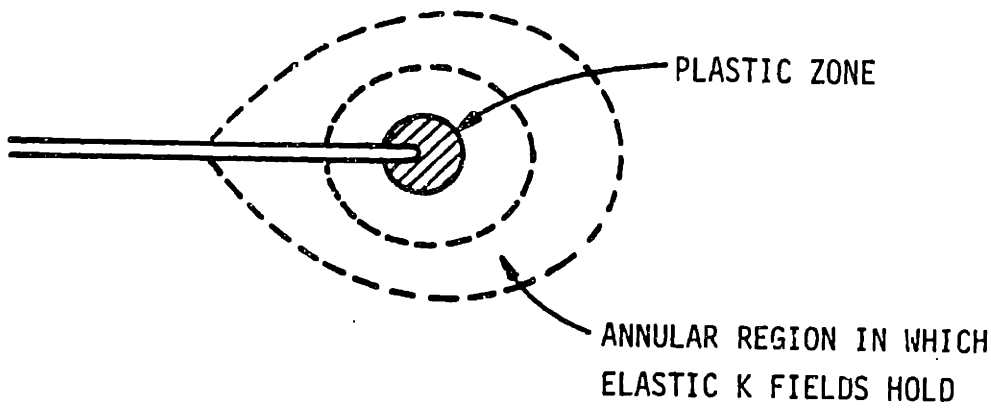

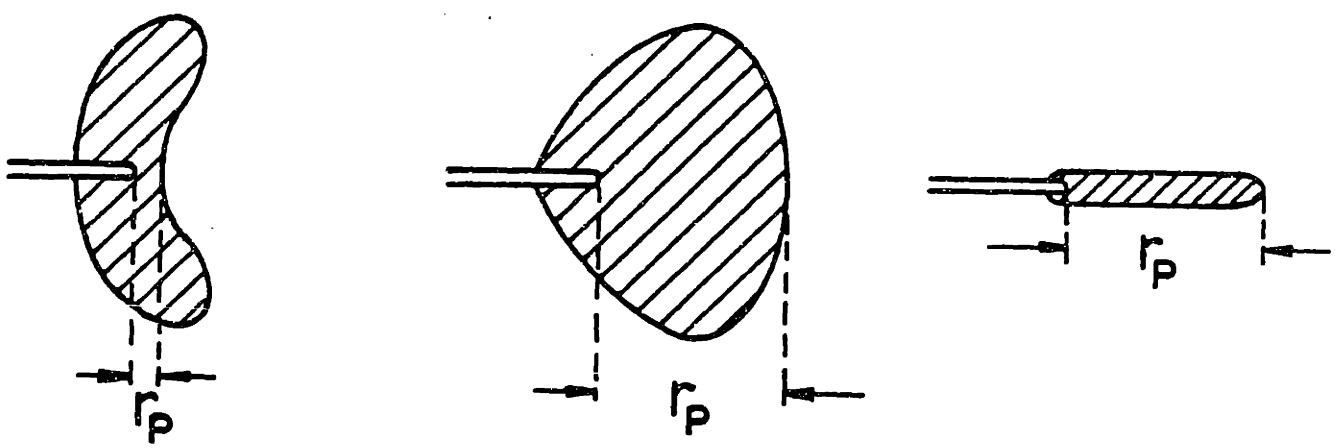

PLANE STRAIN

PLANE STRESS

PLANE STRESS
(DUGDALE MODEL)

Figure 4.1 Crack tip plastic zones for various conditions [27,47]

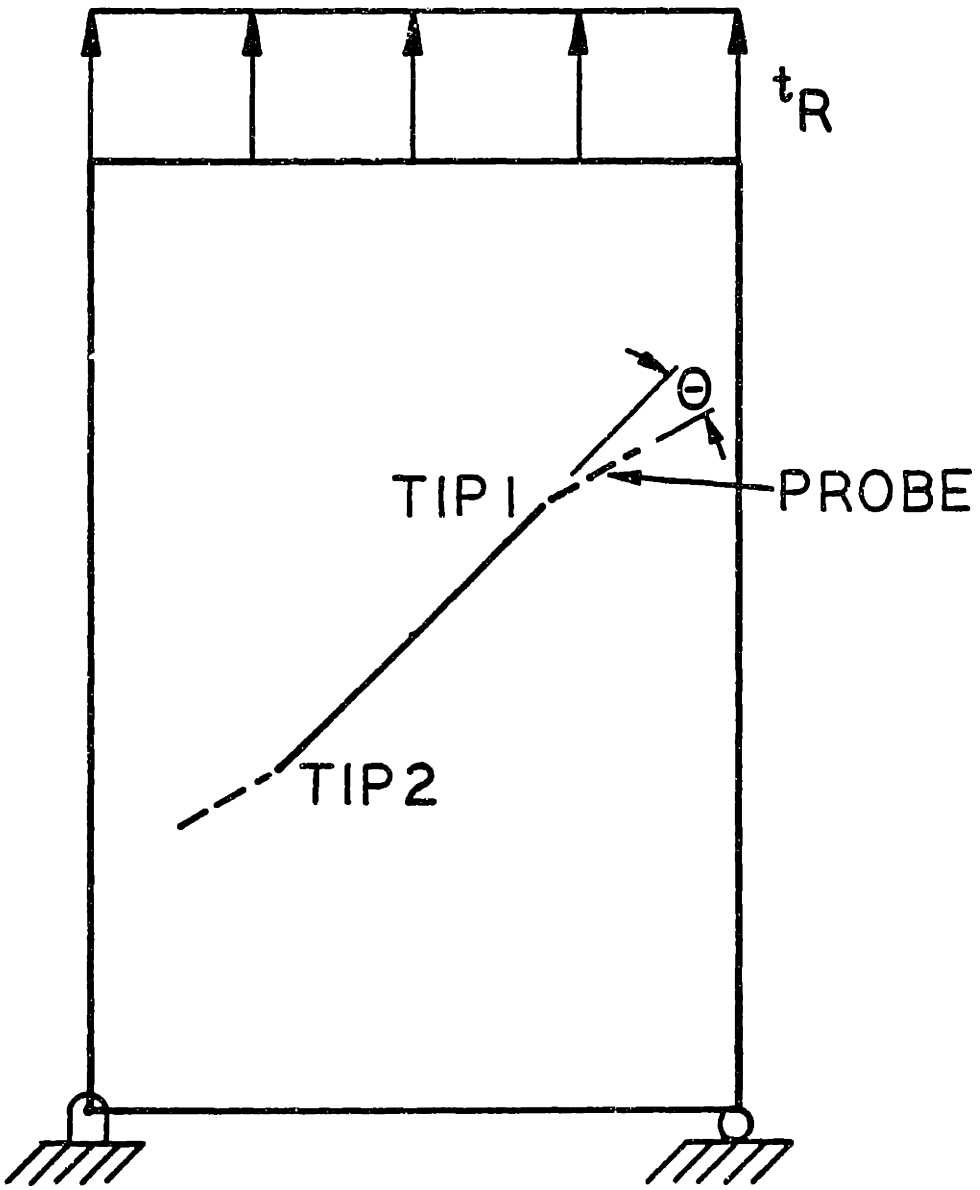

Figure 4.2 Crack propagation by use of probes

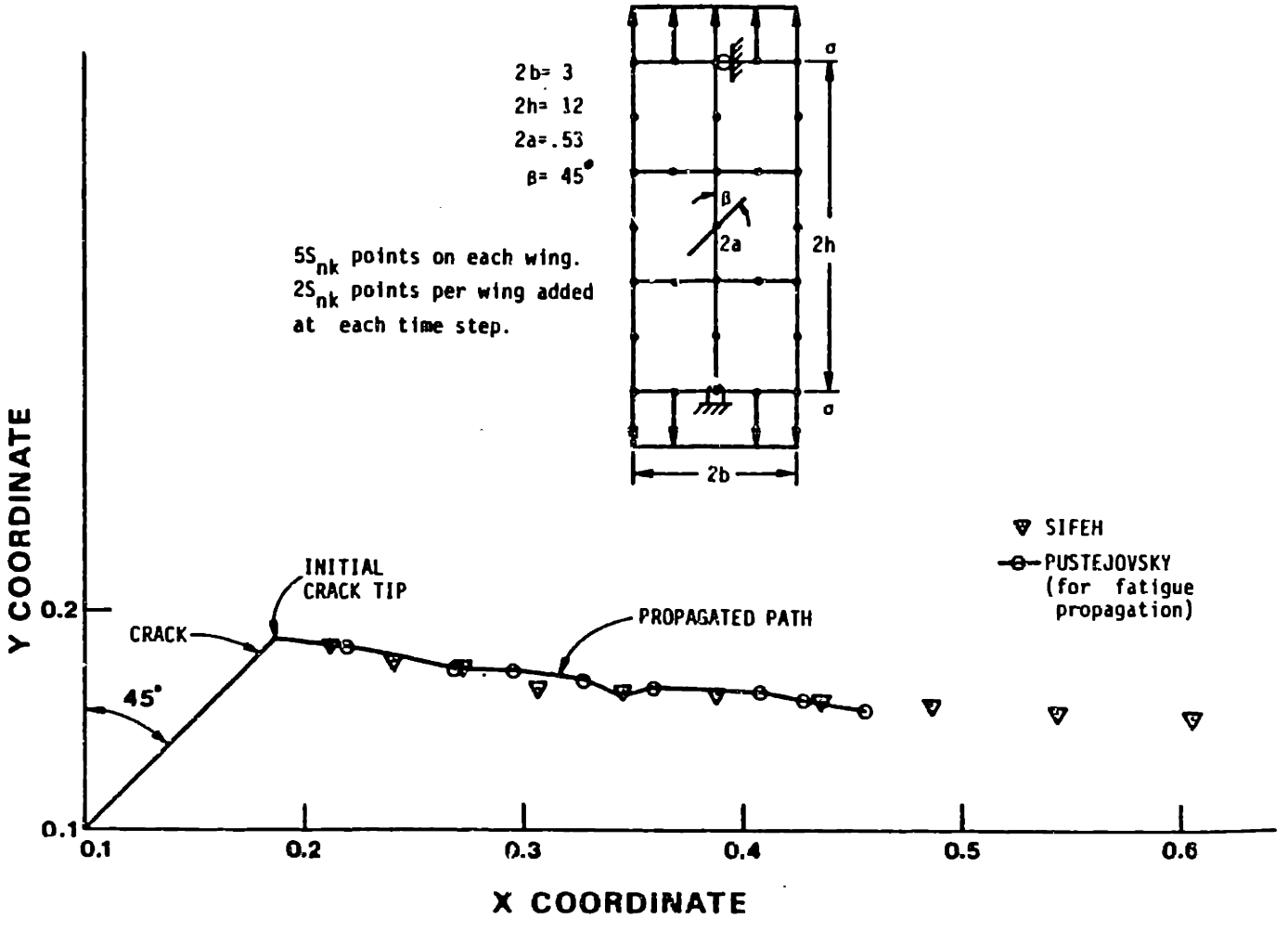

Figure 4.3 Mixed mode crack propagation in center cracked titanium specimen

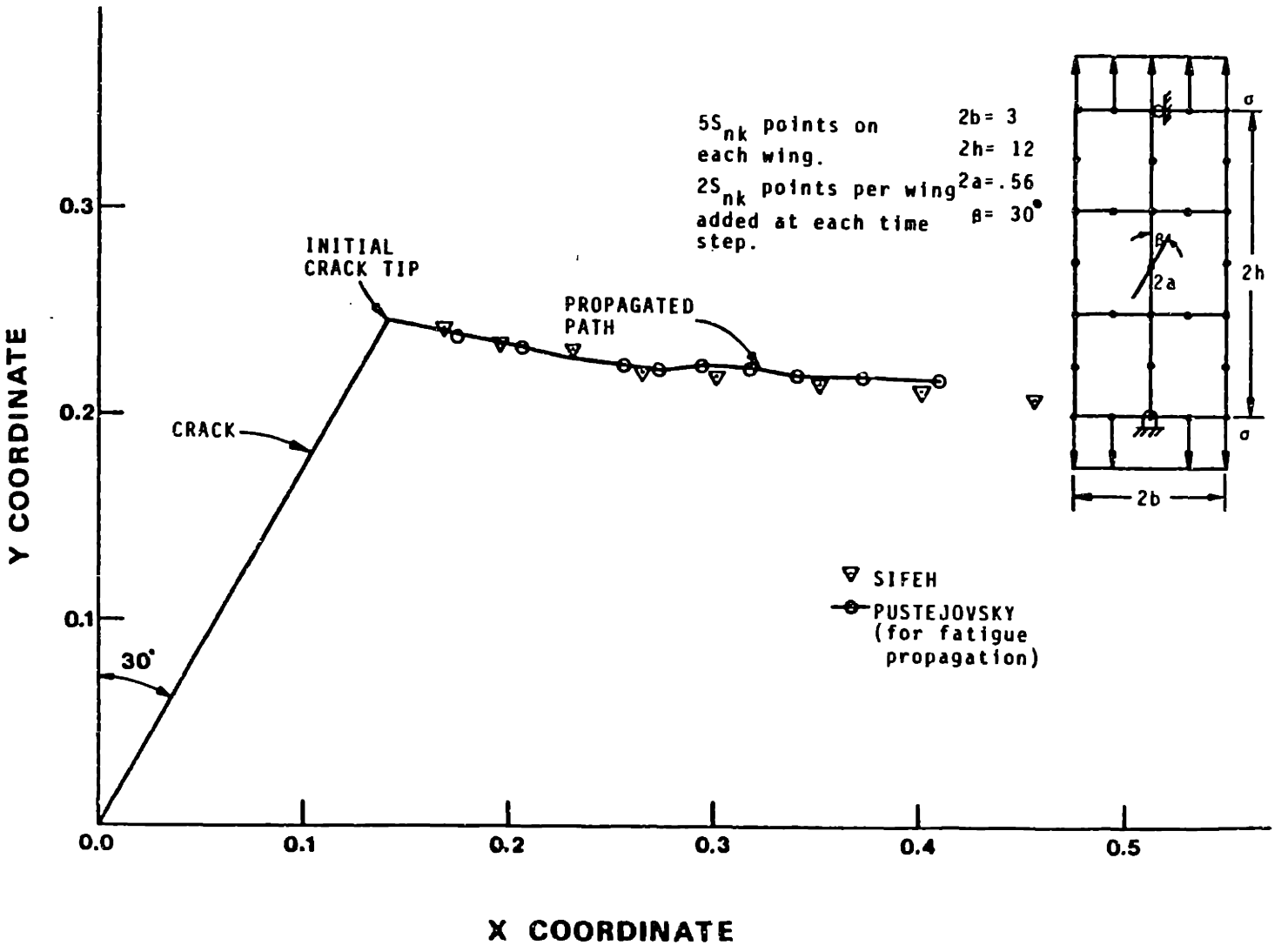

Figure 4.4 Mixed mode crack propagation in center cracked titanium specimen

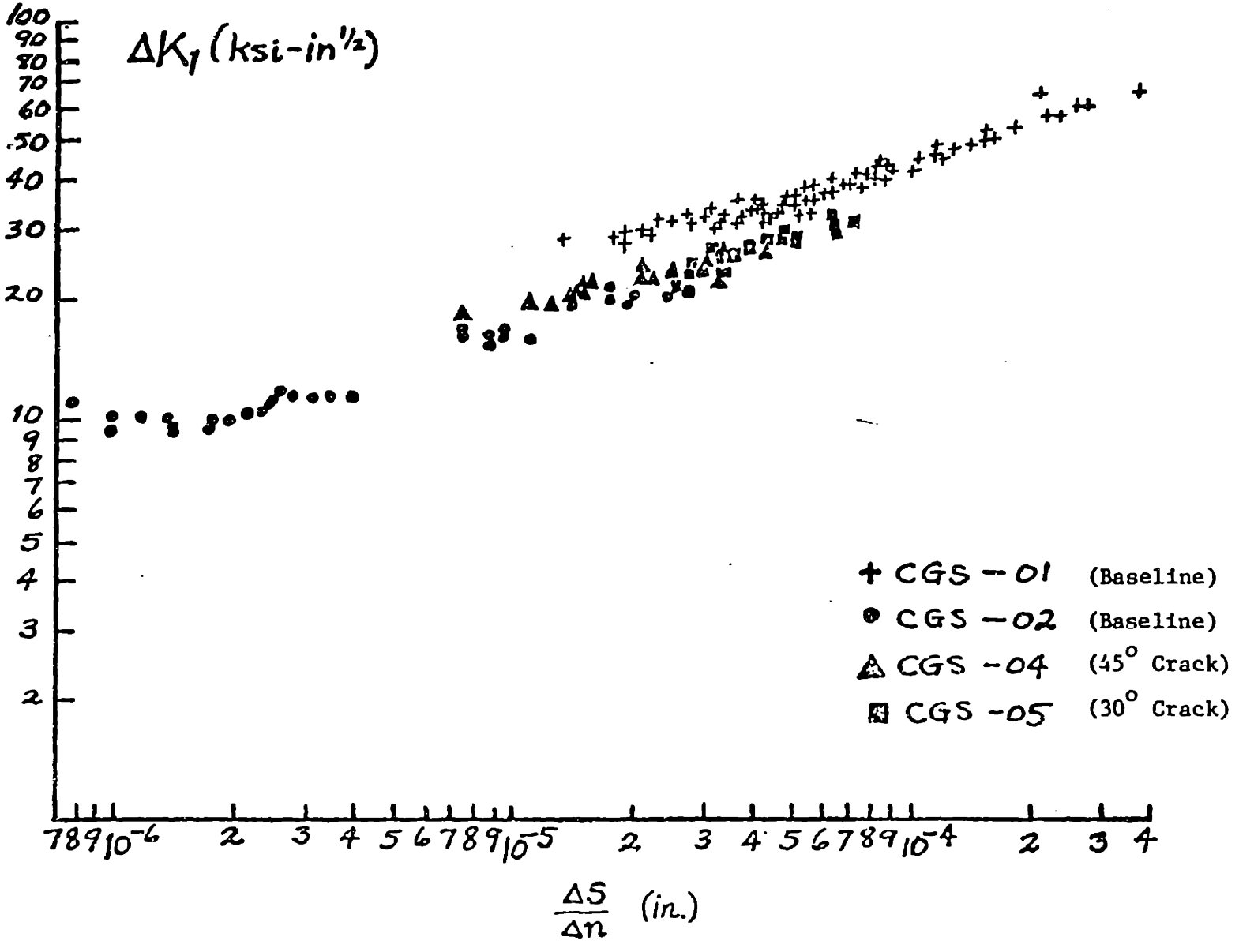

Figure 4.5 Correlation of Numerical and Experimental Results for Fatigue Crack Propagation [46]

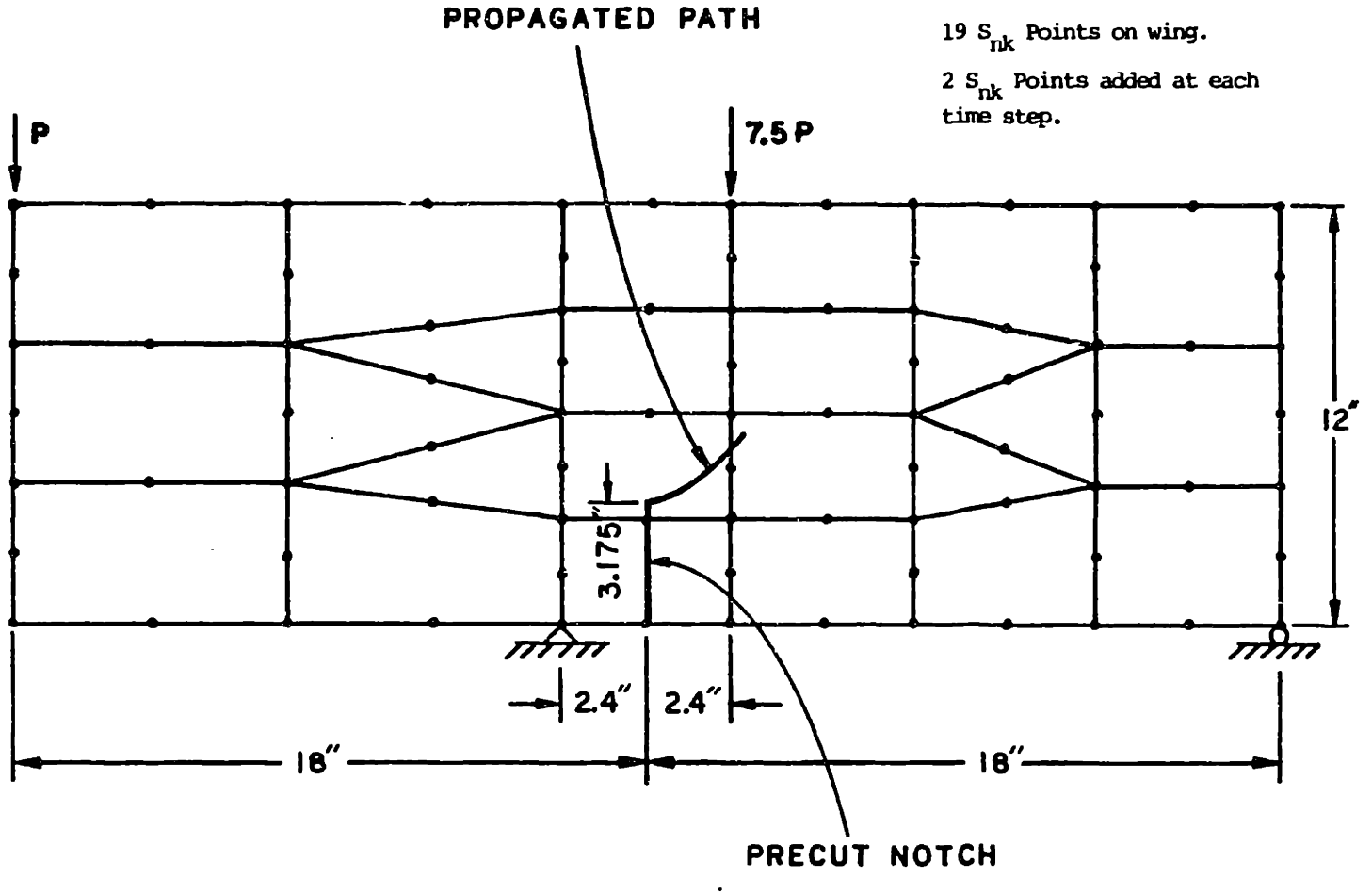

Figure 4.6 Propagation of a surface crack in a beam specimen [59]

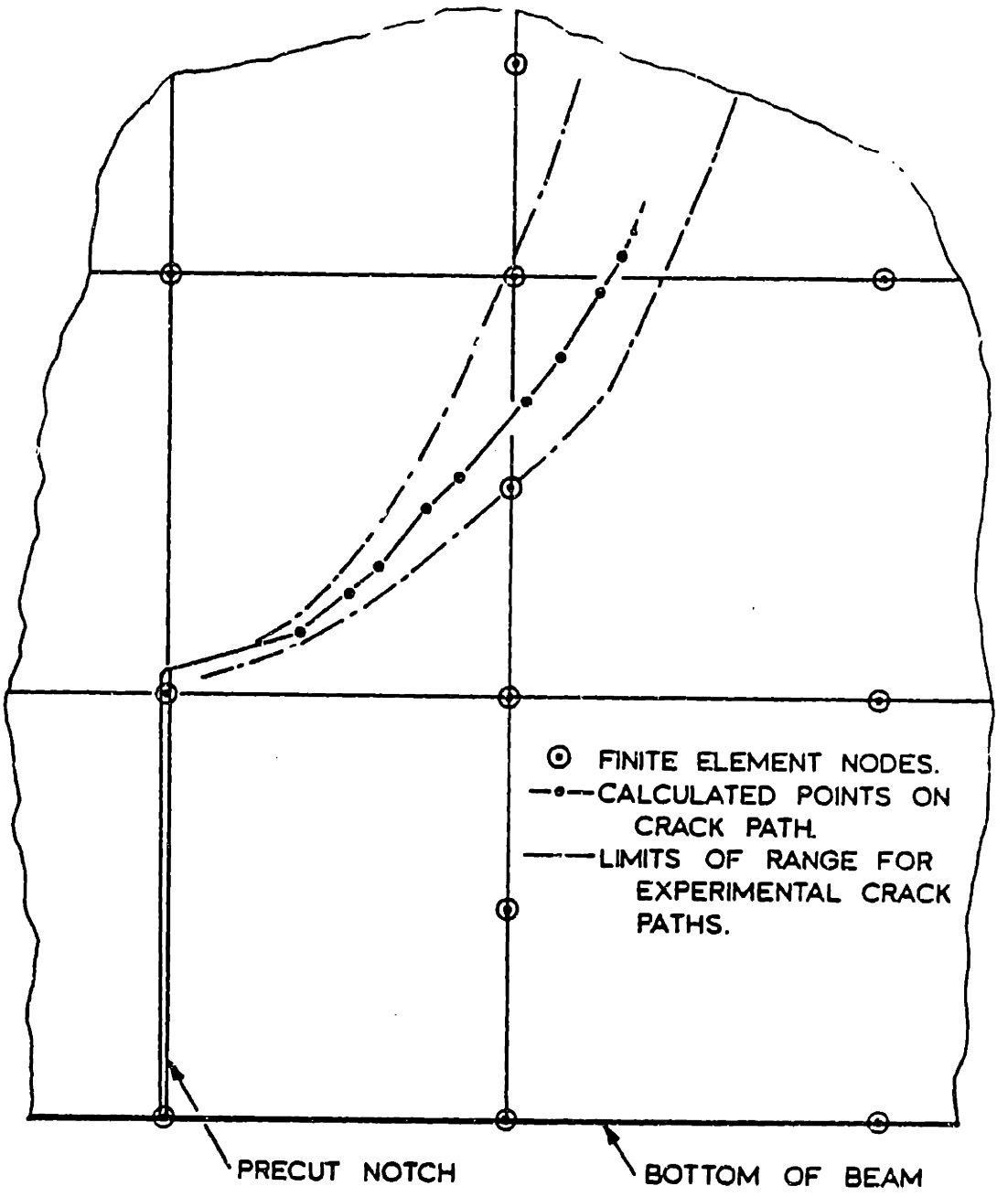

Figure 4.7 Propagated path for beam specimen [59]

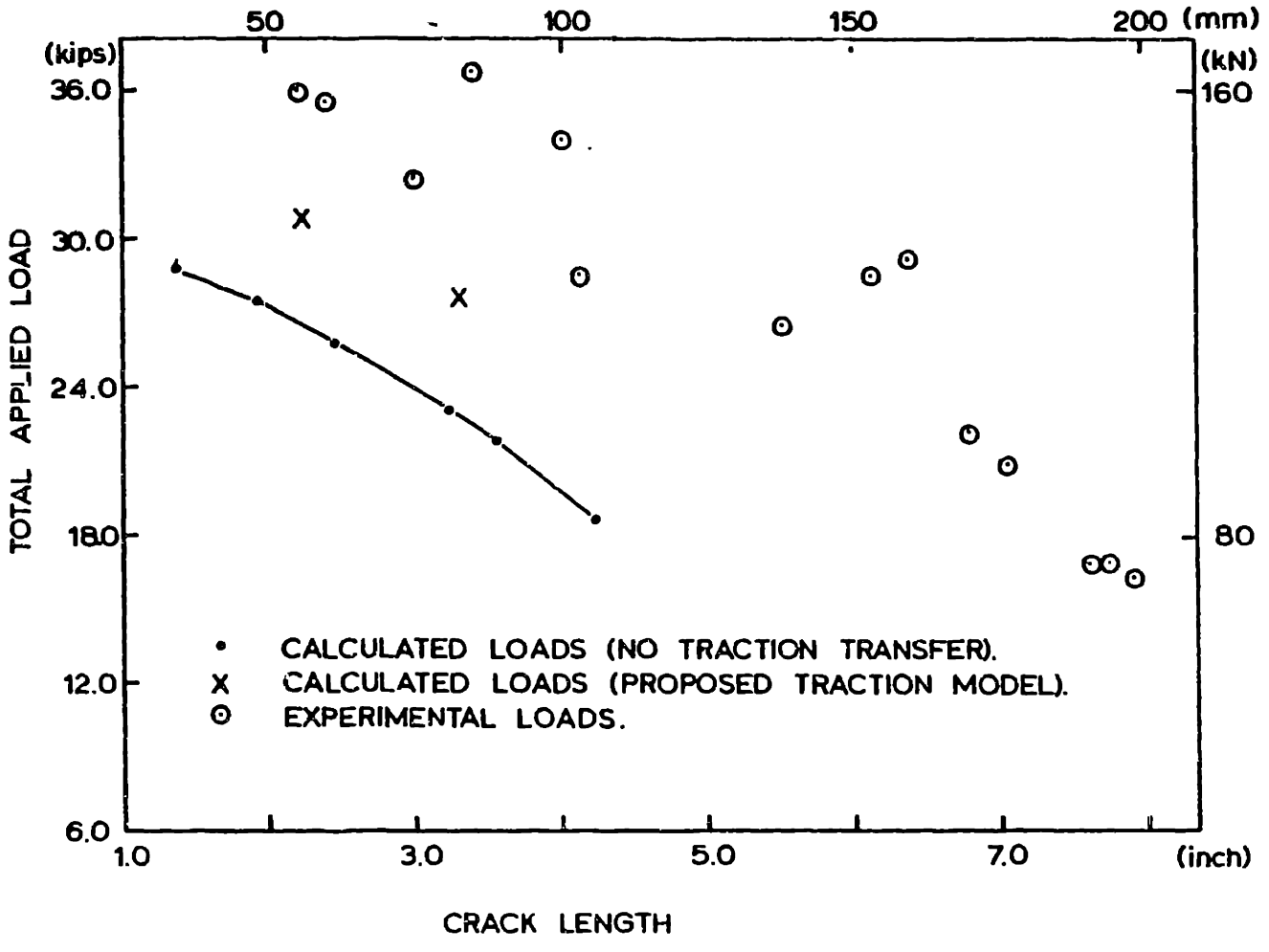

Figure 4.8 Calculated loads for beam specimen [59]

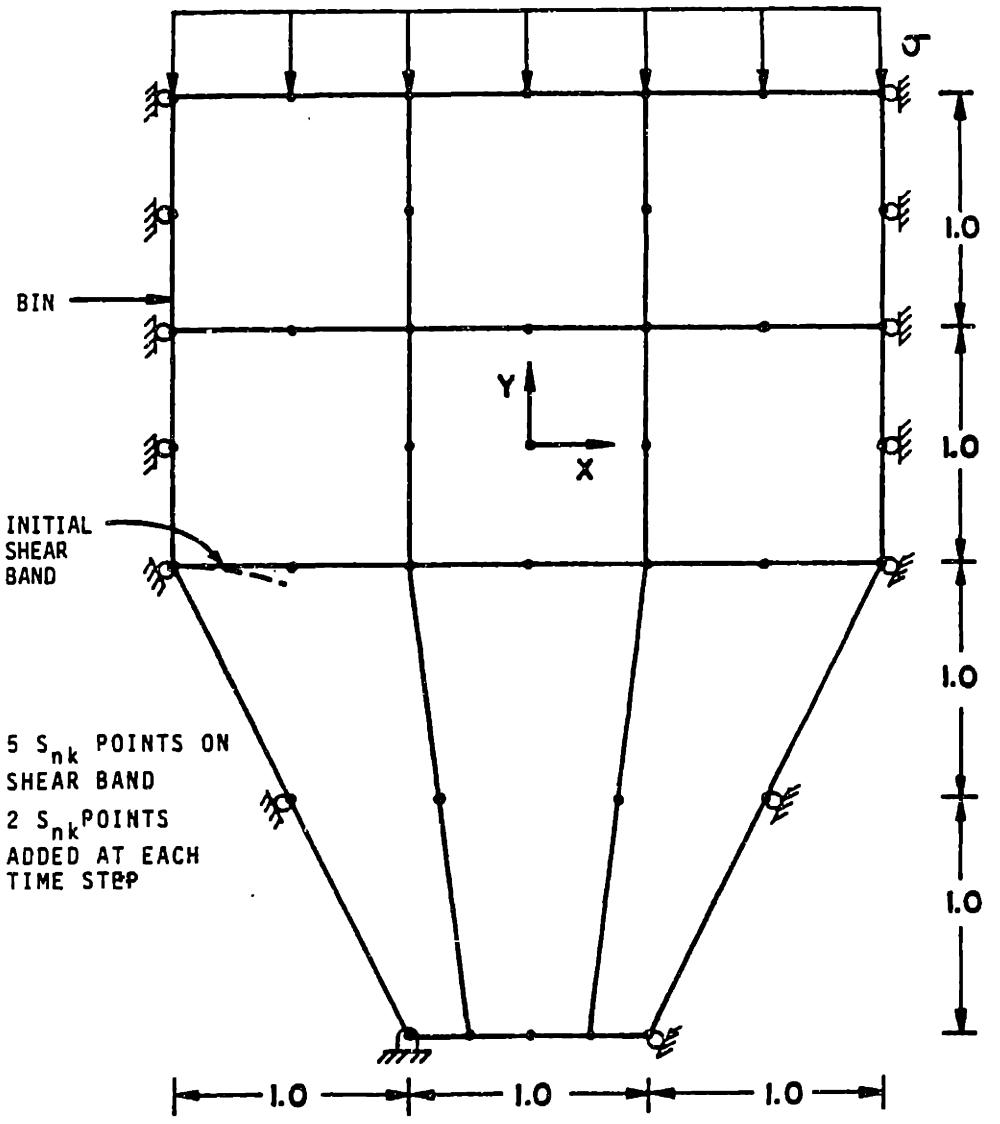

Figure 4.9 SIFEH model for flow of granular material in a hopper

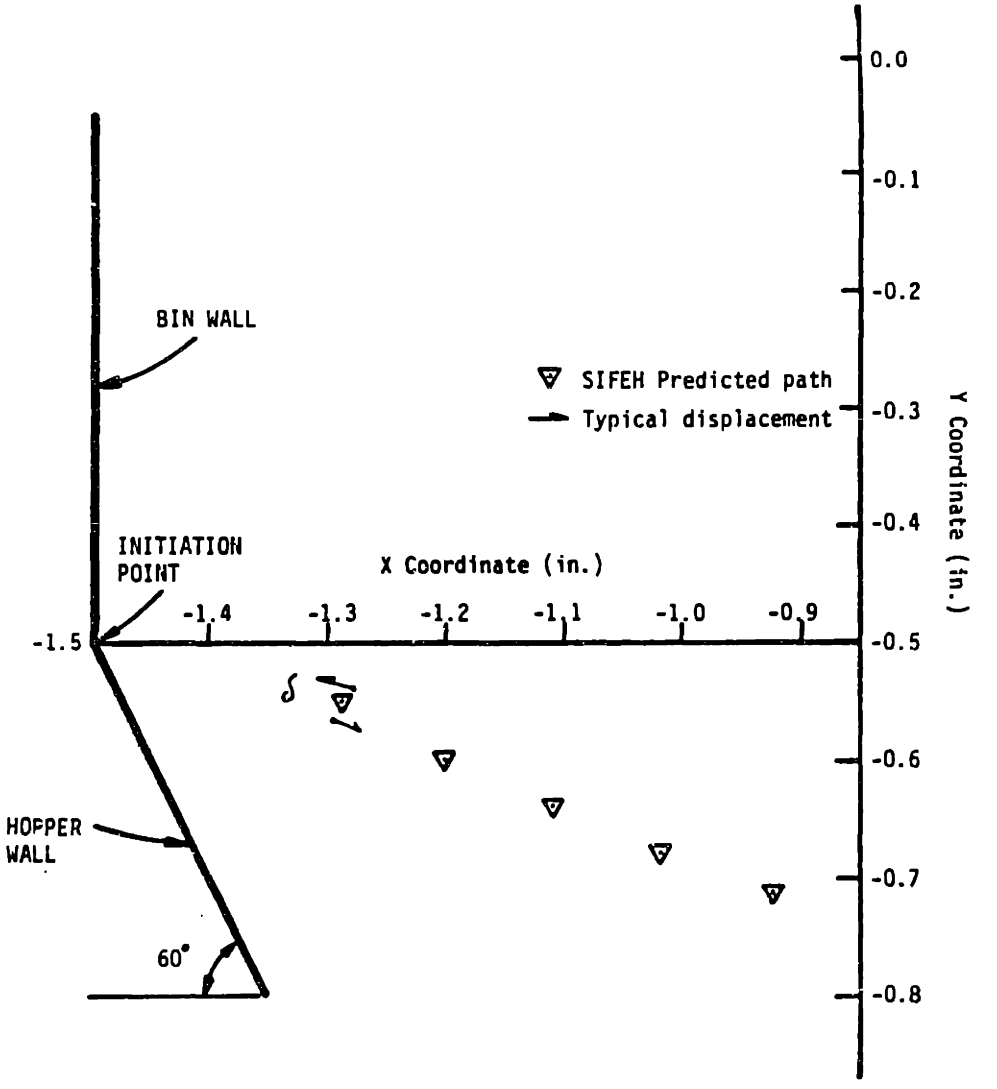

Figure 4.10 Propagation of a shear band in hopper flow (zero friction along the band)

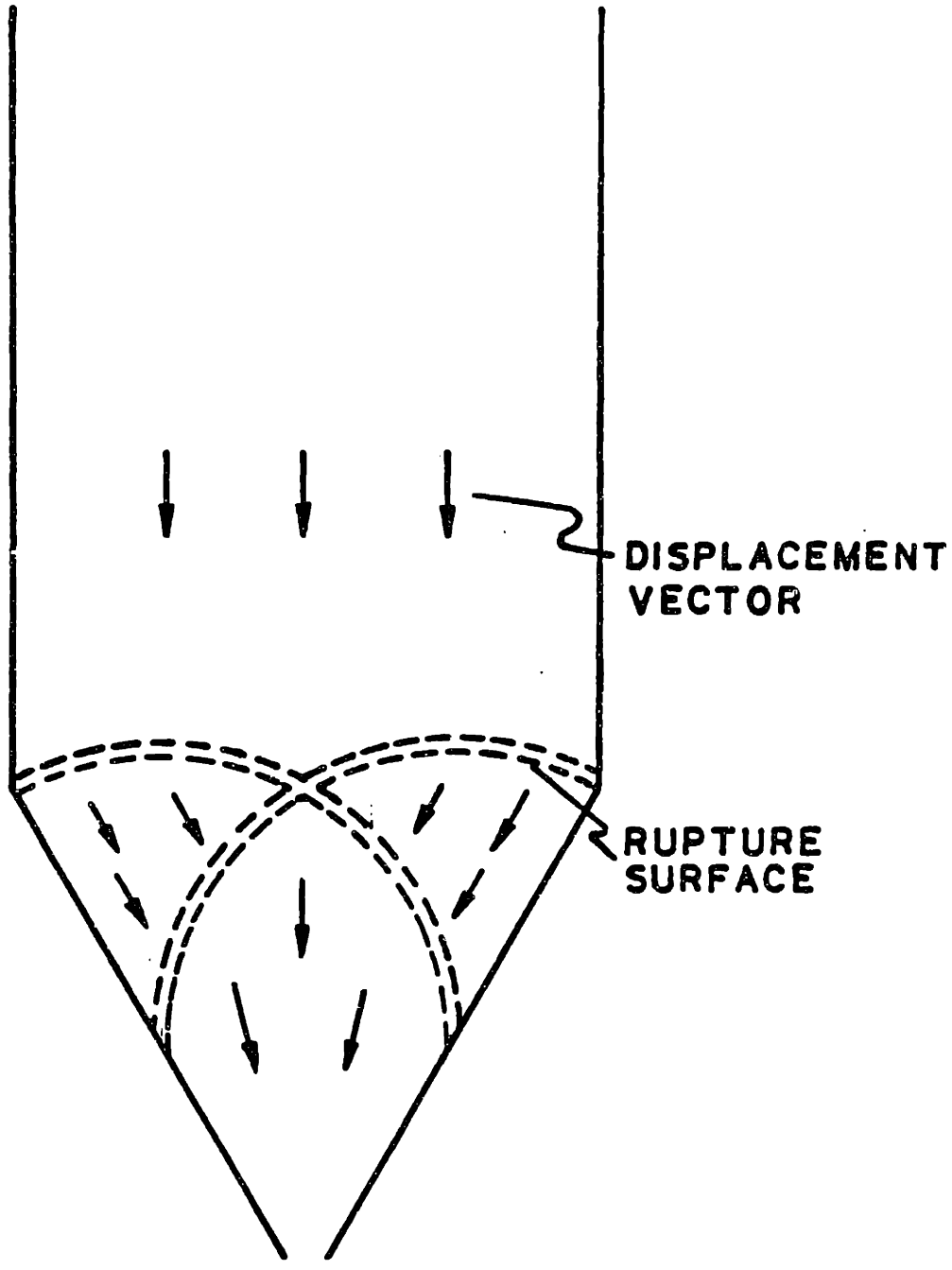

Figure 4.11 Schematic displacement field for a later increment of flow in a test on dense sand in a bunker with the walls of the hopper inclined at 60° to horizontal [61]

CHAPTER 5

FORMULATION AND IMPLEMENTATION OF THE SIFEH METHOD FOR (MATERIALLY) NONLINEAR ANALYSIS

As was discussed in Chapter 1, this SIFEH method was developed so that the best features of the surface integral and the finite element methods be utilized to be able to effectively model localized problems for linear and (materially) nonlinear continuum response.

The presence of a crack or a shear band causes intensification of the stresses and strains near the tip resulting in singularities. However, materials in reality cannot respond in this manner and the result is yielding of the material near the tip (Refer to figure 4.1). If the plastic zone is very small compared to the length of the crack and is contained by a dominant elastic stress field near the crack tip, then it is possible to define a plastic stress intensity factor which is related to the elastic stress intensity factor [63,64]. The plastic intensity factors can be obtained by either solving the governing (dominant) bi-harmonic differential equation [63] or by using the path independent property of the J integral by using paths through the plastic zone and through the far elastic field respectively [63,65]. The yielding at the crack tip has also been modelled by some researchers using shear bands at the crack tip [66,67,68,69]. However, it is the intent of the formulation presented here to also account for the far field plasticity. First, the decoupled method of solution of the governing equations for the hybrid method is presented, then the theoretical formulation for the nonlinear analysis is developed.

5.1 THE DECOUPLED SOLUTION METHOD AND IMPLEMENTATION IN NONSAP

The governing equation for the hybrid scheme is given by equation (2.14) and is given below.

$$\begin{bmatrix} K & G^* \\ S & C^* \end{bmatrix} \begin{Bmatrix} U \\ F \end{Bmatrix} = \begin{Bmatrix} R \\ T \end{Bmatrix} \tag{5.1}$$

From equation (5.1),

$$K\,U + G^*\,F = R \tag{5.2}$$

or,

$$U = K^{-1}\,(R - G^*\,F) \tag{5.3}$$

Also from equation (5.1),

$$S\,U + C^*\,F = T \tag{5.4}$$

Substituting equation (5.3) in (5.4),

$$S\,K^{-1}\,(R - G^*\,F) + C^*\,F = T \tag{5.5}$$

Collecting terms in F and rearranging

$$[C^* - S\,K^{-1}\,G^*]\,F = [T - S\,K^{-1}\,R] \tag{5.6}$$

From equation (5.6) the F vector can be computed. The displacement vector U is computed using equation (5.3) and noting that $K^{-1}R$ and $K^{-1}G^*$ have already been computed in (5.6). Thus the decoupling has been achieved. At present the SIFEH method is available in two computer programs. The first computer program is the coupled version where the

entire K, G*, S and C* matrices are stored in a system matrix A. This system matrix is unsymmetric since $S^T \neq G^*$ and C* is unsymmetric; also the stiffness matrix K is stored with all its zeros and no advantage is taken of the symmetry or sparsity. Clearly storing the matrices in this manner is a limitation which has been alleviated by developing the decoupled method. The second computer program is the implementation of the SIFEH method in NONSAP. In this program the K matrix is stored in a compact form using the sykline or active bandwidth scheme [24] and only storing half the matrix to take advantage of its symmetry. In equation (5.6) it is to be noted that K^{-1} is never computed explicitly. Instead K is triangularized using the familiar $L\ D\ L^T$ factorization (noting that this L is not the same as the L matrix for surface integral displacements); $K^{-1}\ G^*$ is computed by forward reduction and back substitution on each column of G* and $K^{-1}\ R$ is computed similarly. The $L\ D\ L^T$ factorization is performed by a column solver subroutine (COLSOL) in NONSAP; equation (5.6) is solved using a pivoting solver subroutine (SIMQ) for a full matrix. Thus with the decoupled scheme the SIFEH method has utilized the best numerical and computational features of the two component methods. The decoupled method is essentially substructuring and can be used effectively in a variety of problems e.g. soil structure interaction, fluid structure interaction, and contact problems. A major feature of incorporation of the SIFEH method in NONSAP is that dynamic storage allocation has been used and all the matrices and vectors are stored in a vector A; this allows changing the size of the program very easily by changing the dimensions of the A vector.

5.2 THEORETICAL FORMULATION FOR MATERIALLY NONLINEAR ANALYSIS

5.2.1 A SIMPLE NONHOMOGENEOUS PROBLEM

In this section the development for nonlinear analysis is motivated by considering the following problem.

At first consider a problem of a bi-material panel under tensile load as shown in Figure 5.1. The panel is modelled by two finite elements and a linear constitutive law is assumed. Using conventional finite element analysis this problem can be solved in one step by assembling the appropriate stiffness of the two finite elements. This same problem can be solved in another (admittedly longer) way:

1. As the first step consider that the panel is made up of one material with properties E_1, and ν_1. This problem is solved for the applied load R, and the corresponding stresses and strains at the Gauss points $\{\sigma_A\}$ and $\{\varepsilon_A\}$ are computed. In this step equilibrium is satisfied, compatibility is satisfied (by virtue of assumed displacements for finite elements and using complete integration) but the constitutive law is not satisfied in region 2 (Refer to figure 5.1).

2. In the second step the constitutive law is updated in region 2. Since the constitutive law is updated the stresses obtained from the strains $\{\varepsilon_A\}$ computed from the first step will not be in equilibrium with the applied load. In this step compatibility and the constitutive relations are satisfied but equilibrium is not satisfied. The out of balance

load is calculated by computing the misfit stress and by proceeding as follows. The misfit or unbalanced stress is given by:

$$\sigma_A - \sigma_B = \sigma_A - D_B \varepsilon_A \tag{5.7}$$

where:

σ_A = Stress vector at the finite element Gauss points based on step 1.

ε_A = Strain vector at the finite element Gauss points based on step 1.

σ_B = Stress vector at the finite element Gauss points based on step 2.

D_A = Constitutive matrix for the first step.

D_B = Constitutive matrix for the second step.

ε_A is calculated as follows:

$$\varepsilon_A = D_A^{-1} \sigma_A \tag{5.8}$$

The unbalance in the load (computed for all the finite elements m and noting that the terms inside the integral sign are for an element) is computed as:

$$R - \hat{R} = \sum_m \int_{V^{(m)}} B^T (\sigma_A - \sigma_B) \, dV^{(m)} \tag{5.9}$$

where:

$\hat{R}$ = Internal nodal force vector corresponding to the internal stress state at the Gauss points.

Using (5.7) through (5.9),

$$R - \hat{R} = \sum_m \int_{V(m)} B^T [I - D_B D_A^{-1}] \{\sigma_A\} dV^{(m)} \qquad (5.10)$$

I = Identity matrix.

3. The unbalanced load vector is applied to the updated model from step B. The stress and strain vector in this step are given by $\{\sigma_C\}$ and $\{\varepsilon_C\}$. The total solution is given by:

$$\{\sigma\}_{TOTAL} = \{\sigma_B\} + \{\sigma_C\} \text{ (Stress vector)}$$

$$\{\varepsilon\}_{TOTAL} = \{\varepsilon_A\} + \{\varepsilon_C\} \text{ (Strain vector)} \qquad (5.11)$$

$$\{U\}_{TOTAL} = \{U_A\} + \{U_C\} \text{ (Nodal displacement vector)}$$

This example has been run using NONSAP and the same results have been obtained using the direct method and the indirect method described above. Since the constitutive law is linear the problem can be solved with one iteration using this indirect method. The concepts developed here (similar to the procedures used for finite element nonlinear analysis) are used later to formulate the governing equations for nonlinear analysis using the SIFEH method.

5.2.2 DERIVATION OF THE SIFEH GOVERNING EQUATIONS FOR THE NONHOMOGENEOUS CASE

Consider the case of a crack in a nonhomogeneous but elastic body. Similar to the development presented in Chapter 2 the governing SIFEH equations are derived below.

For the finite element model the equations are:

$$K\ U^{FE} = R - R^{c} - R^{cnh} \tag{5.12}$$

Where all the terms have been defined in Chapter 2 except R^{cnh}:

R^{cnh} = Additional correction to the load vector R due to the presence of nonhomogeneity.

Let R^{cnh} be a function of the dislocation density amplitude vector F:

$$R^{cnh} = \bar{K}\ F \tag{5.13}$$

$\bar{K}$ = Nonhomogeneity correction matrix

For the surface integral model (considering the crack to be in one medium),

$$C\ F = T - T^{c} \tag{5.14}$$

Using equation (2.6) in (5.14),

$$S\ U^{FE} + C\ F = T \tag{5.15}$$

Using $U = U^{FE} + U^{SI}$ (From equation 2.9) and $R^c = G\ F$ (from equation 2.2) and equations (5.12) through (5.15) the following is obtained:

$$\begin{bmatrix} K & G - (KL - \bar{K}) \\ S & C - S\ L \end{bmatrix} \begin{Bmatrix} U \\ F \end{Bmatrix} = \begin{Bmatrix} R \\ T \end{Bmatrix} \qquad (5.16)$$

R^{cnh} can be calculated using the misfit stress concept introduced in section 5.2.1.

$$R^{cnh} = \sum_m \int_{V^{(m)}} B^T \left(\{ \sigma_A^{SI} \} - \{ \sigma_B^{SI} \} \right) dV^{(m)} \qquad (5.17)$$

where:

σ_A^{SI} = Stresses at the finite element Gauss points due to the surface integral model for homogeneous media.

σ_B^{SI} = Stresses at the finite element Gauss points due to the surface integral model after updating the constitutive relations.

Using results from section 5.2.1 in equation (5.17):

$$R^{cnh} = \sum_m \int_{V^{(m)}} B^T \left(I - D_B\ D_A^{-1} \right) \{ \sigma_A^{SI} \}\ dV^{(m)} \qquad (5.18)$$

D_A = The constitutive matrix of the homogeneous body used in the surface integral model.

D_B = The constitutive matrix at the finite element Gauss points for the nonhomogeneous body.

The R^{cnh} vector has been evaluated assuming that the stresses due to the surface integral model $\{\sigma_A\}$ have been interpolated using the finite element B matrix; (Convergence will be achieved using more finite elements.

The concepts that have been developed in this section have been verified for the following center cracked specimen problem. The finite element and surface integral discretization is shown in figure 5.4. The specimen is homogeneous and the correct value of Young's modulus is used to compute the K and the S matrices; however, incorrect value is used for the C and the G matrices (note that for plasticity a similar situation exists). By using the $\overline{K}$ matrix as per equation (5.18) a body force correction is provided and solving equation (5.16) has resulted in crack face displacements which are very close to those using the correct moduli for the C and G matrices. It is to be noted that to achieve this result a fine finite element mesh was required to pick up the R^{cnh} effect.

Secondly, the crack in a bi-material plate as shown in figure 5.3 was analyzed using equation (5.16) (Note: a similar problem was solved using a substructuring technique earlier as shown in section 3.9). Superb agreement with known analytical solutions has been obtained as shown in table 5.1. The finite element model as shown in figure 5.3 is adequate as the C and G matrices are modelled using

correct material properties; noting that the G matrix is obtained by traversing the complete perimeter of the finite element model as opposed to the substructure as was done in section 3.9. Also the L matrix is evaluated for all the finite element nodes. At present, inhomogeneties in the elastic regime can be handled for cracks that are not intersecting the bi-material interface; however, appropriate known influence functions for an edge dislocation near a bi-material interface can be utilized to solve intersecting crack problems using the theory developed in this section.

5.2.3 GOVERNING EQUATIONS FOR MATERIALLY NONLINEAR ANALYSIS

The concepts developed in section 5.2.2 for solving nonhomogeneous problems using the SIFEH method are utilized to develop the governing equations for materially nonlinear analysis. The governing equations which are based on incrementally linear superposition with equilibrium iteration and also using the initial stiffness method are as follows:

$$\begin{bmatrix} {}^{o}K & {}^{o}G^{*} \\ {}^{o}S & {}^{o}C^{*} \end{bmatrix} \begin{Bmatrix} \Delta U \\ \Delta F \end{Bmatrix}^{i} = \begin{Bmatrix} {}^{t+\Delta t}R - {}^{t+\Delta t}\hat{R}^{(i-1)} \\ {}^{t+\Delta t}T - {}^{t+\Delta t}\hat{T}^{(i-1)} \end{Bmatrix} \qquad (5.19)$$

where

${}^{o}K$ = Initial stiffness matrix at time t=o.

${}^{o}G^{*}$ = Initial boundary force matrix at time t=o ($G^{*}={}^{o}G-{}^{o}K\ L$).

${}^{o}S$ = Initial stress feedback matrix at time t=o.

$^{o}C^{*}$ = Initial Coefficient matrix at time t=o ($C^{*} = {}^{o}C - {}^{o}S\ L$).

ΔU^{i} = Incremental total displacement vector at iteration i.

ΔF^{i} = Incremental dislocation density amplitude vector at iteration i.

$^{t+\Delta t}R$ = Applied nodal force vector at time $t+\Delta t$.

$^{t+\Delta t}\hat{R}^{(i-1)}$ = Internal nodal force vector corresponding to the (total) Cauchy stresses at the Gauss points at iteration i-1.

$^{t+\Delta t}T$ = Applied traction vector along the crack at time $t+\Delta t$.

$^{t+\Delta t}\hat{T}^{(i-1)}$ = Internal traction vector corresponding to the (total) Cauchy stresses at the Gauss points at iteration i-1.

The internal nodal force vector and traction vector are calculated as follows (for both elasticity and plasticity):

$$^{t+\Delta t}\hat{R}^{(i-1)} = \int_{V} B^{T}\ {}^{t+\Delta t}\tau_{FE}^{(i-1)}\,dV + ({}^{o}G + {}^{t+\Delta t}\tilde{K}^{i-1})\ {}^{t+\Delta t}F^{(i-1)} \qquad (5.20)$$

and,

$^{t+\Delta t}\tilde{K}^{i-1}$ = Nonhomogeneity correction matrix (for plasticity) at time $t+\Delta t$ iteration (i-1).

$$^{t+\Delta t}\hat{T}^{(i-1)} = {}^{t+\Delta t}\tilde{T}_{FE}^{(i-1)} + {}^{o}C\ {}^{t+\Delta t}F^{(i-1)} \qquad (5.21)$$

where,

$^{t+\Delta t}_{\tau}{}_{FE}^{(i-1)}$ = Cauchy stresses (due to only the finite element continuous stress field) at time $t+\Delta t$ for iteration (i-1).

$^{t+\Delta t}\tilde{T}_{FE}^{(i-1)}$ = Smoothed tractions (only continuous stress field) at the collocation points (obtained from Gauss point stresses) at time $t+\Delta t$ for iteration (i-1).

In equation (5.20) it should be noted that for elasticity the right hand side is consistent with the left hand side of equation (5.19); $\bar{K}$ is activated at the Gauss points which go plastic. In equation (5.21) $^{t+\Delta t}\tilde{T}_{FE}^{(i-1)}$ is the smoothed traction vector and is not identically equal to ${}^{o}S^{t+\Delta t}U^{FE(i-1)}$ (however, exact consistency could easily be obtained by computing a smoothed ${}^{o}S$ matrix). The smoothing is necessary for plasticity and the traction vector (at the collocation points along the crack) is obtained by extrapolation of the Gauss point stresses to the finite element nodal points and then obtaining the collocation point tractions by performing a bi-linear interpolation of the nodal point stresses. The extrapolation is done in a least square sense, the details of this local smoothing procedure are provided in [70,71]. At present the smoothing is applicable to finite elements with constant determinants of the Jacobians i.e. parallelograms or rectangles. However extension to curved elements is possible but would require additional calculations [70]. Also global smoothing of stresses can be performed where the smoothing also depends on the size (volume) of the neighboring finite elements.

The incremental equations (5.19) are solved using the

decoupled scheme as described in section 5.1 and the modified Newton - Raphson scheme . Convergence is achieved when the ratio of the Eucledian norms $||\Delta U^{(i)}||_2 / ||^{t+\Delta t}U||_2$ is less than or equal to a small tolerance [24] .

5.2.4 PROCEDURE FOR COMPUTING STRESSES FOR ELASTO-PLASTIC ANALYSIS

The incremental equations for elasto-plastic analysis are given below. The solution to the governing equation (5.26) is known at time t and the solution at time t+Δt is to be obtained. For additional details refer to [24]. The Von-Mises yield condition with an isotropic hardening rule is used for this material model [62].

- DISPLACEMENTS

$$^{t+\Delta t}U = {}^{t}U + \Delta U \qquad (5.22)$$

$$^{t+\Delta t}_{U}FE = {}^{t+\Delta t}U - L^{t+\Delta t}F$$

ΔU = Increment in the nodal displacement vector from time t to t+Δt

- STRAINS

$$^{t+\Delta t}\varepsilon = B^{t+\Delta t}_{U}FE + {}^{t+\Delta t}_{\varepsilon}SI \qquad (5.23)$$

$$^{t+\Delta t}_{\varepsilon}SI = N^{t+\Delta t}F \quad \text{N=Surface Integral Strain Matrix}$$

- STRESSES

$$^{t+\Delta t}\sigma = {}^{t}\sigma + \Delta\sigma \qquad (5.24)$$

$^{t}\sigma$ = Stresses at Gauss points at time t.

$\Delta\sigma$ = Increment in the stresses from time t to $t+\Delta t$.

$\Delta\sigma$ is obtained as follows [24]:

Let,

$^{t+\Delta t}\varepsilon \equiv$ STRAIN , $^{t}\varepsilon \equiv$ EPS

$^{t+\Delta t}\sigma \equiv$ TAU , $^{t}\sigma \equiv$ SIG

- COMPUTE STRAIN INCREMENT (DELEPS)

DELEPS = STRAIN-EPS (5.25)

- COMPUTE STRESS INCREMENT (DELSIG)

DELSIG = D^E DELEPS (5.26)

D^E = Elastic constitutive matrix

- COMPUTE TOTAL STRESSES (TAU)

TAU = SIG+DELSIG (5.27)

- CHECK IF WITHIN YIELD SURFACE

IF F(TAU) $\leq$0 RETURN

IF F(TAU) >0 CONTINUE (5.28)

- IF PREVIOUS STATE OF STRESS WAS PLASTIC SET RATIO = 0 AND GO TO NEXT STEP. OTHERWISE FIND RATIO TO DETERMINE THE PORTION OF THE STRAIN TO BE TAKEN ELASTICALLY.

F [SIG + RATIO * DELSIG] = 0

- DETERMINE STRESS $^{t+\Delta t}\sigma$ BY PERFORMING EULER FORWARD INTEGRATION.

TAU = SIG + RATIO * DELSIG

DEPS = (1 - RATIO) * DELSIG, DEPS IS BROKEN INTO SUB-INCREMENTS DDEPS

$$TAU \leftarrow TAU + D^{EP} * DDEPS \qquad (5.29)$$

D^{EP} = Elastoplastic constitutive matrix [24,72].

It should be noted that iterations are being performed and hence (5.22) can be rewritten as follows (Similar right superscripts can be used for the other variables):

$$^{t+\Delta t}U^{(i)} = {}^{t+\Delta t}U^{(i-1)} + \Delta U^{(i)} \qquad (5.30)$$

5.3 RESULTS FOR MATERIALLY NONLINEAR ANALYSIS

The SIFEH model for a center cracked test specimen is shown in figure 5.4. The bi-linear constitutive law used for this problem is as shown in figure 5.2. All material parameters used are shown in table 5.2. The following equation derived by J. Hutchinson [63] are reproduced here. For small scale yielding around the crack tip the "plastic" stress intensity factor (obtained by asymptotic analysis) for plane strain conditions is given by (also noting that the factor $\sqrt{2}$ is not included in our definition of K):

$$K^H = (1-\nu^2)^{1/2}\sigma^\infty[1 + \frac{1}{2}\xi^2 - \frac{3}{2}\nu\xi + \frac{1}{6}\lambda(4-3\xi + 2\xi^2)]^{-\frac{1}{2}} \quad (5.31)$$

where,

$$\xi = \frac{\nu + \frac{1}{2}(\frac{E}{E_T} - 1)}{\frac{E}{E_T}} \quad (5.32)$$

and

$$\lambda = \frac{3}{2}(\frac{E}{E_T} - 1) \quad (5.33)$$

The plastic stress intensity factors (for different values of E_T) obtained by SIFEH analysis agree well with those obtained using equation (5.31). It should be noted that the plastic stress intensity factor given by equation (5.31) is valid for small scale yielding around the crack tip and the loading used for SIFEH analysis was such that this condition was satisfied. The values used for E_T were upto a ratio of E/E_T=30. The plastic stress intensity factors have been obtained from the dislocation density amplitude at the interpolation point near the crack tip. It is recommended that these intensity factors should be also obtained by using the path independent J integral to provide additional verification. The convergence of the solution is controlled by the tolerance on the displacement norm as was described in section 5.2.3.

Table 5.1 Stress intensity factors for a bi-material panel with an edge crack (refer to figure 5.3)

E_1/E_2	$K_I/P\sqrt{a/2}$ Lu-Erdogan [77]	$K_I/P\sqrt{a/2}$ SIFEH	$\frac{K_I^{SIFEH}}{K_I^{Lu\text{-}Erdogan}}$
0.5	2.3	2.45	1.06
1	2.16	2.26	1.05
2	2.00	2.08	1.04

Table 5.2 Elastic and plastic stress intensity factors

E (psi)	E_T (psi)	Yield (psi)	$\frac{K_I^{el*}}{\sigma\sqrt{\pi a}}$	$\frac{K_I^{pl*}}{\sigma\sqrt{\pi a}}$	$\frac{K_I^{H**}}{\sigma\sqrt{\pi a}}$	$\frac{K_I^{pl}}{K_I^{H}}$	Remarks
$.3\times10^8$	$.15\times10^8$	3500	1.206	.85	.884	0.96	Small yielded zone[1]
$.3\times10^8$	$.1\times10^8$	3500	1.206	.652	.735	0 89	Small yielded zone[1]
$.3\times10^8$	$.3\ 10^7$	3500	1.215	.387	.416	0.93	Small yielded Zone[1,2]
$.3\times10^8$	$.1\ 10^7$	3500	1.198	.208	.238	0.87	Yielded zone was larger[2]

* SIFEH analysis

** Based on Hutchinson's bi-linear results

1 Only one element near the crack tip was fully plastic.

2 SIFEH model used 1st row of finite elements closer to the crack

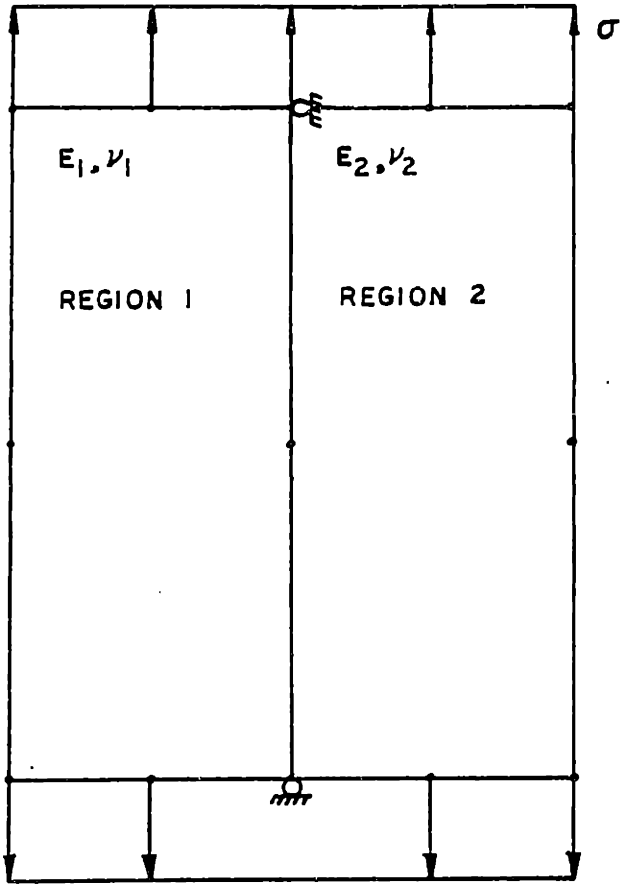

Figure 5.1. A Simple Nonhomogeneous Problem

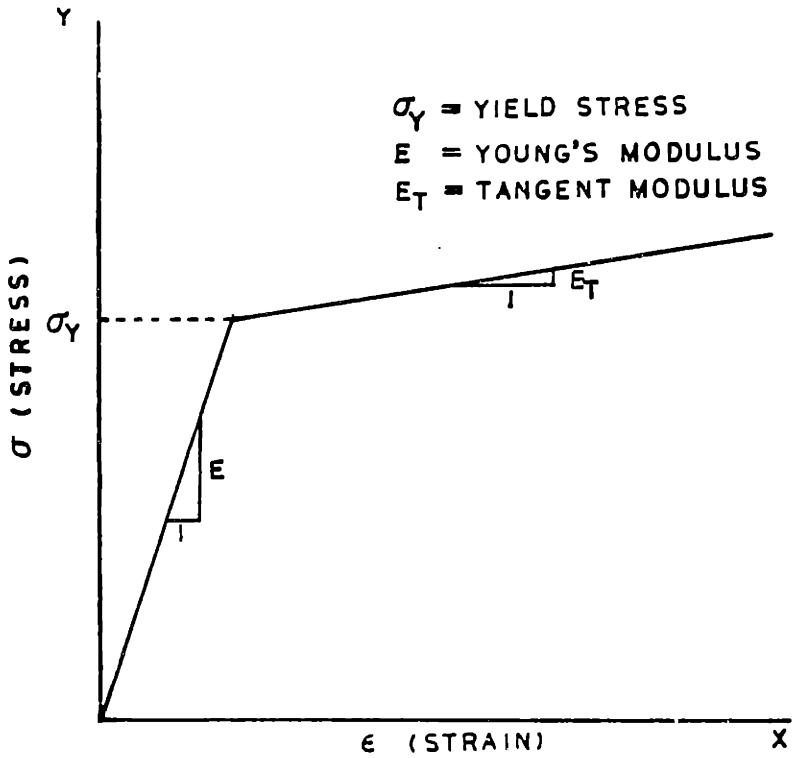

Figure 5.2. Bi-linear Constitutive Law

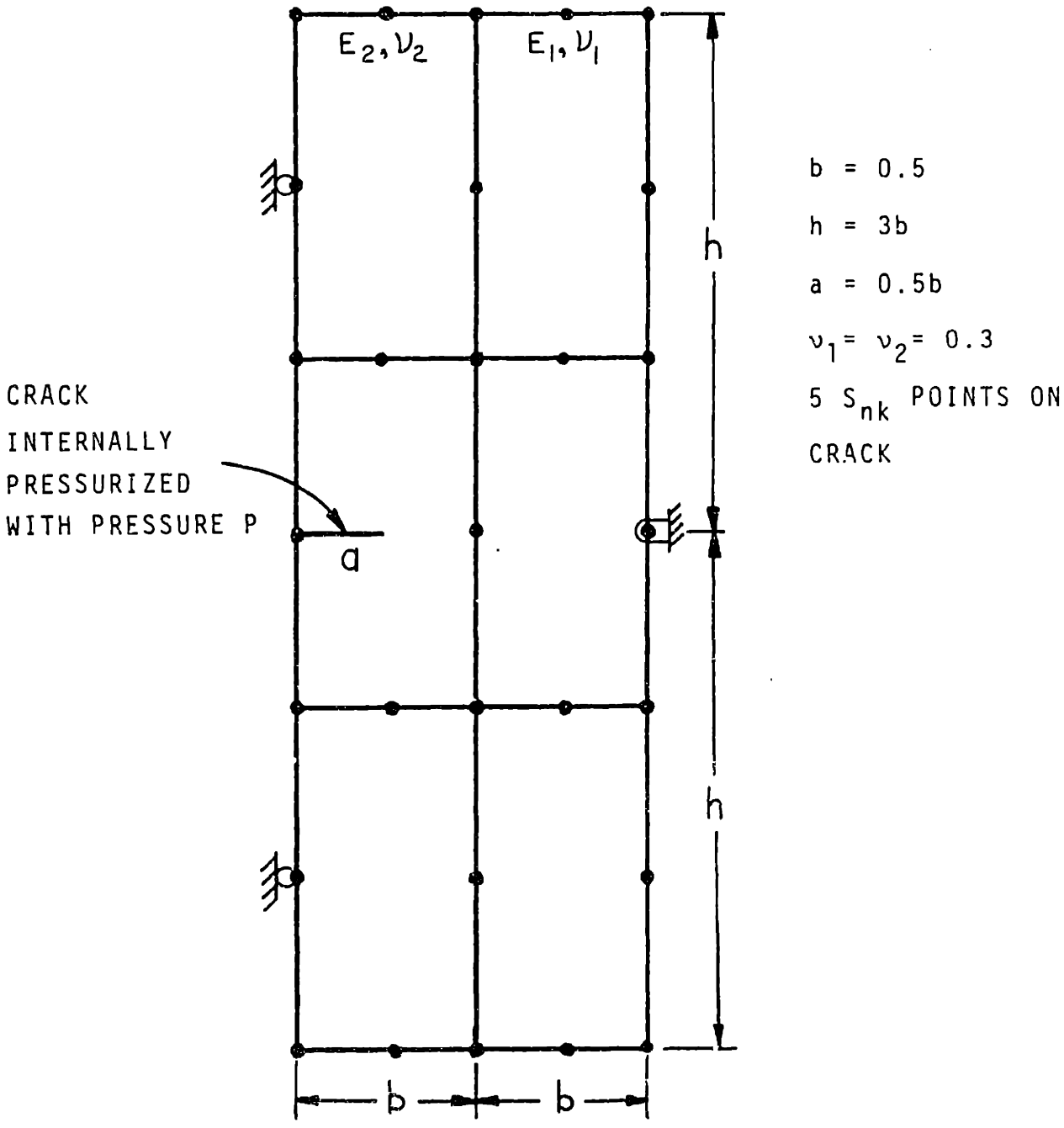

Figure 5.3 Edge crack in a bi-material panel.

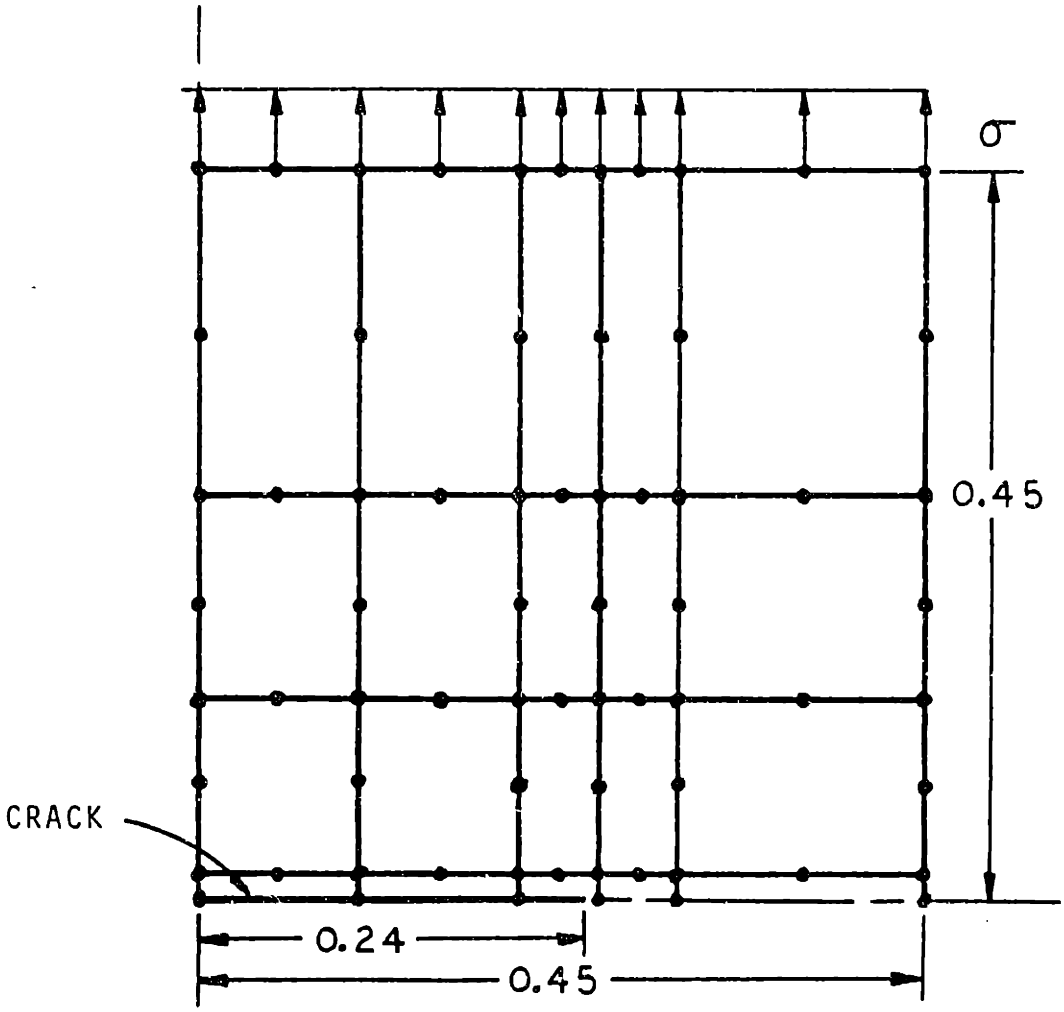

Figure 5.4 Center cracked test specimen (quarter geometry shown)

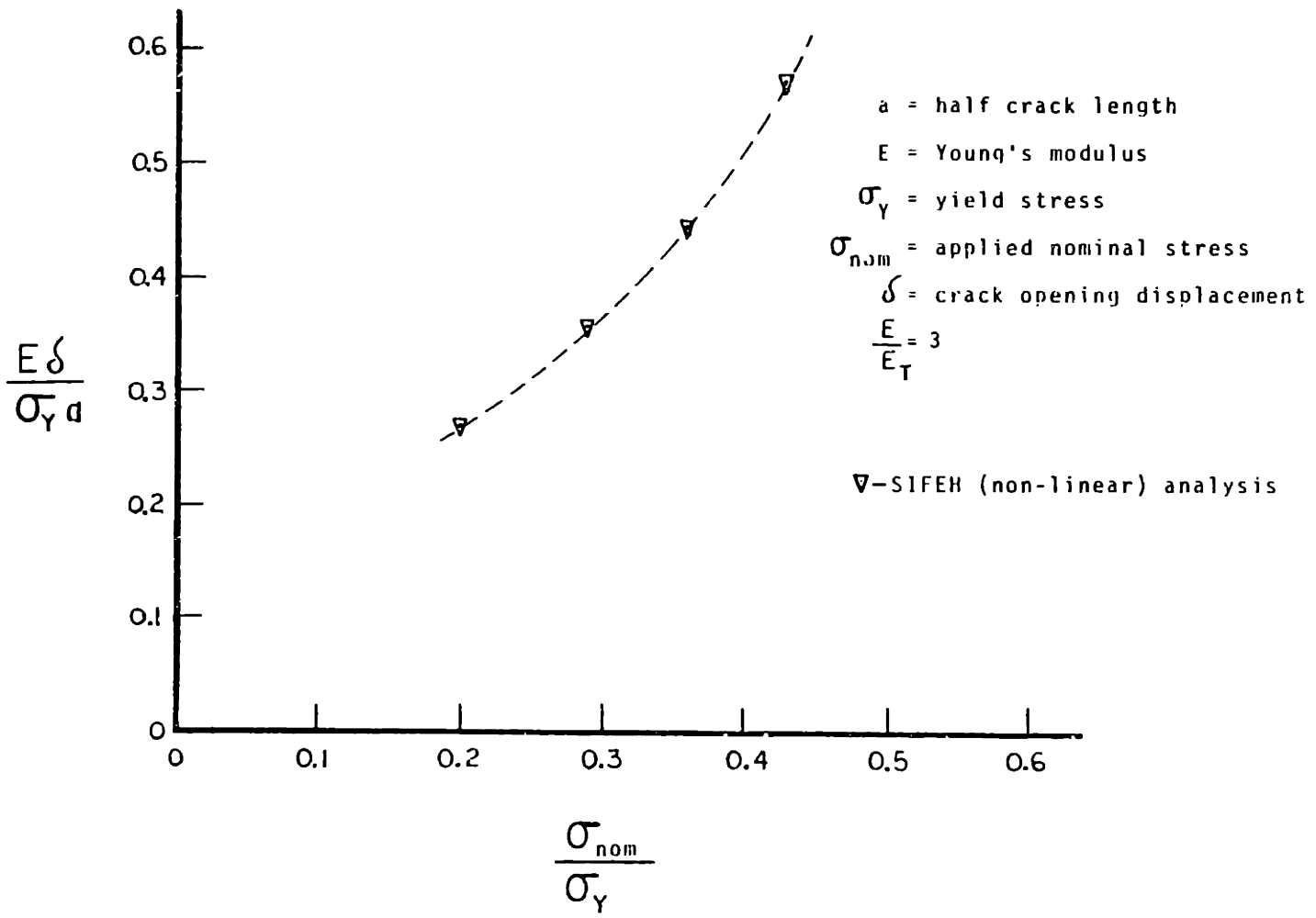

Figure 5.5 Evolution of crack opening displacement at collocation point(near crack tip)for center cracked test specimen.

CHAPTER 6

CONCLUSIONS AND RECOMMENDATIONS FOR FURTHER RESEARCH

An effective hybrid method has been formulated and implemented to solve localized problems in continuum mechanics with emphasis on fracture mechanics in this thesis. Qualification of this method has been performed by comparing results with known analytical and experimental solutions and excellent agreement has been obtained. The advantage of this method for evolution of fractures and shear bands has been demonstrated and excellent agreement with experimental observations has been shown. For this SIFEH method improvements to the existing program and further developments are recommended as follows.

1. The S matrix should be based on stress smoothing so that even if a non-linear material model is used convergence would be achieved in one step for the linear part of the stress excursion.

2. A Paris type law for fatigue propagation should be built in the computer program so that the number of cycles needed to propagate cracks a certain distance can be computed directly.

3. Computer graphics should be effectively used in conjunction with the method for ease of visualizing propagated paths and deflected shapes and also to be able to interactively run the program.

4. Dynamic fracture problems can be modelled using

influence functions which not only have spatial dependence but also temporal with dynamic effects included. An example of formulation of singular integral equations using such influence functions can be found in [80].

5. Initiation criteria for cracks or for localization of deformation could be studied and also used as the basis for nucleation of cracks/shear bands (This study could include bifurcation problems).

6. This method has formed the basis for three dimensional fracture analysis where force dipoles are used to model the discontinuity in displacement and again finite elements model the finite body.

The nonlinear analysis in the SIFEH method was implemented using a square root singular behavior near the crack/shear band tip which was shown by Hutchinson [63] and Hilton and Hutchinson [65] to be valid for the bi-linear and multi-linear hardening cases. Other singulariaties (e.g. 1/r or power law) could be investigated by explicitly employing such dependence near the tip. It is recommended that the evolution of the plastic zone obtained by the SIFEH method should be compared with results obtained by using the finite element method. Propagation of cracks with nonlinear material behavior is an important area of research which can be pursued. It is hoped that difficulties which are associated with remeshing of finite elements (for crack propagation) in non-linear analysis will be alleviated or reduced using the SIFEH method. The nonlinear analysis has been introduced using the SIFEH method but more research is needed to study in detail other aspects of nonlinear analysis.

Another application for the SIFEH method would be fracture analysis in shells as solutions for dislocations in cylindrical geometries are known. A possible extension would be to model geometrical non-linear effects (large rotations) but small strain (dominantly elastic) for thin shell structures where the feed back of stress to the line of the crack could still be the Cauchy stress but the geometry will have to be kept track of. Such possibilities should be investigated.

It has been brought to the author's attention that a technique called the Shwarz's alternating algorithm [29] has been used in reference [81] to solve fracture problems, however, the formulation developed is limited. Iterations are needed for linear analysis and the crack has to lie along a finite element side (this is a serious limitation). Also a large number of degrees of freedom are required (even though the analysis is for linear elasticity).

The SIFEH method has been demonstrated for fracture but it can be effectively applied in principle to solve field problems such as potential flow over airfoils using known influence functions for fluid dipoles; other applications include diffusion, electromagnetism, heat transfer etc. For example, for the airfoil problem shown in figure 1.3, fluid source and sink dipoles can be distributed around the airfoil with the requirement that $V^{\infty} \cdot n = -V \cdot n$ where V^{∞} is the free stream velocity, V is the velocity on the airfoil surface and n is the normal to the airfoil surface. The corresponding integral equation can be generated (similar to the procedures described for fracture) using appropriate influence functions for the fluid dipoles. It is hoped that in the future, application of the SIFEH method to other areas apart from fracture will verify its effectiveness as a method for solving localized problems in continuum mechanics.

APPENDIX A

I. VIRTUAL WORK FORMULATION FOR THE FINITE ELEMENT METHOD

The governing finite element equations for the plate without the crack can be obtained by invoking the virtual work principle or by using variational principles [24,25,5]. This discussion is within the context of small displacement and linear elastic analysis. The virtual work equation for a body (refer figure A.1) is given by [24]

$$\int_V {}^{t+\Delta t}\tau_{ij}\ \delta\, {}_{t+\Delta t}e_{ij}\ dV = {}^{t+\Delta t}R \qquad (A.1)$$

${}^{t+\Delta t}\tau_{ij}$ = Cartesian components of the Cauchy stress tensor at time $t+\Delta t$

$\delta\, {}_{t+\Delta t}e_{ij}$ = Variation in the Cartesian components of the infinitesimal strain tensor at time $t+\Delta t$.

${}^{t+\Delta t}R$ = External virtual work at time $t+\Delta t$ corresponding to compatible variation in displacement which satisfies the essential boundary conditions.

V = Volume of the body under consideration. Remains constant for the small displacement assumption.

Using linear elastic constitutive law

$$\tau_{ij} = D_{ijrs}\, e_{rs} \qquad (A.2)$$

Using equation (A.2) in (A.1) and for convenience omitting the time variable:

$$\int_V D_{ijrs}\, e_{rs}\, \delta e_{ij}\, dV = R \qquad (A.3)$$

D_{ijrs} = Components of the linear constitutive tensor.

When the continuum is discretized by finite elements (using local interpolation of displacements over the element subspace) the following is obtained by expressing the integral as a sum over all the m elements.

Using for convenience matrix notation:

$$\int_V D_{ijrs}\, e_{rs}\, \delta e_{ij}\, dV = \sum_m \int_{V^{(m)}} \delta\, \underline{\varepsilon}^{(m)T}\, \underline{D}\, \underline{\varepsilon}^{(m)} dV^{(m)} \qquad (A.4)$$

Where for two dimensional analysis:

$$\underline{\varepsilon}^{(m)T} = [\varepsilon_{XX}\ \varepsilon_{YY}\ \varepsilon_{XY}],\quad \delta\underline{\varepsilon}^{(m)} = \text{variation of } \underline{\varepsilon}^{(m)} \qquad (A.5)$$

$$\underline{\varepsilon}^{(m)} = \underline{B}^{(m)}\, \underline{U},\quad \delta\underline{\varepsilon}^{(m)} = \underline{B}^{(m)}\, \delta\underline{U} \qquad (A.6)$$

$\underline{U}$ = Nodal displacement for all degrees of freedom.

$\underline{B}^{(m)}$ = Strain displacement interpolation matrix for element m.

$$\underline{D} = \frac{E}{1-\nu^2}\begin{bmatrix} 1 & \nu & 0 \\ \nu & 1 & 0 \\ 0 & 0 & \frac{1-\nu}{2} \end{bmatrix}, \text{ for plane stress} \qquad (A.7)$$

$$\underline{D} = \frac{E(1-\nu)}{(1+\nu)(1-2\nu)}\begin{bmatrix} 1 & \frac{\nu}{1-\nu} & 0 \\ \frac{\nu}{1-\nu} & 1 & 0 \\ 0 & 0 & \frac{1-2\nu}{2(1-\nu)} \end{bmatrix}, \text{for plane strain} \qquad (A.8)$$

The external virtual work can be computed using

$$R = \int_V \delta\underline{U}^T \underline{f}^B \, dV + \int_S \delta\underline{U}^{S^T} \underline{f}^S \, dS + \delta\underline{U}^T \underline{P} \qquad (A.9)$$

$\underline{f}^B$ = Body force vector.

$\underline{f}^S$ = Surface force vector.

$\delta\underline{U}$ = Variation in nodal displacement vector.

$\delta\underline{U}^S$ = Variation in nodal displacement vector along the surface.

$\underline{P}$ = Applied external concentrated force vector.

Summing over all elements:

$$\int_V \delta\underline{U}^T \underline{f}^B \, dV = \sum_m \int_{V^{(m)}} \delta\underline{U}^{(m)^T} \underline{f}^{B(m)} \, dV^{(m)} \qquad (A.10)$$

$$\int_S \delta\underline{U}^{S^T} \underline{f}^S \, dS = \sum_m \int_{S^{(m)}} \delta\underline{U}^{S(m)^T} \underline{f}^{S(m)} \, dS^{(m)} \qquad (A.11)$$

Also,

$$\delta \underline{U}^{(m)} = \underline{H}\ \delta \underline{U} \qquad \text{(A.12)}$$

$\underline{H}$ = Displacement interpolation matrix.

Using equations (A.10) (A.11) and (A.12) in (A.9) and removing $\delta \underline{U}^T$ outside the integral sign (justified since the variations are arbitrary)

$$R = \delta \underline{U}^T \left[\sum_m \int \underline{H}^{(m)^T}\ \underline{f}^{B(m)}\ dV^{(m)} + \sum_m \int_{S^{(m)}} \underline{H}^{S(m)^T}\ \underline{f}^{S(m)}\ dV^{(m)} + P \right] \qquad \text{(A.13)}$$

From equations (A.4),(A.5),(A.6) and (A.13):

$$\sum_m \int_{V^{(m)}} \underline{B}^{(m)^T}\ \underline{D}^{(m)}\ \underline{B}\ U = \sum_m \int \underline{H}^{(m)^T}\ \underline{f}^{B(m)}\ dV^{(m)} + \sum_m \int_{S^{(m)}} \underline{H}^{S(m)^T}\ \underline{f}^{S(m)}\ dV^{(m)} + \underline{P} \qquad \text{(A.14)}$$

or,

$$\underline{K}\ \underline{U} = \underline{R} \qquad \text{(A.15)}$$

Where

$$\underline{K} = \sum_m \int_{V^{(m)}} \underline{B}^{(m)^T}\ \underline{D}^{(m)}\ \underline{B}$$

$$\underline{R} = \sum_m \int_{V^{(m)}} \underline{H}^{(m)^T}\ \underline{f}^{B(m)}\, dV^{(m)} + \sum_m \int_{S^{(m)}} \underline{H}^{S(m)^T}\ \underline{f}^{S(m)}\, dV^{(m)} + \underline{P}$$

(External consistent load vector).

The above equations have been derived for statics and generalization of these equations for initial stresses, thermal stresses, dynamics, material and geometric nonlinearities etc. can be found in [24].

II. COMPUTATION OF THE STIFFNESS MATRIX K.

Eight noded isoparametric finite elements have been used and the elemental stiffness matrix K_m is evaluated using numerical integration (Gaussian quadrature). The stiffness matrix of the complete structure is evaluated by summing over all the elements.

$$K = \sum_{m} \int_{V^{(m)}} \underline{B}^{(m)T} \underline{D} \underline{B}^{(m)} \, dV^{(m)} \qquad (A.16)$$

m = Total number of finite elements.

$\underline{B}$ = Strain displacement interpolation matrix.

$\underline{D}$ = Constitutive matrix.

All quantities shown below with indices "ij" are calculated at Gauss points with co-ordinates (r_i, s_j) in the intrinsic (isoparametric) co-ordinate system where i,j depend on the order of numerical integration.

$$K_m = \sum_{i,j} t_{ij} \alpha_{ij} F_{ij} \qquad (A.17)$$

t_{ij} = Thickness of the finite element.

α_{ij} = Weighting factors.

$$F_{ij} = B_{ij}\, D\, B_{ij} \det J_{ij} \qquad (A.18)$$

J_{ij} = Determinant of the Jacobian of the transformation.

$$\underline{K} = \sum_{m} \underline{K}_{m} \qquad (A.19)$$

The other matrices needed viz. $\underline{H}$ and $\underline{B}$ etc. for the eight noded isoparametric element can be obtained using procedures developed in [24].

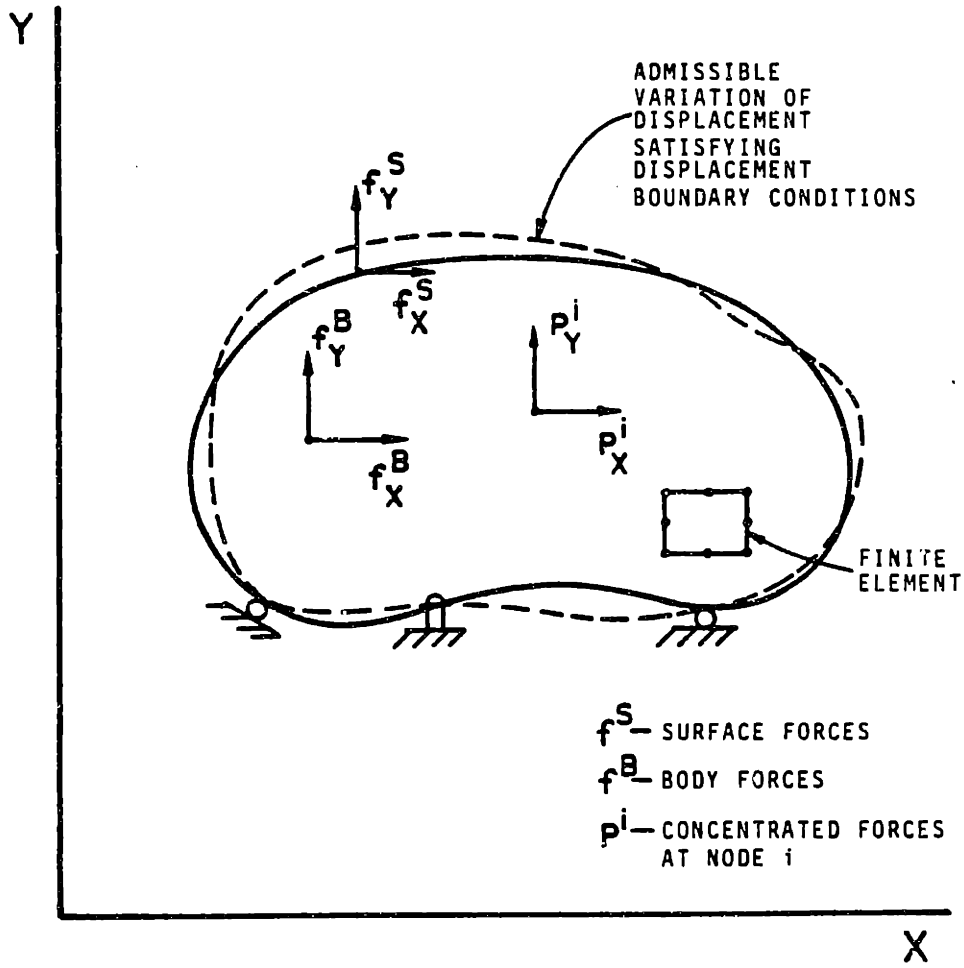

Figure A.1 Application of the virtual work principle for finite element analysis

APPENDIX B

I. COMPUTATION OF THE S MATRIX

The elements of the S matrix are the shear and normal stresses at collocation points (S_{mr} points) along the crack in the local tangential and normal directions, due to unit displacements at the finite element nodes.

The stress at any point in a finite element is obtained as follows [24].

$$\sigma_m(r,s) = \begin{Bmatrix} \sigma_{XX} \\ \sigma_{YY} \\ \sigma_{XY} \end{Bmatrix} = \left\{ D^{(m)} \; B^{(m)} \; U^{(m)} \right\} \quad (B.1)$$

r,s = Intrinsic co-ordinates of the collocation points.

$B^{(m)}$ = Strain-displacement interpolation matrix for the element m evaluated at the collocation point S_{mr}.

$D^{(m)}$ = Constitutive matrix for the element m.

$U^{(m)}$ = Nodal displacement vector for the element m.

σ_{XX} = Normal stress in the global X direction.

σ_{YY} = Normal stress in the global Y direction.

σ_{XY} = Shear stress in the global X-Y plane.

Elements of the S matrix are obtained by computing the

product DB and using Mohr's circle transformation to obtain shear and normal stresses in the local tangential and normal directions at the collocation points along the crack.

Deleting the element superscript for convenience, the stresses are given by:

$$\left\{ \begin{array}{c} \sigma_{XX} \\ \sigma_{YY} \\ \sigma_{XY} \end{array} \right\}_{S_{mr}} = \underline{D}\ \underline{B}\ \underline{U} \qquad (B.2)$$

Let

$$\underline{D} = \underline{D}_1\ \underline{D}_2\ \underline{D}_3 \qquad (B.3)$$

Where the columns of $\underline{D}$ are given by:

$$\underline{D}_1 = \left\{ \begin{array}{c} D_{11} \\ D_{21} \\ D_{31} \end{array} \right\} \quad \underline{D}_2 = \left\{ \begin{array}{c} D_{12} \\ D_{22} \\ D_{32} \end{array} \right\} \quad \underline{D}_3 = \left\{ \begin{array}{c} D_{13} \\ D_{23} \\ D_{33} \end{array} \right\} \qquad (B.4)$$

$$\sigma_{XX} = \underline{D}_1^T \underline{B}\ \underline{U} \qquad \sigma_{YY} = \underline{D}_2^T \underline{B}\ \underline{U} \qquad , \sigma_{XY} = \underline{D}_3^T \underline{B}\ \underline{U} \qquad (B.5)$$

Since the constitutive matrix $\underline{D}$ is symmetric:

$$\underline{D}_1^T = \underline{D}_1, \qquad D_2^T = \underline{D}_2, \qquad \underline{D}_3^T = \underline{D}_3 \qquad (B.6)$$

The components of the stress tensor in the local co-ordinate system X'-Y' [Refer to figure B.1] are given by [28]:

$$\sigma_{Y'X'} = \sigma_{XY}(\cos^2\theta - \sin^2\theta) + (\sigma_{YY} - \sigma_{XX})\sin\theta\cos\theta \qquad (B.7)$$

$$\sigma_{Y'Y'} = \sigma_{XX}\cos^2\theta + \sigma_{YY}\sin^2\theta + 2\tau_{XY}\sin\theta\cos\theta$$

Using $\cos^2\theta - \sin^2\theta = \cos2\theta$, $2\sin\theta\cos\theta = \sin2\theta$

$$\text{and } \cos^2\theta = \frac{1+\cos2\theta}{2}\ ,\ \sin^2\theta = \frac{1-\cos2\theta}{2} \tag{B.8}$$

$$\sigma_{Y'X'} = \sigma_{XY}\cos2\theta + \frac{\sigma_{YY}-\sigma_{XX}}{2}\sin2\theta$$

$$\sigma_{Y'Y'} = \sigma_{XX}\left[\frac{1+\cos2\theta}{2}\right] + \sigma_{YY}\left[\frac{1-\cos2\theta}{2}\right] + \sigma_{XY}\sin2\theta \tag{B.9}$$

Using (B.5) in (B.9)

$$\sigma_{Y'X'} = \left[D_3\cos2\theta + \frac{D_2 - D_1}{2}\sin2\theta\right] \cdot B \cdot U \tag{B.10}$$

$$\sigma_{Y'Y'} = \left[\frac{D_1 + D_2}{2} + \frac{D_1 - D_2}{2}\cos2\theta + D_3\sin2\theta\right] \cdot B \cdot U$$

The terms in the parentheses times the matrix B are the components of the matrix S (for this collocation point).

In the computer program the sign convention for the shear stress has been reversed so as to facilitate using a right handed sign convention for the applied shear tractions along the crack; this is consistent with the sign convention for the shear terms of the C matrix.

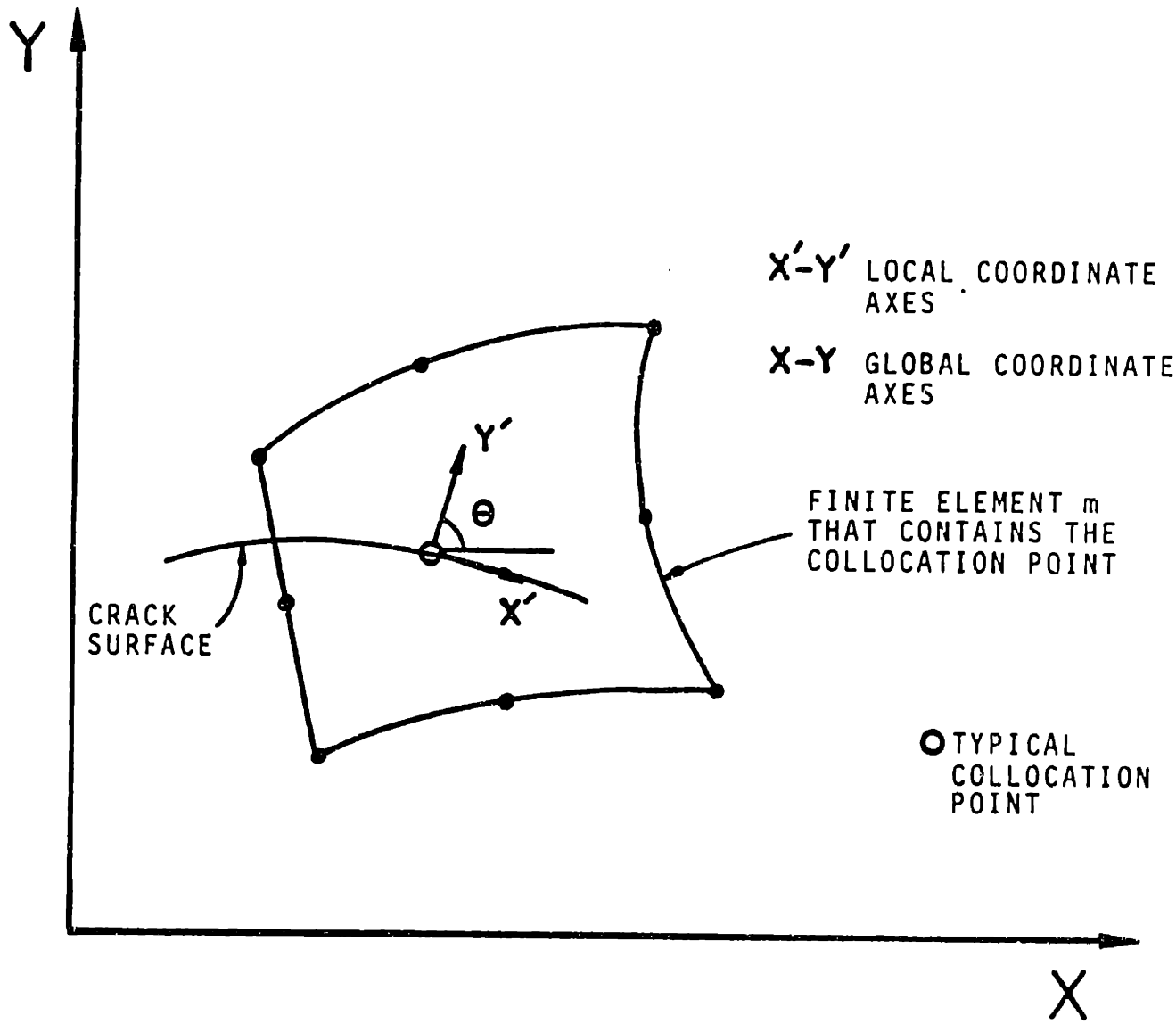

Figure B.1 Computation of the S matrix by locating the finite element that contains the collocation point

APPENDIX C

I. COMPUTATION OF THE C MATRIX

The concept of modelling cracks using a continuous distribution of dislocations is well established [17,39,40]. Consider a system of cracks in an infinite domain as shown in Figure C.1. Slip (gliding) dislocations and opening (climbing) dislocations are used to model the slip and opening discontinuities in displacement. The cracks can be loaded due to remotely applied stresses and also due to tractions applied along the cracks (e.g. an internally pressurized crack). Using linear superposition, this problem can be modelled as a sum of the infinite domain without the cracks with remote stresses applied and the infinite domain with the cracks with reversed tractions applied along the cracks. Essentially this implies that the tractions (on a prospective crack locus) are relieved due to the formation of the fracture. The elasticity problem of the infinite domain without the cracks can be solved using complex variable or other available techniques [23,28,29,52], however this problem does not have singular fields. The second problem of the cracks with remotely applied tractions reversed has singular fields which are modelled very effectively using a continuous distribtuion of dislocations. The governing integral equation is given by the following:

$$\sigma_{ij}(\underset{\sim}{X}_o) = \int_{S_c} \Gamma^P_{ij}(\underset{\sim}{X}_o, \underset{\sim}{X}) \cdot \mu^P(\underset{\sim}{X})\, dS_c \qquad (C.1)$$

$\Gamma^P_{ij}(\underset{\sim}{X}_o, \underset{\sim}{X})$ = Stress influence function for a

dislocation. Stress component Γ_{ij} at $\underset{\sim}{X}_o$ due to a unit dislocation density in the p direction at $\underset{\sim}{X}$.

$\mu^P(\underset{\sim}{X})$ = Dislocation density in the p direction (p=1,2 for slip and opening respectively).

$\sigma_{ij}(\underset{\sim}{X}_o)$ = Stress component at $\underset{\sim}{X}_o$ due to a distribution of dislocations along the crack surface S_c.

S_c = Crack Surface.

$$\mu^P(\underset{\sim}{X}) = \frac{d\delta(\underset{\sim}{X})}{dS_c} \qquad (C.2)$$

$\delta(\underset{\sim}{X})$ = Discontinuity in displacement at $\underset{\sim}{X}$.

The governing integral equation (C.1) is further modified so that the applied traction conditions on the crack surfaces are satisfied.

$$T_{im}(\underset{\sim}{X}_o) = \sum_{n=1}^{M} \sum_{p=1}^{2} \int_{S_n} \Gamma_{im}^{pn}(\underset{\sim}{X}_o, \underset{\sim}{X})\, \mu^{pn}(\underset{\sim}{X})\, dS_n \qquad (C.3)$$

where,

$T_{im}(\underset{\sim}{X}_o)$ = Applied traction component in the i direction on the m^{th} crack surface at $\underset{\sim}{X}_o$.

$\Gamma_{im}^{pn}(\underset{\sim}{X}_o, \underset{\sim}{X})$ = Traction component in the i direction

on the m^{th} crack surface at $\underset{\sim}{X}_o$ due to a unit dislocation density in the p direction on the n^{th} crack surface at $\underset{\sim}{X}$.

$\mu^{pn}(\underset{\sim}{X})$ = Dislocation density in the p direction on the n^{th} crack surface at $\underset{\sim}{X}$.

S_n = Crack surface of the n^{th} crack.

N = Total number of cracks.

Note: (i) p=1,2 refers to components of the dislocation density in the global X-Y directions

(ii) Traction components are along the local normal and tangential directions along the crack surfaces.

The integral over the surface S_n is effectively evaluated in the Cauchy principal value sense using a Gauss-Chebyshev scheme. The crack surfaces (which could be curved in the plane) are mapped onto a (-1,+1) interval for numerical integration and equation (C.3) becomes:

$$\begin{Bmatrix} T_\tau(S_m) \\ T_\sigma(S_m) \end{Bmatrix} = \sum_{n=1}^{N} \sum_{p=1}^{2} \int_{-1}^{1} \begin{Bmatrix} \Gamma_\tau^p(S_m,S_n) \\ \Gamma_\sigma^p(S_m,S_n) \end{Bmatrix} \mu^p(S_n)\, ds_n \quad (C.4)$$

$T_\tau(S_m)$ = Applied shear traction in the local tangential direction at point S_m.

$T_\sigma(S_m)$ = Applied normal traction in the local normal direction at point S_m.

$\Gamma_i^p(S_m,S_n)$ = Traction component in the local i direction ($i=\tau$ for shear, σ for normal) at point S_m due to a unit normalized dislocation density $\mu^p(S_n)$ in the p direction at S_n. These components are obtained from dislocation influence functions for stresses [19,53] and using Mohr's circle transformation [19,20].

$\mu^{pn}(S_n)$ = Normalized dislocation density ($= \mu^{pn}(\underset{\sim}{X})/a_n$) where a_n is half the length of crack n.

ds_n = Differential length of the mapped surface of the n^{th} crack.

The dislocation density is given by [19]:

$$\mu^{pn}(S_n) = \frac{F^{pn}(S_n)}{(1+S_n)^{\alpha}(1-S_n)^{\beta}} \quad \text{, in general} \qquad (C.5)$$

For homogeneous isotropic media $\alpha = \beta = 0.5$ which results in the familiar square root singular dislocation density:

$$\mu^{p}(S_n) = \frac{F^{pn}(S_n)}{\sqrt{1-S_n^2}} \qquad (C.6)$$

$F^{pn}(S_n)$ = Amplitude of the normalized dislocation density (S_n).

using (C.6), equation (C.4) takes the form:

$$\begin{Bmatrix} T_\tau(S_m) \\ T_\sigma(S_m) \end{Bmatrix} = \sum_{n=1}^{N} \sum_{p=1}^{2} \int_{-1}^{1} \begin{Bmatrix} \Gamma_\tau{}^p(S_m, S_n) \\ \Gamma_\sigma{}^p(S_m, S_n) \end{Bmatrix} \frac{F^{pn}(S_n)}{\sqrt{1-S_n^2}} \, ds_n \quad (C.7)$$

The integral is evaluated numerically using the Gauss-Chebyshev formulae as per [18]:

$$\begin{Bmatrix} T_\tau(S_{mr}) \\ T_\sigma(S_{mr}) \end{Bmatrix} = \sum_{n=1}^{N} \frac{\pi}{M_n} \sum_{p=1}^{2} \sum_{k=1}^{M_n} F^p(S_{nk}) \begin{Bmatrix} \Gamma_\tau{}^p(S_{mr}, S_{nk}) \\ \Gamma_\sigma{}^p(S_{mr}, S_{nk}) \end{Bmatrix} \quad (C.8)$$

N = Total number of cracks

m = 1,2, ... N

n = 1,2, ... N

r = 1,2, ... M_m-1

k = 1,2, ... M_n

S_{nk} = M_n zeros of T_{M_n}, the Chebyshev polynomials of the first kind.

S_{mr} = M_m-1 zeros of U_{M_m-1}, the Chebyshev polynomials of the second kind.

S_{mr} and S_{nk} are obtained from the following:

$$S_{mr} = \cos\left(\frac{\pi r}{M_m+1}\right) \quad (C.9)$$

$$S_{nk} = \cos\left[\frac{(2k-1)\pi}{2M_n}\right] \quad (C.10)$$

It is important to identify that in the Gauss-Chebyshev integration scheme as suggested by Erdogan and Gupta [18] the total number of collocation points is one less than the

total number of interpolation points. Additional equations are needed to solve equation (C.8). These equations are obtained as follows:

INTERNAL (EMBEDDED) CRACK

The entrapped dislocation $a_n \delta^{pn}$ for crack n is given by (using Gauss-Chebyshev quadrature):

$$\delta^{pn} = \int_{-1}^{1} \mu^{pn}(S_n)\, ds_n = \int_{-1}^{1} \frac{F^{pn}(S_n)\, ds_n}{\sqrt{(1-S_{nk}^2)}} \simeq \frac{\pi}{M_n} \sum_{k=1}^{M_n} F^{pn}(S_{nk}) \qquad (C.11)$$

p = 1,2 which provides two additional equations per crack.

Usually δ^{pn} is zero but the above formula can be used for nonzero δ^{pn}. For a system of N cracks 2N additional equations are obtained. The above equation is adequate for non- intersecting cracks and has to be modified for branch cracks and intersecting cracks.

SURFACE CRACK

Let us examine the state of stress at the point where a crack intersects a free surface. Let the crack be along the X axis and let a free surface be defined by X = c. At the intersectio σ_{XX} and σ_{XY} should vanish and σ_{YY} should remain finite. This condition is best modelled by setting the dislocation density at the intersection to be zero. This was also pointed out in [19]. In the work presented in [19] the influence functions for a semi-infinite medium were used; in this hybrid SIFEH formulation however finite elements capture the boundary and influence functions for an infinite medium are used. Thus the additional equation for a surface crack is given by:

$$\mu^{pn}(S_{n1}) = 0 \quad , \quad p = 1,2 \tag{C.12}$$

It can also be argued that for a deep surface cracked plate under in plane bending that the surface condition is correctly represented by enforcing the derivative of the dislocation density to be zero (by noting that near the edge the crack faces are almost straight):

$$\frac{\partial \mu^{pn}(S_{n1})}{\partial S_n} = 0 \quad , \quad p = 1,2 \tag{C.13}$$

Again using (C.12) or (C.13) additional 2N equations are obtained.

Both these conditions have been modelled in the computer program and experience indicates that imposing (C.13) does not make appreciable difference in either displacements or stress intensity factors. Using equations C.8 through C.12 the following is obtained:

$$C\ F = T \tag{C.14}$$

where C evaluated at collocation point S_{mr} is given by:

$$[C]_{S_{mr}}\{F\} = \sum_{n=1}^{N} \frac{\pi}{M_n} \sum_{p=1}^{2} \sum_{k=1}^{M_n} \begin{Bmatrix} \Gamma_\tau^{p}(S_{mr}, S_{nk}) \\ \Gamma_\sigma^{p}(S_{mr}, S_{nk}) \end{Bmatrix} F^{pn}(S_{nk}) \tag{C.15}$$

Note: After C is computed at all the collocation points for the crack, closure or matching equations are added as given by (C.11), (C.12) or (C.13) and as discussed further in this appendix, to make C a square matrix.

$$F = F^{pn}(S_{nk}), \quad \begin{aligned} p &= 1,2 \\ n &= 1,2, \ldots . N \\ k &= 1,2, \ldots . M_n \end{aligned} \tag{C.16}$$

$$T = \begin{Bmatrix} T_\tau(S_{mr}) \\ T_\sigma(S_{mr}) \end{Bmatrix}, \quad \begin{matrix} m = 1,2, \ldots . N \\ r = 1,2, \ldots . M_m - 1 \end{matrix} \qquad (C.17)$$

II. CLOSURE AND MATCHING CONDITIONS FOR RADIAL CRACKS AND BRANCH CRACKS

Figure C.2 shows examples of radial cracks with branch cracks. The arms or wings of the cracks may have different lengths and these wings are modelled on a (0,+1) interval and the branch cracks on a (-1,+1) interval. For a system of M main cracks and B branch cracks for an origin, 2(M+B) extra equations are required to make C a square matrix. The closure condition is obtained by summing over all the cracks for a given origin [20]:

$$\sum_{m=1}^{M} \left\{ a_m \int_0^{+1} \frac{F^{pm}(S_n)\, dS_n}{\sqrt{1 - S_n^2}} + \sum_{b=1}^{B_m} a_b \int_{-1}^{1} \frac{F^{pb}(S_n)}{\sqrt{1 - S_n^2}} \right\} = \delta^{pe} \qquad (C.18)$$

$$p = 1,2$$

a_m = Crack length of main crack wing.

a_b = Half crack length of branch crack b of main crack wing m.

δ^{pe} = Entrapped dislocation in the p direction

The above equation is discretized using the Gauss-Chebyshev integration formula:

$$\sum_{m=1}^{M} \left\{ \frac{2}{M_{nm}} a_m \sum_{k=1}^{M_{nm}} \left\{ \frac{\pi}{4} + \sum_{\ell=1}^{M_{nm}-1} \frac{1}{\ell} \cos \frac{\ell(M_{nm}-2k+1)}{2M_{nm}} \sin\left(\frac{\pi}{2}\ell\right) \right\} F^{pm}(S_{mk}) \right.$$

$$\left. + \sum_{b=1}^{B_m} \left\{ \frac{\pi}{M_{nb}} a_b \sum_{k=1}^{M_{nb}} F^{pb}(S_{bk}) \right\} \right\} = \delta^{pe} \qquad (p = 1,2) \qquad (C.19)$$

Equation (C.19) provides 2 additional equations. Additional 2B equations are provided by the matching conditions where the dislocation density at the point of intersection of a main and branch crack or two branch cracks are enforced to be equal. Additional (2M-2) equations are provided by zeroing out the dislocation densities for the other wings.

III. CURVED CRACKS

Curved cracks are modelled by using piecewise linear segments as shown in figure C.3. The length of crack n is given by:

$$L_n = \sum_{i=1}^{k-1} [(X_{i+1}-X_i)^2+(Y_{i+1}-Y_i)^2]^{1/2} \quad (C.20)$$

L_n = Total length of crack n.

(X_j,Y_j) = Co-ordinates of discrete points defining the linear segments, j = 1 . . . . . k.

k = Total number of segments

The total length upto the j^{th} end point is given by:

$$l_{nj} = \sum_{i=1}^{j-1} [(X_{i+1}-X_i)^2+(Y_{i+1}-Y_i)^2]^{1/2} \quad (C.21)$$

Gauss-Chebyshev interpolation and collocation points defined by (S_{nr},S_{nk}) are mapped to the physical space on the

linear segments (defining the crack) by:

$$X(S_n) = X_{j+1} - \frac{l_{(nj+1)} - L_n S_n}{l_{(nj+1)} - l_{nj}} (X_{j+1} - X_j) \qquad (C.22)$$

$$S_n = S_{nr} \text{ or } S_{nk}$$

Equation (C.22) is applied when:

$$l_{nj} < L_n \cdot S_n < l_{(nj+1)} \qquad (C.23)$$

Once $X(S_n)$ is determined $Y(S_n)$ can be found from the end point co-ordinates of the j^{th} segment.

IV. EDGE DISLOCATION INFLUENCE FUNCTIONS FOR STRESSES

The stress tensor Γ^P_{ij} at evaluation point (X_o, Y_o) due to an edge dislocation of strength b^p at source point (X,Y) in an infinite, homogeneous and linear elastic medium is given by the third order influence function tensor $\Gamma^P_{ij}(Xo,Yo;X,Y)$ defining:

E = Young's modulus

ν = Poisson's ratio

Φ = $E/4\pi(1-\nu^2)$

X_m = $X-X_o$

Y_m = Y_o-Y

b^X = Burger's vector in the X direction

b^Y = Burger's vector in the Y direction

$$\Gamma^X_{XX} = \phi b^X \frac{-Y_m (Y_m^2 + 3X_m^2)}{(Y_m^2 + X_m^2)^2}$$

$$\Gamma^Y_{XX} = \phi b^Y \frac{Y_m^2 - X_m^2}{(Y_m^2 + X_m^2)^2}$$

$$\Gamma^X_{YY} = \phi b^X \frac{Y_m (X_m^2 - Y_m^2)}{(Y_m^2 + X_m^2)^2}$$

$$\Gamma^Y_{YY} = \phi b^Y X_m \left[\frac{-(3Y_m^2 + X_m^2)}{(Y_m^2 + X_m^2)^2} \right]$$

$$\Gamma^X_{XY} = \phi b^X \frac{X_m (Y_m^2 - X_m^2)}{(Y_m^2 + X_m^2)^2}$$

$$\Gamma^Y_{XY} = \phi b^Y \frac{Y_m (X_m^2 - Y_m^2)}{(Y_m^2 + X_m^2)^2} \qquad \text{(C.24)}$$

The normalized influence functions are obtained by using X_m/a and Y_m/a (where a is half crack length or wing length) instead of X_m and Y_m in the above equations. The influence functions given above are of the form 1/r (where r=radius to evaluation point) and hence the normalized function will have an extra a in the denominator. This a is however cancelled by the a in the numerator obtained from $dS_n = a\, ds_n$ during the mapping process of the crack to the (-1,+1) interval. Hence equation (C.4) is obtained. However for other influence functions (e.g. displacement influence function) appropriate transformations are required during the mapping process.

V. OBTAINING TRACTION COMPONENTS FROM INFLUENCE FUNCTIONS

Using Mohr's circle transformation for stress, the traction components Γ_τ^p and Γ_σ^p as used in equation (C.4) are obtained as follows (after reversing the sign for the shear stress):

$$\Gamma_\tau^p = \Gamma_{xy}^p \cos 2\psi + \frac{\Gamma_{yy}^p - \Gamma_{xx}^p}{2} \sin 2\psi \qquad \text{(C.25a)}$$

$$\Gamma_\sigma^p = \Gamma_{xx}^p \frac{1+\cos 2\psi}{2} + \Gamma_{yy}^p \frac{1-\cos 2\psi}{2} + \Gamma_{xy} \sin 2\psi \qquad \text{(C.25b)}$$

p = 1, 2 for mode I and II respectively.

Γ's = Normalized influence functions.

ψ = Angle made by the local tangent along the crack, with the vertical (positive anti-clockwise).

VI. COMPUTATION OF STRESS INTENSITY FACTORS

The amplitude F^p_{snk} of the dislocation density at the crack tip is directly related to the stress intensity factor as shown in [22,39]. As a greater number of interpolation points are used to model the crack, the tip interpolation points approach the physical location of the crack tips. Referring to figure C.1 the stress intensity factors for a homogeneous elastic medium are given by [19], [53]:

$$\begin{Bmatrix} K_I(\underset{\sim}{X}^a_m) \\ K_{II}(\underset{\sim}{X}^a_m) \end{Bmatrix} = \bar{E}(\pi a_m)^{1/2} \begin{bmatrix} -\cos\psi_{ml} & -\sin\psi_{ml} \\ -\sin\psi_{ml} & \cos\psi_{ml} \end{bmatrix} \begin{Bmatrix} F^1(S_{ml}) \\ F^2(S_{ml}) \end{Bmatrix} \qquad \text{(C.26)}$$

$K_I(\underset{\sim}{X}_m^a)$ = Crack opening or mode I stress intensity factor.

$K_{II}(\underset{\sim}{X}_m^a)$ = Crack shearing or mode II stress intensity factor.

$\underset{\sim}{X}_m^a$ = Tip vector for crack m, corresponds to interpolation point S_{m1}.

a_m = Half the crack length for crack m.

$\bar{E}$ = $E/4(1-\nu^2)$, for plane strain conditions.

$\bar{E}$ = E, for plane stress conditions.

E = Young's modulus.

ν = Poisson's ratio.

$F^1(S_{m1})$ = Amplitude of the shear dislocation density at the interpolation points at the tips.

$F^2(S_{m1})$ = Amplitude of the opening dislocation density at the interpolation points at the tips.

Ψ_{m1} = Angle (at the crack tip interpolation point) made by the local tangent along the crack with the vertical (positive anti-clockwise).

The sign convention for K_I is positive for the opening

mode I; and for K_{II} it is positive when the crack wants to propagate to the right for the shearing mode II when looking towards the crack tip.

It is to be noted that in equation (C.26) S_{m1} and ψ_{m1} correspond to the location x_m^a and for other crack tips the appropriate interpolation point and angle of the local tangent should be used.

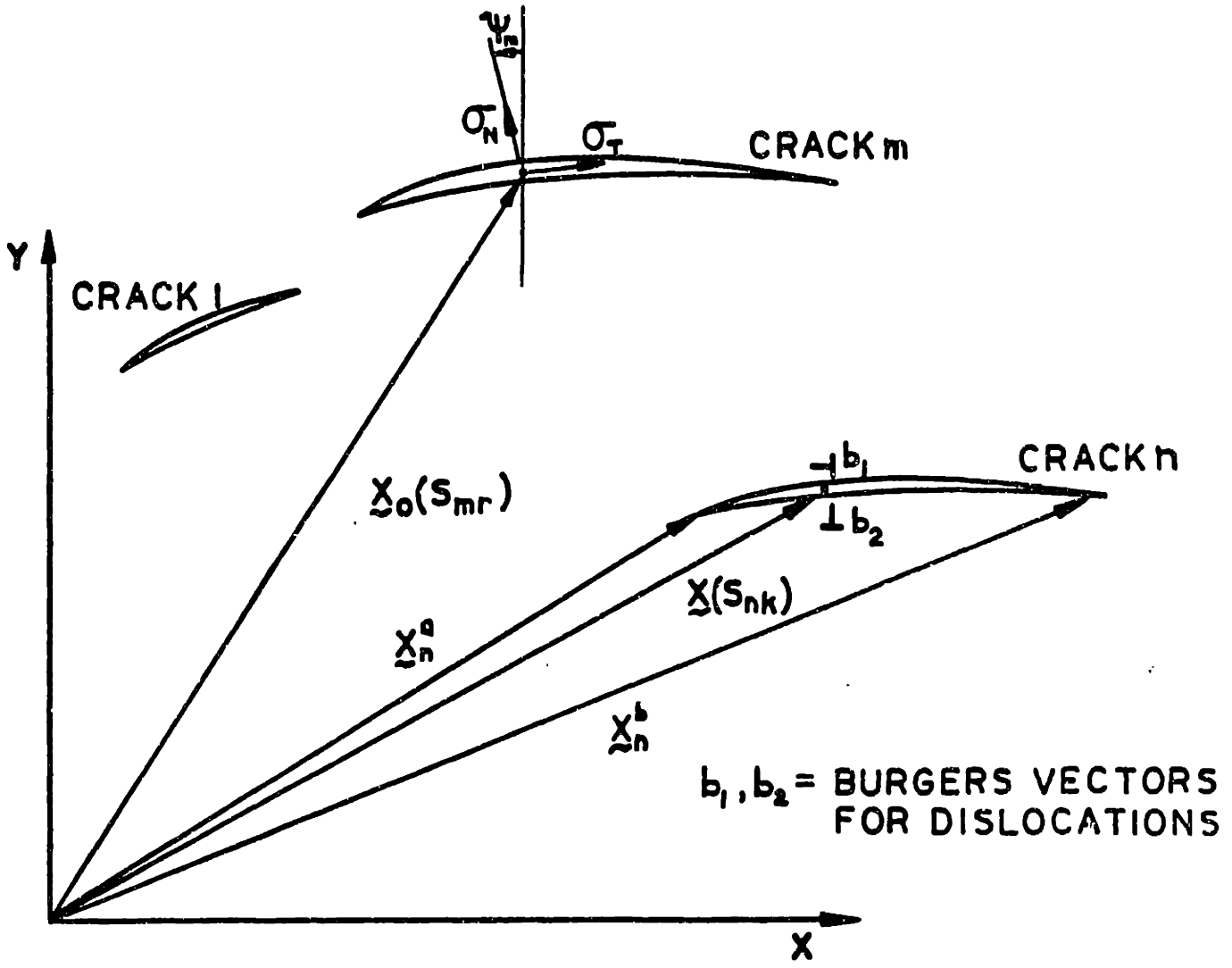

Figure C.1. Modelling System of Cracks Using a Continuous Distribution of Dislocations

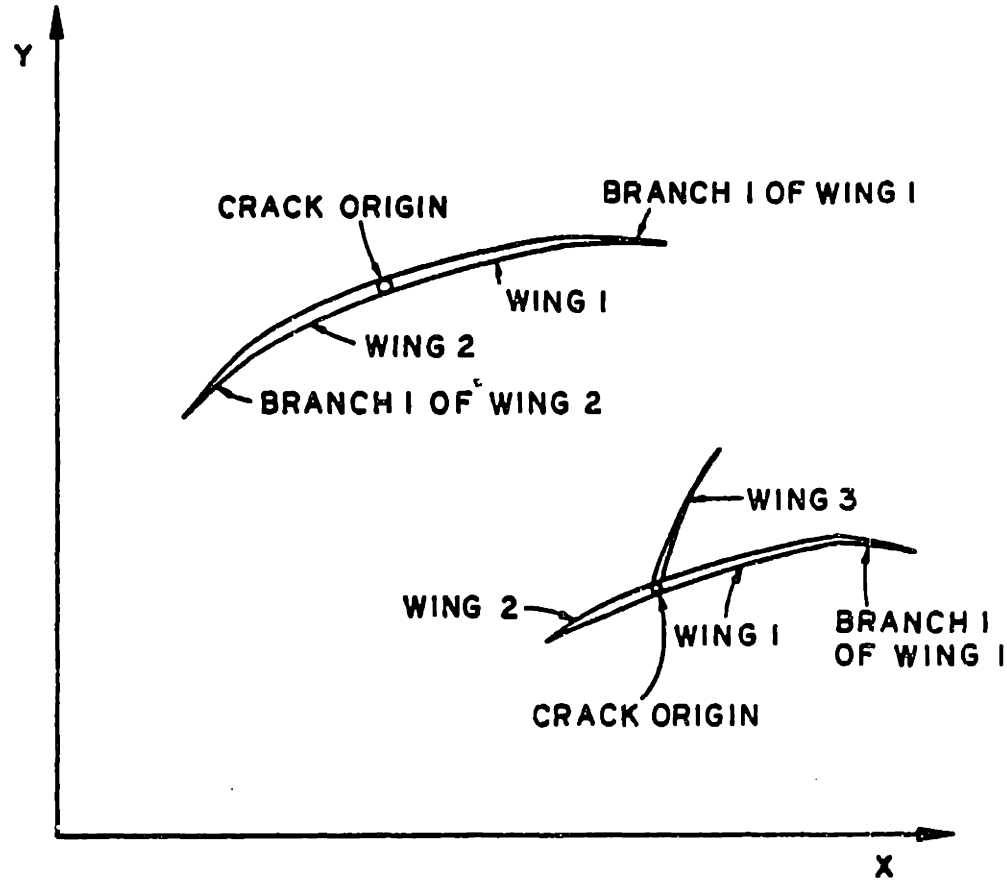

Figure C.2 Examples of multiple (radial) cracks emanating from an origin

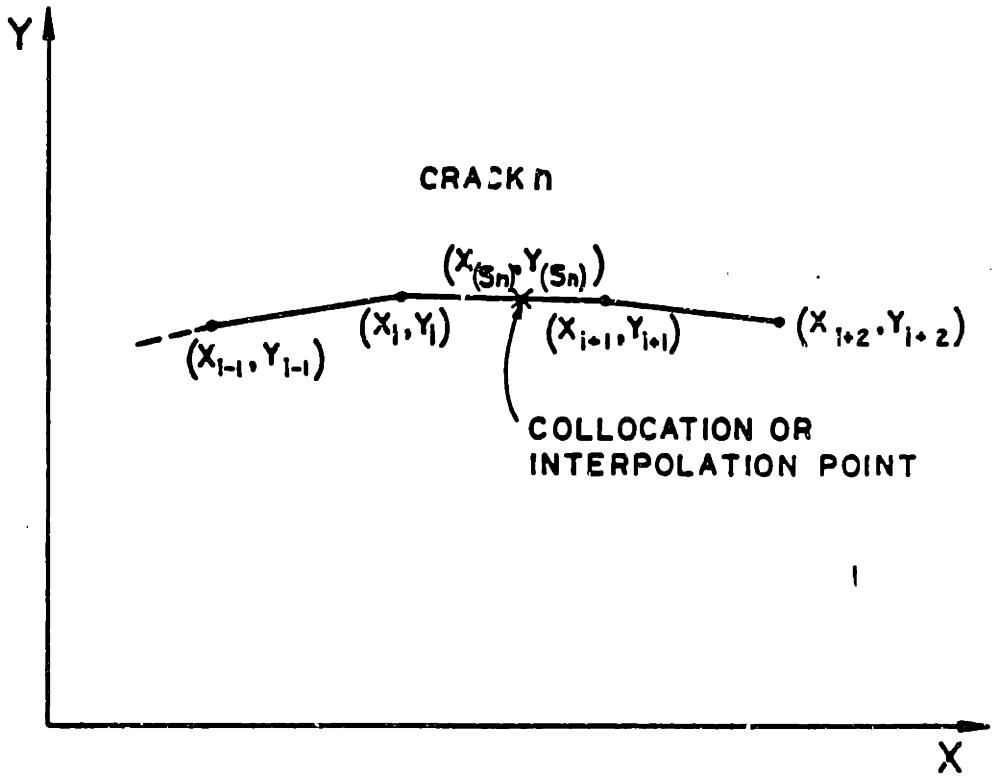

Figure C.3 Modelling of curved cracks using linear segments

APPENDIX D

I. COMPUTATION OF THE G MATRIX

The elements of the G matrix are the consistent loads (in the global X and Y directions) at the finite element boundary nodes due to unit dislocation density amplitudes at the interpolations (S_{nk}) points along the crack surface.

$$[G]_i \quad F = \int_{S_i} H^{Si} \, dS_i \quad n^{Si} \int_{S_c} \Gamma(\underset{\sim}{X}_o, \underset{\sim}{X}) . \mu(\underset{\sim}{X}) dS_c \tag{D.1}$$

$[G]_i$ = Element of the G matrix evaluated at the finite element node i which lies on the boundary.

$\{F\}$ = Vector of amplitudes of dislocation density at interpolation points S_{nk} along the crack.

S_i = Surface defining the finite element boundary associated with node i.

H^{Si} = Displacement interpolation function for the node i on the finite element boundary.

S_c = Crack surface.

n^{Si} = Outer normal vector on the surface S_i. (Note that there could be two normals associated with a node i, e.g. at a corner).

$\Gamma(\underset{\sim}{X}_o, \underset{\sim}{X})$ = Stress tensor (in the global X-Y frame) at a point $\underset{\sim}{X}_o$ due to unit slip and opening dislocations at $\underset{\sim}{X}$.

$\underset{\sim}{X}_o$ = Position vector for the Gauss integration points on the surface S_i.

$\underset{\sim}{X}$ = Position vector for the S_{nk} points along the crack surface.

$\mu(\underset{\sim}{X})$ = Dislocation density vector at S_{nk} points along the crack.

The elements of the G matrix are evaluated using Gauss-Chebyshev integration along the crack surface S_c and Gauss integration along the finite element boundary S_i. The Gauss-Chebyshev integration here is identical to the procedure [19,20] used to obtain the C matrix except that the evaluation of stresses is carried out at the Gauss integration points associated with the node i (noting that the Gauss-Chebyshev integration is valid for the whole domain). Once the normal and tangential stresses are obtained at the Gauss integration points; consistent nodal forces are obtained using standard finite element integration procedure over the surface S_i.

APPENDIX E

I. COMPUTATION OF THE L MATRIX

The elements of the L matrix are the displacements in the global X and Y directions at the finite element nodes due to unit slip and opening dislocation density amplitudes at the interpolation (S_{nk}) points along the cracks.

$$[L]_i \{F\} = \int_{S_c} \Gamma_D (\underset{\sim}{X}_o, \underset{\sim}{X}) \cdot \mu(\underset{\sim}{X}) \, d\underset{\sim}{S}_c \qquad (E.1)$$

$$[L]_i F = \sum_{n=1}^{N} \frac{\pi}{M_n} \sum_{p=1}^{2} \sum_{k=1}^{M_n} \begin{Bmatrix} \Gamma^p_{DX} (\underset{\sim}{X}_o, S_{nk}) \\ \Gamma^p_{DY} (\underset{\sim}{X}_o, S_{nk}) \end{Bmatrix} F^p_{S_{nk}} \qquad (E.2)$$

The integral has been evaluated using Gauss-Chebyshev integration. All parameters used in this appendix are same as those in Appendix D except the following:

$[L]_i$ = Elements of the L matrix evaluated at the finite element node i with position vector $\underset{\sim}{X}_o$.

$\Gamma_D(\underset{\sim}{X}_o, \underset{\sim}{X})$ = Displacement vector at $\underset{\sim}{X}_o$ in the global X and Y directions due to unit slip and opening dislocations at $\underset{\sim}{X}$.

$\Gamma^p_{DX}(\underset{\sim}{X}_o, \underset{\sim}{X})$ = Displacement in the global X direction at $\underset{\sim}{X}_o$ due to unit slip or opening

dislocation at $\underset{\sim}{X}$.

$r^{p}_{DY}(\underset{\sim}{X}_o, \underset{\sim}{X})$ = Displacement in the global Y direction at $\underset{\sim}{X}_o$ due to unit slip or opening dislocation at $\underset{\sim}{X}$.

II. EDGE DISLOCATION INFLUENCE FUNCTIONS FOR DISPLACEMENTS

The displacement influence functions for an edge dislocation are given in references [26,43]. These displacement functions as described in these references with a modification to the U_Y component of displacement are given below for Mode II:

$$U_X^{II} = \frac{b^X}{2\pi}\left[-\tan^{-1}\left(\frac{X}{Y}\right) + \frac{XY}{2(1-\nu)(x^2+y^2)}\right] + B \qquad (E.3a)$$

$$U_Y^{II} = -\frac{b^X}{2\pi}\left[\frac{1-2\nu}{4(1-\nu)}\ln(X^2+Y^2) + \frac{X^2-Y^2}{4(1-\nu)(X^2+Y^2)}\right] + C \qquad (E.3b)$$

In the aforementioned references the U_Y displacement field does not have the constant C as shown in equation (E.3b). If a constant is not included in the expression then the equation is dimensionally incorrect. A thorough discussion of this aspect and additional considerations for curved lines of discontinuity etc., is presented in an associated research effort [43]; for completeness, the central features will be outlined here.

The equations (E.3) are transformed to polar co-ordinates by using $X = r\cos\theta$, $Y = r\sin\theta$, $X^2+Y^2=r^2$.

$$U_x^{II} = \frac{b^X}{2\pi}\left[\theta - \pi/2 + \frac{\sin 2\theta}{4(1-\nu)}\right] + B \qquad (E.4a)$$

$$U_y^{II} = -\frac{b^X}{2\pi}\left[\frac{1-2\nu}{2(1-\nu)}\ \ell n(r) + \frac{\cos 2\theta}{4(1-\nu)}\right] + C \qquad (E.4b)$$

The boundary conditions for U_X^{II} are as follows:

$$U_x^{II}(\theta = 0^+) = b/2, \quad U_x^{II}(\theta = 2\pi^-) = -b/2 \qquad (E.5)$$

which gives, B = b

The boundary conditions for U_Y^{II} are as follows:

$U_Y^{II}(r_o,\theta_o) = \overline{U}_Y^{II}$ (known) from which C can be determined. This physically means that if the U_Y^{II} displacement is known anywhere at (r_o,θ_o) in the medium (except at r=o or r=∞ as ln(r) is then unbounded) then U_Y^{II} can be determined. In the SIFEH analysis, however, displacement boundary conditions are always used (in the least to remove rigid body modes) and thus this constant is automatically determined. The complete displacement components for mode I and mode II are given by:

$$U_X^{I} = \frac{b^Y}{2\pi}\left[\frac{1-2\nu}{2(1-\nu)}\ \ell n(r) - \frac{\cos 2\theta}{4(1-\nu)}\right] + C_1 \qquad (E.6a)$$

$$U_Y^{I} = \frac{b^Y}{2\pi}\left[\theta - \pi - \frac{\sin 2\theta}{4(1-\nu)}\right] \qquad (E.6b)$$

and

$$U_X^{II} = \frac{b^X}{2\pi}\left[\theta - \pi + \frac{\sin 2\theta}{4(1-\nu)}\right] \qquad (E.7a)$$

$$U_Y^{II} = -\frac{b^X}{2\pi}\left[\frac{1-2\nu}{2(1-\nu)}\ln(r) + \frac{\cos 2\theta}{4(1-\nu)}\right] + C_2 \qquad (E.7b)$$

In equations (E.6a) and (E.7b) the constants corresponding to the rigid body shift are C_1 and C_2 respectively. For an edge dislocation (opening Mode I or sliding Mode II) with a line of discontinuity along the X axis (Refer figure E.1) the range of θ is given by:

$$0 \leq \theta \leq 2\pi \qquad (E.8)$$

For a curved line of discontinuity the angle θ at which the discontinuity occurs has to be tracked (See [43] for more details). Also while computing elements of the L matrix at finite element node i, the location of the node with respect to the curved crack has to be determined so that the angle θ can be correctly computed. Since for the SIFEH modelling b^X and b^Y are the Burgers vectors in the global X and Y directions; the displacements are computed in the local directions and then rotated to the global directions. Refer to figure E.2: Let the displacement at a point (X_o, Y_o) due to opening and sliding dislocation of strength $b^X L$ and $b^Y L$ respectively at (X,Y) be given by U^L.

$$\underset{\sim}{U}^L = \begin{Bmatrix} U^{X_L} \\ U^{Y_L} \end{Bmatrix} = \underset{\sim}{L}^L \underset{\sim}{b}^L = \begin{bmatrix} L_{XX} & L_{XY} \\ L_{YX} & L_{YY} \end{bmatrix} \begin{Bmatrix} b^{X_L} \\ b^{Y_L} \end{Bmatrix} \qquad (E.9)$$

The vector b^L represents components of the Burgers

vector in the local co-ordinate system. The L matrix has been evaluated for these two dislocations as shown in figure E.2. The b vector in the global co-ordinate system is given by

$$\{b\} = \begin{Bmatrix} b^X \\ b^Y \end{Bmatrix} \tag{E.10}$$

The global displacement vector $\underset{\sim}{U}$ is obtained as

$$\{U\} = [R^{LG}]\{U^L\} \tag{E.11}$$

where R^{LG} is the local to global rotation matrix given by:

$$[R^{LG}] = \begin{bmatrix} \cos\phi & -\sin\phi \\ \sin\phi & \cos\phi \end{bmatrix} \tag{E.12}$$

Also,

$$\{b^L\} = [R^{GL}]\{b\} \tag{E.13}$$

where R^{GL} is the global to local rotation matrix given by:

$$[R^{GL}] = \begin{bmatrix} \cos\phi & \sin\phi \\ -\sin\phi & \cos\phi \end{bmatrix} \tag{E.14}$$

Using equations (E.9) through (E.14) the displacements in the global co-ordinate system are obtained as follows:

$$\{U\} = [R^{LG}][L^{L}][R^{GL}]\ \{b\} \qquad (E.15)$$

The terms in the parentheses are the components of the L matrix in the global co-ordinate system.

Crack opening and slip displacements are evaluated by setting up a matrix similar to the L matrix; the only difference being that the evaluation points are the collocation points instead of the finite element nodes.

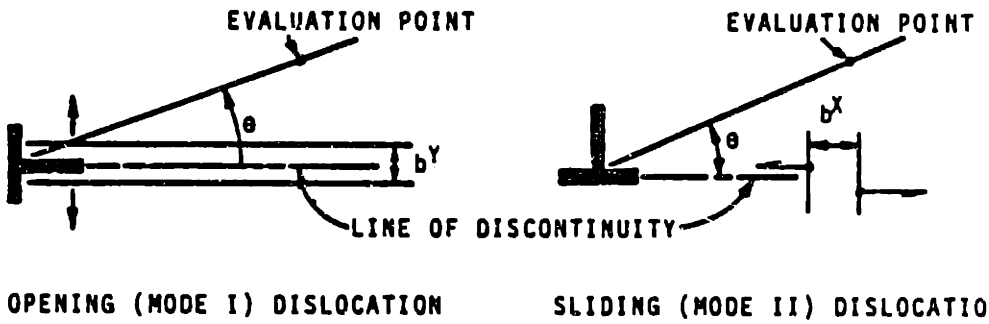

Figure E.1 Opening and sliding dislocations

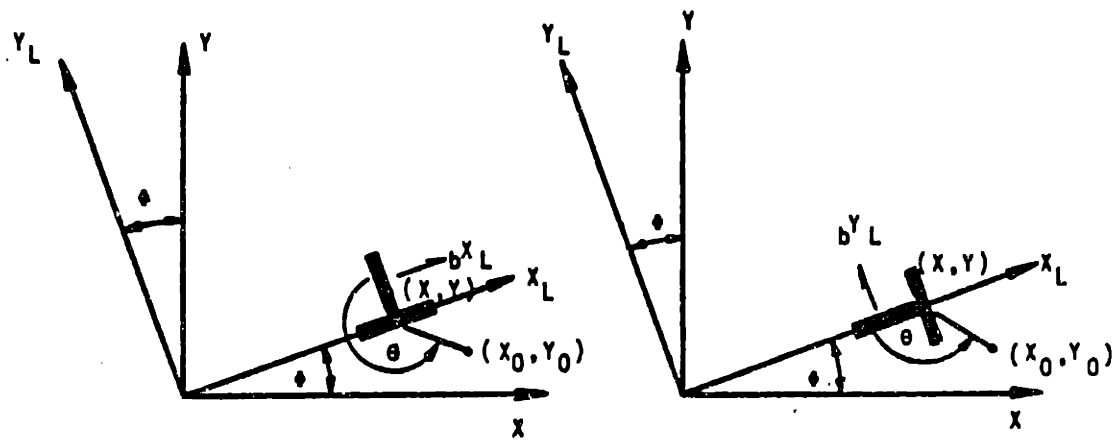

Figure E.2 Computation of the angle θ for opening and sliding dislocations

REFERENCES

1. R.S. Barsoum, "On the use of isoparametric finite elements in linear fracture mechanics", Int'l. J. Num. Meth. Eng., Vol. 10, 25-37, (1976).

2. R.S. Barsoum, "Triangular quarter-point elements as elastic and perfectly-plastic crack tip elements", Int'l. J. Num. Meth. Eng., Vol. 11, 85-98, (1977).

3. R.D. Henshell and K.G. Shaw, "Crack tip finite elements are unnecessary", Int'l. J. Num. Meth. Eng., Vol. 9, 495-507, (1975).

4. D.M. Parks, "A stiffness derivative finite element technique for determination of crack tip stress intensity factors", Int. J. of Fracture, Vol. 10.. No. 4, Dec., (1974).

5. T.H.H. Pian, "Variational and finite element methods in structural analysis", RCA Review, Vol. 39, Dec., (1978).

6. E.P. Sorensen, "A finite element investigation of stable crack growth in anti-plane shear", Int. J. of Fracture, Vol. 14, No. 5, Oct., (1978).

7. V.E. Saouma, "Interactive finite element analysis of reinforced concrete: A fracture mechanics approach", Report 81-5, Department of Structural Engineering, Cornell Univ., Jan., (1981).

8. T.A. Cruse, "Mathematical Foundations of the boundary integral equation method in solid mechanics", AFOSR-

TR77-1002 Jul., (1977).

9. T.A. Cruse and R.B. Wilson, "Advanced applications of boundary-integral equation methods", Nuclear Eng. Des. 46, 223-234, (1978).

10. T.A. Cruse and R.B. Wilson, "Boundary-integral equation method for elastic fracture mechanics analysis", AFOSR-TR-78-0355, Nov., (1977).

11. J.C. Lachat and J.O. Watson, "Effective numerical treatment of boundary integral equations: A formulation for three dimensional elastostics," Int'l. J. Num. Meth. Eng., Vol. 10, 991-1005, (1976).

12. C.A. Brebbia, The Boundary Element Method for Engineers, John Wiley & Sons, New York, NY (1978).

13. G.E. Blandford, A.R. Ingraffea, J.A. Liggett, "Automatic two dimensional quasi-static and fatigue crack propagation using the boundary element method", Report 81-3, Department of Structural Engineering, Cornell Univ., Jan., (1981).

14. P. Bettess, "Infinite elements", Int'l. J. Num. Meth. Eng., Vol. 11, 53-64, (1977).

15. H. Pircher and G. Beer, "On the treatment of "Infinite" boundaries in the finite element method", Int'l. J. Num. Meth. Eng., Vol. 11, 1194-1197, (1977).

16. P. Bettess and O.C. Zienkiewicz, "Diffraction and refraction of surface waves using finite and infinite elements", Int'l. J. Num. Meth. Eng., Vol. 11, 1271-1290, (1977).

17. M.P. Cleary, "Continuously distributed dislocation model for shear bands in softening materials", Int'l. J. Num. Meth. Eng., Vol. 10, 679-702, (1976).

18. F. Erdogan and G.D. Gupta, "On the numerical solution of singular integral equations", Quart. Appl. Math, 525-534, (1972).

19. D.T. Barr, "Thermal Cracking in Nonporous Geothermal Reservoirs", S.M. Thesis in Mechanical Engineering, M.I.T., May, (1980).

20. V. M. Narendran, "Elastostatic interaction of multiple arbitrarily shaped cracks in plane inhomogeneous regions", S.M. Thesis in Mechanical Engineering, M.I.T., (1982).

21. J.L. Dong, "Analyses of Deformation and Failure in Geological Materials", S.M. Thesis in Mechanical Engineering, M.I.T., (1980).

22. M.P. Cleary, "Moving singularities in elasto diffusive solids with applications to fracture propagation", Int. J. Solids and Structures, Vol. 14, 81-97, (1978).

23. A.E.H. Love, A Treatise on the mathematical theory of elasticity, Dover (1944).

24. K.J. Bathe, Finite Element Procedures in Engineering Analysis, Prentice-Hall, Englewood Cliffs, N.J. (1982).

25. O. C. Zienkiewicz, The Finite Element Method. McGraw-Hill, New York, NY, (1977).

26. J.P. Hirth and J. Lothe, Theory of Dislocations, McGraw-Hill, (1968).

27. H. Tada, P.C. Paris, and G.R. Irwin, The stress analysis of cracks handbook, Del Research Corporation, Hellertown, Pennsylvania (1973).

28. S. Timoshenko and J.N. Goodier, Theory of Elasticity, McGraw-Hill Book Company, New York, NY, (1951).

29. I.S. Sokolnikoff, Mathematical Theory of Elasticity, McGraw Hill Book Company, New York, NY, (1956).

30. J.W. Rudnicki and J.R. Rice, "Conditions for the localization of deformation in pressure-sensitive dilatant materials", J. Mech. Phy. Solids. Vol. 23, 371-394, (1975).

31. A. Argon, "Plastic deformation in metallic glasses", Acta Metall., Vol. 27, 47-58, (1979).

32. L. Anand and W.A. Spitzig, "Shear-band orientations in plane strain", Acta Metall., Vol. 30, 553-561, (1982).

33. M.P. Cleary, M. Kavvadas and K.Y. Lam, "Development of a fully three dimensional simulator for analysis and design of hydraulic fracturing", MIT Resource Extraction Laboratory, Report No. REL-82-12, (1982).

34. L. Prandtl and O.G. Tietjens, Fundamentals of Hydro and Aeromechanics, Dover Publications, New York, NY, (1957).

35. V.M. Narendran and M.P. Cleary, "Analysis of the growth and interaction of multiple hydraulic

fractures", MIT Resource Extraction Laboratory, Report No. REL-82-11, (1982).

36. M.P. Cleary, A.R. Crockett, J.I. Martinez, V.M. Narendran and S. Sutsky, "Surface Integral Schemes for Fluid Exchange and Induced Stresses around Fractures in Underground Reservoirs", Report No. REL-82-9, (1982).

37. D.M. Parks, Private Communication.

38. J.C.F. Telles, The Boundary Element Method Applied to Inelastic Problems, Springer Verlag, (1983).

39. J. R. Rice, "Mathematical analysis in the mechanics of fracture", Chap. 3 of Fracture: An Advanced Treatise, Vol. 2, H. Liebowitz, ed., Academic Press, New York, 191-311, (1968).

40. B.A. Bilby and J.D. Eshelby, "Dislocations and the theory of fracture", Chapter 2 of Fracture: An Advanced Treatise, Vol. 1, H. Liebowitz, ed., Academic Press, New York, 99-182, (1968).

41. O.L. Bowie, C.E. Freese and D.M. Neal, "Solution of plane problems of elasticity utilizing partitioning concepts", J. Appl. Mech., 767-772, Sept., (1973).

42. F.A. McClintock and A.S. Argon, eds., Mechanical Behavior of Materials., Addison-Wesley Publishing Co. Inc., Mass., (1966).

43. D.J.W. Wium, B.S. Annigeri, M.P. Cleary, V. Li and O. Buyukozturk, "Displacement field for a single dislocation", submitted for publication in Int. J.

Frac., (1984).

44. F.A. McClintock, J. Tirosh, L. Miller, J. Eckerle, J. H. Im, R. Cipolla, J. Joyce, R. Casler, J. Fleming, "Calculating Plane Elasticity by an integral formulation using dislocation pairs", Research Memorandum No. 177, Revision 2, Fatigue and Plasticity laboratory, Dept. of Mechanical Engineering, M.I.T., (1974).

45. F. A. McClintock, L. Miller, J. Eckerle, "User's manual for solving plane strain elasticity by superposing dislocation pairs", Research Memorandum No. 155 Revision 6, Fatigue and Plasticity labboratory, Dept. of Mechanical Engineering, M.I.T., (1974).

46. M.A. Pustejovsky, "Fatigue crack propagation in titanium under general in-plane loading", Ph.d thesis, Aeronautics and Astronautics Dept., M.I.T., (1976).

47. J. W. Hutchinson, Nonlinear Fracture Mechanics Department of Solid Mechanics, The Technical University of Denmark, (1980).

48. G. Strang and G J. Fix, An Analysis of the Finite Element Method, Prentice Hall Inc., Englewood Cliffs, N.J., (1973).

49. J.T. Oden, Finite Elements of Nonlinear Continua, McGraw-Hill Book Company, New York, (1972).

50. T.H. Greene, B.S. Annigeri and M.P. Cleary, "Computation of stress and displacement using the surface integral method", MIT Resource Extraction

Laboratory, Report No. REL-83-1, (1983).

51. O.L. Bowie, "Solutions of plane crack problems by mapping techniques", in Methods of Analysis and Solution of Crack Problems, G.C. Sih, Ed., Noordhoff, 1, (1973).

52. N. I. Muskhelishvilli, Some Basic Problems of the Mathematical Theory of Elasticity, Noordhoff, (1963).

53. D.T. Barr and M.P. Cleary, "Thermoelastic fracture solutions using distributions of singular influence functions - I", Int. J. Solids Structures, Vol. 19, 73-82, (1983).

54. F. Erdogan and G.C. Sih, "On the crack extension in plates under plane loading and transverse shear", ASME J. Basic Eng., Vol 85, 519-527, (1963).

55. G.C. Sih, "Strain energy density factor applied to mixed mode crack problems", Int. J. Fract., Vol. 10, 305-321, (1974).

56. M.A. Pustejovsky, "Fatigue crack propagation in titanium under general in-plane loading - I: Experiments, Eng. Frac. Mech., Vol. 11, 9-15, (1979).

57. M.A. Pustejovsky, "Fatigue crack propagation in titanium under general in-plane loading - II: Analysis, Eng. Frac. Mech., Vol. 11, 17-31, (1979).

58. B. Carnahan, H.A. Luther and J.O. Wilkes, Applied Numerical Methods, John Wiley and Sons Inc., New York, (1969).

59. D.J.W. Wium, O. Buyukozturk, and V.C. Li, "Hybrid model for discrete cracks in concrete", submitted for publication in J. Eng. Mech. Division, ASCE, (1983).

60. M. Arrea and A.R. Ingraffea, "Mixed-mode crack propagation in mortar and concrete", Report No. 81-13, Department of Structural Engineering, Cornell Univ., Ithaca, N.Y., Feb., (1982).

61. P.L. Bransby and P.M. Blair - Fish, "Wall Stresses in Mass-Flow Bunkers", Chem. Eng. Sci., Vol. 29, 1061-1074, (1974).

62. K.J. Bathe, E.L. Wilson, R.H. Iding, "NONSAP - A structural analysis program for static and dynamic response of nonlinear systems", Univ. of California, Berkeley.

63. J.W. Hutchinson, "Singular behavior at the end of a tensile crack in a hardening material", J. Mech. Phys. Solids, Vol 16, 13-31, (1968).

64. J.R. Rice and G.F Rosengren, "Plane strain deformation near a crack tip in a power-law hardening material", J. Mech. Phys. Solids, Vol 16, 1-12, (1968).

65. P.D. Hilton and J.W. Hutchinson, "Plastic intensity factors for cracked plates", Eng. Frac. Mech. Vol. 3, 435-451, (1971).

66. V. Vitek, "Yielding on inclined planes at the tip of a crack loaded in uniform tension", J. Mech. Phys. Solids, Vol. 24, 263-275, (1976).

67. K.K. Lo, "Modelling of plastic yielding at a crack tip

by inclined slip planes", Int. J. Fracture, Vol. 15, 583-589, (1979).

68. H. Riedel, "Plastic yielding on inclined slip-planes at a crack tip", J. Mech. Phys. Solids, Vol. 24, 277-289, (1976).

69. K.Y. Lam and M.P. Cleary, "General branching and frictional slippage at crack tips with applications to hydraulic fracturing", Report REL-82-1, Jan., (1982).

70. E. Hinton and J.S. Campbell, "Local and global smoothing of discontinuous finite element functions using least squares method", Int'l. J. Num. Meth. Eng., Vol. 8, 461-480, (1979).

71. J. T. Oden and H. J. Brauchli, "On the Calculation of consistent stress distributions in finite element applications", Int'l. J. Num. Meth. Eng., Vol. 3 317-325, (1971).

72. L. E. Malvern, Introduction to the Mechanics of a Continuous Medium, Prentice-Hall, Inc., Englewood Cliffs, N.J., (1965).

73. K. J. Bathe, "ADINA - A finite element program for automatic dynamic incremental nonlinear analysis", Report 82448-1, Acoustics and Vibration Laboratory, Department of Mechanical Engineering, M.I.T., Cambridge, Mass., 1975, rev. Dec., (1978).

74. H.P. Rossmanith, ed., Rock Fracture Mechanics, Springer Verlag, (1983).

75. S.K. Wong and M.P. Cleary, "Numerical analysis of

axisymmetric and other crack problems related to hydraulic fracturing", M.I.T. Resource Extraction Laboratory, Report NO.REL-81-4, (1981).

76. Ming-Che Lu and F. Erdogan, "Stress intensity factors in two bonded elastic layers containing cracks perpendicular to and on the interface" - Part I. Analysis NASA Report No. 159218, January (1980).

77. Ming-Che Lu and F. Erdogan, "Stress intensity factors in two bonded elastic layers containing cracks perpendicular to and on the interface" - Part II. Results NASA Report No. 159219, January (1980).

78. B. S. Annigeri and M.P. Cleary, "Surface integral finite element hybrid (SIFEH) method for fracture mechanics", to be published in Int'l J. Num. Meth. Eng., (1984).

79. B. S. Annigeri and M.P. Cleary, "Quasi-static fracture propagation using the surface integral finite element hybrid method", to be presented at the ASME Pressure Vessels and Piping Conference, San Antonio, Texas, June (1984).

80. Vargas Guadarrama, C. A., "Dynamic Poroelasticity", Ph.D. Thesis, New York University, June (1975).

81. P.S. Theocaris, G. Tsamasphyros and E.E. Theotokoglou, "A combined integral equation and finite-element method for the evaluation of stress intensity factors", Comp. Meth. Appl. Mech. and Eng. 31, 117-127, (1982).